https://doi.org/10.15388/vu.thesis.340
https://orcid.org/0000-0003-2364-6093

VILNIUS UNIVERSITY
CENTER FOR PHYSICAL SCIENCES AND TECHNOLOGY

Augustinas Povilas Fedaravičius

Algorithms of synchronization control in neural networks

DOCTORAL DISSERTATION

Natural sciences,
Physics (N 002)

VILNIUS 2022

The doctoral dissertation was prepared in 2015–2021 at the Center for Physical Sciences and Technology.

Academic supervisor – Prof. Habil. Dr. Kęstutis Pyragas (Center for Physical Sciences and Technology; Natural sciences, Physics – N 002).

Dissertation Defense Panel:

Chairman – Prof. Habil. Dr. Leonas Valkūnas (Vilnius University; Natural sciences, Physics – N 002).
Members:
Dr. Elena Adomaitienė (Center for Physical Sciences and Technology; Natural sciences, Physics – N 002),
PD Dr. Oleksandr Popovych (Institute of Neuroscience and Medicine, Research Centre Jülich, Germany; Natural sciences, Mathematics – N 001),
Prof. Habil. Dr. Kęstutis Staliūnas (Universitat Politècnica de Catalunya; Natural sciences, Physics – N 002),
Habil. Dr. Arūnas Tamaševičius (Center for Physical Sciences and Technology; Natural sciences, Physics – N 002).

The dissertation will be defended at a public meeting of the Dissertation Defense Panel on 1 July 2022 at 14:00 in auditorium D401 of the Center for Physical Sciences and Technology. Address: Saulėtekio av. 3, LT-10257 Vilnius, Lithuania. Phone: +370 5 264 9211, e-mail: `office@ftmc.lt`.

The dissertation is available in the libraries of the Center for Physical Sciences and Technology and Vilnius University, as well as on the Vilnius University website: `www.vu.lt/lt/naujienos/ivykiu-kalendorius`.

https://doi.org/10.15388/vu.thesis.340
https://orcid.org/0000-0003-2364-6093

VILNIAUS UNIVERSITETAS
FIZINIŲ IR TECHNOLOGIJOS MOKSLŲ CENTRAS

Augustinas Povilas Fedaravičius

Neuroninių tinklų sinchronizacijos valdymo algoritmai

DAKTARO DISERTACIJA

Gamtos mokslai,
Fizika (N 002)

VILNIUS 2022

Daktaro disertacija rengta 2015–2021 metais Fizinių ir technologijos mokslų centre.

Mokslinis vadovas – prof. habil. dr. Kęstutis Pyragas (Fizinių ir technologijos mokslų centras; gamtos mokslai, fizika – N 002).

Gynimo taryba:

Pirmininkas – prof. habil. dr. Leonas Valkūnas (Vilniaus universitetas; gamtos mokslai, fizika – N 002).
Nariai:
dr. Elena Adomaitienė (Fizinių ir technologijos mokslų centras; gamtos mokslai, fizika – N 002),
PD dr. Oleksandr Popovych (Neuromokslų ir medicinos institutas, Julicho tyrimų centras, Vokietija; gamtos mokslai, matematika – N 001),
prof. habil. dr. Kęstutis Staliūnas (Katalonijos politechnikos universitetas; gamtos mokslai, fizika – N 002),
habil. dr. Arūnas Tamaševičius (Fizinių ir technologijos mokslų centras; gamtos mokslai, fizika – N 002).

Disertacija ginama viešame Gynimo tarybos posėdyje 2022 m. liepos 1 d. 14:00 val. Fizinių ir technologijos mokslų centro D401 auditorijoje. Adresas: Saulėtekio al. 3, LT-10257 Vilnius. Tel. +370 5 264 9211, el. paštas: `office@ftmc.lt`.

Disertaciją galima peržiūrėti Fizinių ir technologijos mokslų centro ir Vilniaus universiteto bibliotekose bei VU interneto svetainėje adresu: `www.vu.lt/lt/naujienos/ivykiu-kalendorius`.

Contents

Abbreviations **viii**

Introduction **ix**

Objectives xi

Novelty xi

Scientific statements xiii

List of publications xiv

Personal contribution xv

Acknowledgements xv

1 Background **1**

1.1 Neurons and neuron models 1

1.2 Neurons as oscillators 5

1.3 Mean-field reduction 12

1.4 Pontryagin's maximum principle 16

2 Optimal entrainment of a spiking neuron with minimum charge **18**

2.1 Problem formulation 19

2.2 Solving the optimization problem 21

2.3 Analytical example: A Stuart-Landau oscillator 27

2.3.1 Comparing results for different waveforms 32

2.3.2 Small frequency mismatch 35

2.4 Optimal waveform for a small $|\Delta\omega|$ in the general case 36

2.5 Numerical examples 40

2.5.1 A randomly generated phase response curve 40

2.5.2 A Hodgkin-Huxley neuron model 45
2.6 Summary 47

3 Charge-optimal entrainment of a network of interacting neurons 51
3.1 Problem formulation 53
3.2 Optimal waveform for a network of interacting neurons 56
3.3 Numerical examples 59
3.3.1 A network of synaptically coupled FHN neurons . . . 61
3.3.2 A network of electrically coupled FHN neurons 67
3.3.3 A large-scale network of synaptically coupled QIF neurons 69
3.4 Summary 76

4 Spiking suppression in two interacting populations of QIF neurons 78
4.1 The model 79
4.1.1 Microscopic description 79
4.1.2 Macroscopic description: Low-dimensional mean-field equations in the limit $N \to \infty$ 82
4.2 Network dynamics without stimulation 82
4.3 Suppressing synchronous spiking 88
4.3.1 High-frequency stimulation of the inhibitory population 88
4.3.2 Suppression of oscillations by controlling the excitatory population 96
4.4 Modeling microscopic dynamics 100
4.5 Summary 104

Results and conclusions 107

Bibliography 111

Santrauka 123
Įvadas 123
Tikslai 124
Mokslinis naujumas 124
Ginamieji teiginiai 125

Publikacijų sąrašas 126
Asmeninis indėlis 127
Padėka 128
1 Pagrindai 129
2 Valdymo srovė krūviu optimaliai neurono sinchronizacijai . . 130
2.1 Uždavinio formuluotė 130
2.2 Optimizavimo uždavinio sprendimas 131
2.3 Analizinis pavyzdys: Stuart-Landau osciliatorius . . . 133
2.4 Optimalus valdymas mažoms $|\Delta\omega|$ vertėms bendruoju atveju 138
2.5 Skaitiniai pavyzdžiai 139
3 Neuronų tinklo sinchronizacija minimizuojant stimuliacijos krūvį 143
3.1 Uždavinio formuluotė 143
3.2 Optimali valdymo srovė sąveikaujančių neuronų tinklo sinchronizacijai 144
3.3 Skaitiniai pavyzdžiai 145
4 Sinchronizacijos slopinimas sąveikaujančiose neuronų populiacijose 156
4.1 Neuronų tinklo modelis 156
4.2 Tinklo dinamika nesant stimuliacijos 159
4.3 Sinchroninių virpesių slopinimas 160
4.4 Mikroskopinės dinamikos modeliavimas 168
Rezultatai ir išvados 171
Santrumpos 173

Abbreviations

DBS deep brain stimulation

FHN FitzHugh-Nagumo

GPe globus pallidus externus

HF high-frequency (stimulation)

HH Hodgkin-Huxley

LPC limit point of cycles

PRC phase response curve

QIF quadratic integrate-and-fire

RHS right-hand side

STN subthalamic nucleus (nucleus subthalamicus)

Introduction

Synchronization processes in large populations of interacting dynamical units are the focus of intense research in physical, technological, and biological systems [1], such as smart grids [2], Josephson junction arrays [3], coupled mechanical devices [4], optical networks [5], and neural networks [6]. In neural networks, synchronization can play a dual role. Under normal conditions, synchronization is responsible for cognition and learning [7, 8], while excessive synchronization can cause abnormal brain rhythms associated with neurological diseases such as Parkinson's disease [9], epilepsy [10, 11], tinnitus [12], and others. Various open-loop and closed-loop control algorithms have been developed to suppress unwanted synchronized network oscillations, e.g., coordinated reset stimulation [13, 14], time-delayed feedback control [15–17], separate stimulation-registration setup [18], act-and-wait algorithm [19, 20], optimal open-loop desynchronization [21], and many others [22–24].

In many applications, optimization of the entrainment of nonlinear oscillators to an external signal is desired. A representative example in neural networks is deep brain stimulation (DBS) [25–28], which is a powerful therapeutic tool for the treatment of patients with Parkinson's disease, essential tremor, dystonia, and even psychiatric disorders [29–33]. In theoretical and computational neuroscience, the research on stimulus optimization mainly focuses on developing *minimum-energy* or *minimum-power* controls [34–43]. The energy or power is a natural performance measure for optimal control problems when seeking to minimize a general intervention of the applied stimulus to the biological system and to reduce the power consumption of an implantable pulse generator. However, it is known that an improperly designed electrical stimulation system can damage neural tissue and/or the

DBS electrode itself [44]. For the specific aim to minimize this damage, an alternative performance measure can be chosen.

In various neurological stimulation protocols, one typically uses periodic, charge-balanced, biphasic stimuli [45]. Usually, the two phases are not symmetric. Charge balance is necessary to avoid any adverse long-term effects such as pH shift, ionic charges near the implanted electrodes, and erosion of the electrode material [46–49]. Neural tissue damage in such stimulation protocols depends on electrode properties, such as electrode material, geometry, and size, as well as on pulse properties, i.e., the pulse amplitude and duration [50–53]. For a given electrode, along with the resulting charge density, the tissue damage threshold is determined by the charge per phase of a stimulus pulse [50, 51]. For the periodic charge-balanced stimulation, this quantity is proportional to the mean absolute value of the stimulating current. Thus, the mean absolute value of the stimulating current can be chosen as a performance measure for optimizing stimulating waveform parameters in order to minimize tissue damage [49, 54].

The mechanism of action of DBS, however, is still poorly understood [55, 56]. Clinical observations show that the effects of lesioning and electrical stimulation of the same anatomical target area are similar [57]. This suggests that high-frequency stimulation suppresses neuronal activity in the target area. The hypothesis of local inhibition is also supported by some experiments in animals [58, 59] and in humans [60, 61]. In this context, the effect of high-frequency stimulation can be explained in terms of stabilizing the neuron's resting state [62]. However, there is no clear theoretical understanding of how high-frequency stimulation affects synchronization processes in neural networks. Recent advances in dynamical systems theory, namely, mean-field reduction of microscopic model equations in large-scale oscillatory networks to a low-dimensional system of differential equations that accurately describes the macroscopic evolution of the system in the infinite-size limit, provides not only a better understanding of the occurrence of synchronization in such large-scale oscillatory networks but also has the potential to explain the effect of stimulation on synchronization processes.

Objectives

1. To adapt the methods of phase reduction, averaging, and mean-field reduction of systems in the thermodynamic limit to problems of synchronization control in networks of nonlinear oscillators;

2. To derive an optimal charge-balanced waveform that ensures entrainment of a spiking neuron to external periodic stimulation with the minimum mean absolute value of the stimulating current;

3. To extend and apply the minimum-charge control algorithm to networks of interacting dynamical elements as well as macroscopic equations derived in the thermodynamic limit for a network of spiking neurons;

4. To analyze the effect of various stimulation algorithms on a large-scale network of two interacting populations of excitatory and inhibitory quadratic integrate-and-fire (QIF) neurons.

Novelty

- To minimize tissue damage, we have chosen the mean absolute value of the stimulating current as a performance measure for optimal control. The resulting minimum-charge control problem differs from typical optimization problems considered before. Usually, the problem of optimal entrainment of a spiking neuron is considered as a minimum-power control problem and deals with the minimization of a mean energy functional. The energy delivered to the neuron is proportional to the square of the stimulating current rather than its absolute value. The minimum-charge waveform derived here by the minimization of the mean absolute value of the stimulating current differs significantly from the minimum-power waveform.

- Along with the minimization of tissue damage, the minimum-charge control algorithm has another practical advantage over the minimum-

power control approach. For a small frequency mismatch, the minimum-power waveform is proportional to the phase response curve of the neuron, and thus its construction requires the knowledge of the whole phase response curve. On the contrary, the minimum-charge waveform is of the bang-off-bang type and is determined only by the distance between the absolute extrema of the phase response curve and its amplitude. This allows estimating the parameters of the optimal bang-off-bang waveform empirically, without recourse to the neuron model and the phase reduction theory. Furthermore, the widths and the amplitudes of the pulses can be generally different since the optimization problem considers an asymmetric amplitude restriction of the stimulating current. In previous theoretical considerations, only symmetric amplitude restriction has been considered. Searching for asymmetric optimal waveforms is highly important since stimulation protocols in vivo typically employ positive and negative pulses that are not symmetric.

- The method for constructing the signal for the optimal entrainment of a single neuron can be applied to a network of interacting neurons exhibiting collective periodic oscillations. However, for this purpose, the knowledge of the effective PRC of the network is required. For a small frequency mismatch, as in the case of a single neuron, only knowledge of the distance between the absolute extrema of the PRC and the PRC amplitude is required.

- Thorough bifurcation analysis of a system of two interacting excitatory and inhibitory populations of quadratic integrate-and-fire neurons revealed the mechanisms of action of various stimulation algorithms. The effect of high-frequency stimulation is explained using mean-field equations averaged over the stimulation period. Such methodology can serve as an effective tool for developing various stimulation algorithms to control synchronization processes in large-scale neural networks.

Scientific statements

1. The optimal waveform that provides the entrainment of a spiking neuron to a periodic charge-balanced external stimulating current is of the bang-off-bang type: it consists of two rectangular pulses, one positive and the other negative, located at the extrema of the phase response curve of the neuron.

2. For a small frequency mismatch, in the linear part of the Arnold tongue, where the amplitude restriction is not significant, the minimum-charge current is determined only by the distance between the absolute extrema of the phase response curve and its amplitude.

3. The same method can be applied to a network of interacting neurons by replacing the phase response curve of a single neuron with an effective phase response curve of the network; the optimal waveform for the network is also of the bang-off-bang type with periodically repeated positive and negative rectangular pulses, generally of different amplitudes and widths.

4. In a network of two globally connected neural populations of excitatory and inhibitory quadratic integrate-and-fire neurons, high-frequency stimulation applied to the inhibitory population effectively changes the distribution center of the excitability parameter, thereby increasing the proportion of spiking neurons in that population. This leads to the stabilization of the incoherent resting state and the termination of collective oscillations.

5. In the high-frequency domain, the threshold amplitude of high-frequency stimulation, which stabilizes the unstable incoherent resting state of the network, is proportional to the frequency of stimulation.

6. Suppression of network oscillations by controlling the excitatory population can be achieved provided that the system parameters are in a region of bistability. By applying a rectangular inhibitory pulse to the excitatory

population, the network state can be switched from the stable limit cycle to the stable incoherent state of rest.

List of publications

Scientific articles

1. Kestutis Pyragas, Augustinas P. Fedaravičius, Tatjana Pyragienė, and Peter A. Tass. "Optimal waveform for entrainment of a spiking neuron with minimum stimulating charge". In: *Physical Review E* 98.4 (Oct. 2018), p. 042216.

2. Kestutis Pyragas, Augustinas P. Fedaravičius, Tatjana Pyragienė, and Peter A. Tass. "Entrainment of a network of interacting neurons with minimum stimulating charge". In: *Physical Review E* 102.1 (July 2020), p. 012221.

3. Kestutis Pyragas, Augustinas P. Fedaravičius, and Tatjana Pyragienė. "Suppression of synchronous spiking in two interacting populations of excitatory and inhibitory quadratic integrate-and-fire neurons". In: *Physical Review E* 104.1 (July 2021), p. 014203.

Conferences

1. Augustinas P. Fedaravičius and Kestutis Pyragas. "Optimal waveform for the entrainment of a spiking neuron with the minimum mean absolute value of the stimulating current". In: *Open Readings 2018*. Vilnius, Mar. 2018, p. 77.

2. Augustinas P. Fedaravičius, Kestutis Pyragas, Tatjana Pyragienė, and Peter A Tass. "Optimal entrainment of a network of interacting neurons with minimum stimulating charge". In: *Dynamics Days Digital 2020*. Aug. 2020, p. 48.

3. Tatjana Pyragienė, Kęstutis Pyragas, and Augustinas P. Fedaravičius. "Sinchronizacijos slopinimas dviejose sąveikaujančiose neuronų populiacijose". In: *44-oji Lietuvos nacionalinė fizikos konferencija*. Vilnius, Oct. 2021, p. 169.

Personal contribution

The author, together with publication co-authors, derived the minimum-charge control for the entrainment of a single neuron as well as a network of interacting neurons to the frequency of a periodic external stimulation, conducted the bifurcation analysis and averaging of a large-scale network of two populations of QIF neurons perturbed by a high-frequency stimulation, and confirmed the theoretical results by performing numerical simulations.

Acknowledgements

I would like to express my sincere gratitude to my supervisor, prof. habil. dr. Kęstutis Pyragas, for his knowledge, clarity and accuracy in both physics, when reducing and controlling complex systems, and everyday communication, and endless patience for no doubt the most chaotic doctoral student over his long academic career;

To the supervisor of my bachelor's and master's theses, prof. habil. dr. Minvydas Ragulskis, who introduced me to nonlinear dynamics and chaos, and thus further propelled me into the field of neuroscience;

To my parents, Lilija and Algimantas, who, through their upbringing and support, enabled me to delve into all my areas of interest;

To Eglė Preckailaitė, who keeps my nervous system in a critical state (in the physical sense).

Chapter 1

Background

1.1 Neurons and neuron models

The *neuron* is the structural and functional unit of the nervous system. Despite an enormous diversity of characteristics, all neurons exhibit common morphological and functional identifying features. The cell body (*soma*) gives rise to processes, the *dendrites* and the *axon*, that establish the regionalization of the neuron's functions, its polarity, and its capacity to connect to other neurons and to sensory or effector cells. Neurons are *excitable* cells. In response to various inputs, neurons generate electrical signals that propagate along their processes. They are also *secretory* cells. They secrete *neurotransmitters* – signalling molecules – which are released (with a few exceptions) in a very localized fashion and directed to specific targets. Finally, neurons form contacts called *synapses* which enable information processing and transmission [69].

An important feature of the neuron is its plasma membrane, which consists of a phospholipid bilayer containing a large diversity of transmembrane proteins, such as ionic channels, pumps, transporters and various receptors, essential for the proper functioning of the cell. The plasma membrane acts as a barrier between the intracellular and extracellular environments and maintains a concentration gradient of ions which, in the absence of electrical activity, gives rise to the relatively stable difference in electrical potential across the membrane called the *resting membrane potential*. In this state the inside of the

cell is electrically negative with respect to the extracellular environment. When the membrane potential deviates from the resting potential in the positive or negative direction, the membrane is said to be *depolarized* and *hyperpolarized*, respectively. Electrical signals in neurons are carried by Na^+, Ca^{2+}, K^+, and Cl^- ions, which move through membrane channels according to their electrochemical gradients [70, 71].

The somatodendritic tree is the neuron's receptive pole, it receives up to ten thousand synaptic connections from other neurons. The inputs induce electrical currents, such as the excitatory and inhibitory postsynaptic potentials as well as calcium action potentials, which integrate the afferent information. A sufficient input may give rise to an *action potential* or *spike* – an abrupt and transient depolarization of the membrane, followed by its repolarization and, possibly, hyperpolarization – which originates in the axon initial segment and propagates along the axon. After reaching the axon terminal, the action potential triggers the release of neurotransmitters in the synaptic cleft [72].

From a biophysical point of view, neurons are dynamical systems. They are excitable because the equilibrium corresponding to their resting state is near a bifurcation. The resting state corresponds to a stable equilibrium and the spiking state corresponds to a stable limit cycle attractor. The four possible codimension-1 bifurcations (saddle node, saddle node on an invariant circle, sub- and supercritical Hopf bifurcations) classify neuronal dynamics into four categories: integrators or resonators, monostable or bistable [73].

The main structural and functional elements of a cortical neuron are depicted in Fig. 1.1.

The Hodgkin-Huxley model

The previously described neurophysiological principles can be formalized using a detailed neuron model proposed in 1952 by Hodgkin and Huxley [74]. It is the most accepted formalism to describe neuronal dynamics. This model, in the presence of a direct current I_d and the stimulating alternating current

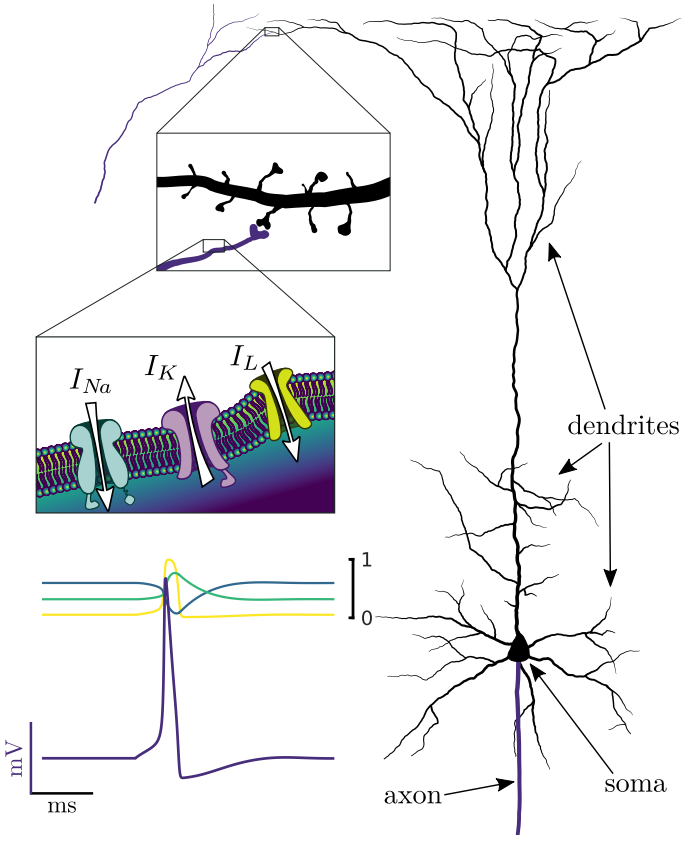

Figure 1.1 Structural and functional elements of a cortical neuron. (right) A diagram of the morphology of a pyramidal neuron. The cell body and cellular processes – dendrites (black) and axon (purple) – are indicated. (top inset) The axon terminal of another neuron (purple) makes contact with a dendritic spine and forms a chemical synapse. (bottom inset) The plasma membrane of the neuron consists of a phospholipid bilayer with embedded ion channels. The ion flows are depicted by white arrows and labeled according to their corresponding currents of the Hodgkin-Huxley (HH) model (1.1). (bottom-left) The action potential (spike) and corresponding dynamics of the gating variables of the HH neuron.

$I(\omega t)$, is defined by the following set of ordinary differential equations:

$$C_m \dot{v} = -I_{Na} - I_K - I_L + I_d + I(\omega t), \tag{1.1a}$$
$$\dot{m} = \alpha_m(v)(1-m) - \beta_m(v)m, \tag{1.1b}$$
$$\dot{h} = \alpha_h(v)(1-h) - \beta_h(v)h, \tag{1.1c}$$
$$\dot{n} = \alpha_n(v)(1-n) - \beta_n(v)n. \tag{1.1d}$$

Here $C_m = 1\ \mu\text{F/cm}^2$ is the membrane capacitance, and v is the membrane potential measured in mV. The Na^+, K^+ and leak currents are given by the following expressions

$$I_{Na} = g_{Na} m^3 h (v - v_{Na}), \tag{1.2a}$$
$$I_K = g_K n^4 (v - v_K), \tag{1.2b}$$
$$I_L = g_L (v - v_L). \tag{1.2c}$$

The parameters are $(v_{Na}, v_K, v_L) = (115, -12, 10.6)$ mV, and $(g_{Na}, g_K, g_L) = (120, 36, 0.3)$ mS/cm^2. The rate parameters defining the dynamics of the gating variables m, h and n measured in ms^{-1} are the following functions of the membrane potential:

$$\alpha_m(v) = (2.5 - 0.1v)/[\exp(2.5 - 0.1v) - 1], \tag{1.3a}$$
$$\beta_m(v) = 4\exp(-v/18), \tag{1.3b}$$
$$\alpha_h(v) = 0.07\exp(-v/20), \tag{1.3c}$$
$$\beta_h(v) = 1/[\exp(3 - 0.1v) + 1], \tag{1.3d}$$
$$\alpha_n(v) = (0.1 - 0.01v)/[\exp(1 - 0.1v) - 1], \tag{1.3e}$$
$$\beta_n(v) = 0.125\exp(-v/80). \tag{1.3f}$$

The parameters for this model have been obtained by fitting its solution to the experimental data on the giant axon of the squid [74]. Here the voltage scale is shifted in such a way that the membrane resting potential without external currents [$I_d = I(\omega t) = 0$] is zero. There are various extensions to this

model, because mammalian neurons have additional currents with different activation and inactivation dynamics.

In this dissertation we will also use simplified models. One example is the FitzHugh-Nagumo (FHN) model [75], which is a modified van der Pol oscillator designed to mimic the generation of action potentials of the Hodgkin-Huxley (HH) neuron. Despite a reduced level of complexity, it retains many features of the HH model and allows geometrical analysis of neuronal excitability and the spike generating mechanism. Another is the quadratic integrate-and-fire neuron (QIF) [76], which is the topological normal form of the saddle node bifurcation [77, 78]. It is the simplest model of a spiking neuron. It foregoes the subtleties of spike generation, but its relative simplicity allows for numerical simulation of large neuronal networks as well as yields to mean field reduction techniques. These models will be introduced as they are needed.

1.2 Neurons as oscillators

It is difficult both conceptually and computationally to analyze higher level neural dynamics using biophysical neuron models. To make such analysis mathematically tractable while retaining the essential properties of neural spiking, neurons are conceptualized as oscillators. It is possible to do so despite somewhat irregular activity (especially in cortical neurons), if the complete state of the neuron can be described using a single variable, called the *phase*.

Let us suppose that we have a general neuron model described by an ordinary differential equation:

$$\dot{\mathbf{X}}(t) = \mathbf{\Phi}(\mathbf{X}), \tag{1.4}$$

where $\mathbf{X} \in \mathbb{R}^n$ is a vector describing the state of the neuron, $\mathbf{\Phi} = (\Phi_1(\mathbf{X}), \ldots, \Phi_n(\mathbf{X}))$ is a function which represents the system dynamics and the dot denotes the time derivative. Suppose that there exists a stable limit cycle $\mathcal{L}$ with a natural period T_0 and natural frequency $\omega_0 = 2\pi/T_0$, such that $\mathbf{X}_{\mathcal{L}}(t) = \mathbf{X}_{\mathcal{L}}(t + T_0)$.

By choosing an arbitrary origin point on the limit cycle it is possible to define the *phase function* in the basin of $\mathcal{L}$:

$$\vartheta = \Theta(\mathbf{X}), \tag{1.5}$$

where the phase satisfies $0 \leq \vartheta < 2\pi$. Although the velocity $\dot{\mathbf{X}}$ of the system as it rotates along the limit cycle is generally nonconstant, the phase always increases with a constant frequency, that is, $\mathbf{X}_{\mathcal{L}}(t)$ is assigned the phase $\vartheta(t) = \omega_0 t$. Phase reduction of an oscillating FHN neuron (3.26) is shown in Fig. 1.2.

In order to characterize the response of the system to external perturbations, which may kick the state of the neuron out of the limit cycle, we extend the definition of the phase function to the basin of attraction of the limit cycle by assigning the same phase $\vartheta(t)$ to all states $\mathbf{X}(t)$ that converge to the same trajectory on the limit cycle as $t \to \infty$. The set of such states is called the *isochron*.

Differentiating Eq. (1.5) with respect to time, we obtain

$$\dot{\vartheta}(t) = \dot{\Theta}(\mathbf{X}(t)) = \boldsymbol{\nabla}_{\mathbf{X}=\mathbf{X}(t)}\Theta(\mathbf{X}) \cdot \dot{\mathbf{X}}(t) = \boldsymbol{\nabla}_{\mathbf{X}=\mathbf{X}(t)}\Theta(\mathbf{X}) \cdot \boldsymbol{\Phi}(\mathbf{X}(t)), \tag{1.6}$$

where the operator $\boldsymbol{\nabla}_{\mathbf{X}=\mathbf{X}(t)}$ is the gradient with respect to $\mathbf{X}$ evaluated at $\mathbf{X}(t)$. If the phase function satisfies

$$\boldsymbol{\nabla}_{\mathbf{X}=\mathbf{X}(t)}\Theta(\mathbf{X}) \cdot \boldsymbol{\Phi}(\mathbf{X}) = \omega_0 \tag{1.7}$$

for every $\mathbf{X}$ on $\mathcal{L}$ and in its basin of attraction, then

$$\dot{\vartheta}(t) = \omega_0 \tag{1.8}$$

holds. Using the above theory, we can define a phase $\vartheta(t)$ of the neuron state $\mathbf{X}(t)$ that increases with constant ω_0 in the whole basin of attraction of the limit cycle $\mathcal{L}$.

We will now describe the phase response of the neuron to a perturbative impulse (Fig. 1.3). Depending on the neuron's intrinsic dynamics, the type of stimulus and the phase at which the stimulus is applied, the neural oscillation

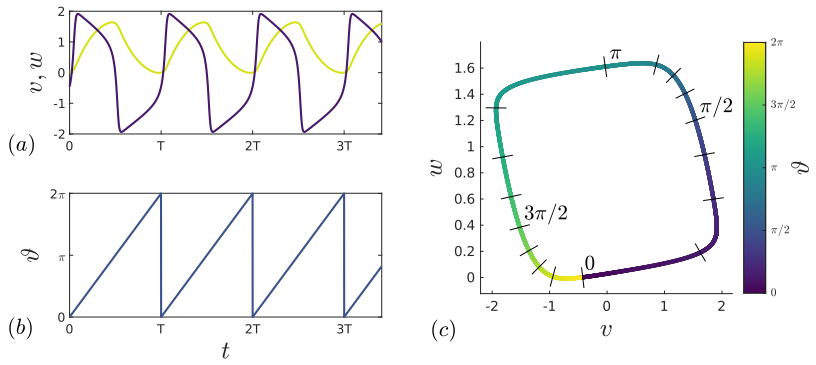

Figure 1.2 Dynamics of an oscillating FHN neuron (3.26) and the corresponding phase model. (a) Time series of the voltage v (purple) and the recovery variable w (yellow) of the FHN neuron model as it is oscillating in a stable limit cycle. (b) Dynamics of the phase variable ϑ corresponding to the limit cycle orbit of the FHN neuron. (c) Definition of the phase ϑ superimposed on the stable limit cycle of the FHN neuron.

may be advanced or delayed, i.e. the phase is shifted forwards or backwards. Let us define a perturbation vector $\mathbf{I} = (I_1, \dots I_n)$ applied to the neuron state $\mathbf{X}_0$ which results in a new state $\mathbf{X} = \mathbf{X}_0(\vartheta) + \mathbf{I}$. The perturbation has to be weak so that the perturbed state remains in the basin of $\mathcal{L}$ and does not cause a separate spike. The perturbation results in a *phase shift* which can be defined using the phase function as

$$g(\vartheta, \mathbf{I}) = \Theta(\mathbf{X}_0(\vartheta) + \mathbf{I}) - \vartheta. \tag{1.9}$$

Because we require $|\mathbf{I}|$ to be small, we can expand the phase function in a Taylor series

$$\Theta(\mathbf{X}_0(\vartheta) + \mathbf{I}) = \Theta(\mathbf{X}_0(\vartheta)) + \nabla_{\mathbf{X}=\mathbf{X}_0}\Theta(\mathbf{X}) \cdot \mathbf{I} + o(|\mathbf{I}^2|) \tag{1.10}$$

to obtain the approximation for the phase shift

$$g(\vartheta, \mathbf{I}) \approx \nabla_{\mathbf{X}=\mathbf{X}_0}\Theta(\mathbf{X}) \cdot \mathbf{I} = \mathbf{z}(\vartheta) \cdot \mathbf{I}, \tag{1.11}$$

where $\mathbf{z}(\vartheta)$ is the *phase response curve* (PRC), also called the infinitesimal phase response curve or phase sensitivity function in the literature. The PRC represents the linear response coefficients of the phase to perturbations.

The PRC of an oscillator can be obtained directly by applying a weak impulse of magnitude I to each component of $\mathbf{X}$ and measuring the resulting phase shift:

$$z_j(\vartheta) = \lim_{I \to 0} \frac{g(\vartheta, I\hat{\mathbf{e}}_j)}{I}, \tag{1.12}$$

where $\hat{\mathbf{e}}_i$ is the unit vector corresponding to the j'th component of $\mathbf{X}$. This method can be used experimentally, however, it is usually only possible to apply an impulse to the component of the state variable corresponding to the neuron's membrane potential. The PRC can also be obtained numerically (and, in rare cases, analytically) by integrating the adjoint equation [79, 80]

$$\omega_0 \frac{\mathrm{d}\mathbf{z}(\vartheta)}{\mathrm{d}\vartheta} = -\mathsf{J}(\vartheta)^T \mathbf{z}(\vartheta) \tag{1.13}$$

backwards in time with the normalization condition

$$\mathbf{z}(\vartheta) \cdot \frac{\mathrm{d}\mathbf{X}_0(\vartheta)}{\mathrm{d}\vartheta} = 1, \tag{1.14}$$

where $\mathsf{J}(\vartheta)^T$ is the transpose Jacobian matrix of $\mathbf{\Phi}(\mathbf{X})$ evaluated at $\mathbf{X} = \mathbf{X}_0$. Another efficient numerical algorithm for computing the PRC by using the direct method adapted to infinitesimal perturbations is described in [81].

If we choose the origin of the phase so that it coincides with the spike of an action potential, the PRC is usually close to zero at 0 and 2π, because a spiking neuron is insensitive to small inputs. Furthermore, we can distinguish two types of neurons by their PRCs: type I PRCs are non-negative, the spikes can only be advanced; and type II PRCs, which are usually biphasic. In such neurons, spikes can be both advanced and retarded. The type of PRC is very important in determining how a neuron behaves in a network.

Using the above reasoning we can perform *phase reduction* of a neuron stimulated with a weak periodic external current

$$\dot{\mathbf{X}} = \mathbf{\Phi}(\mathbf{X}) + \mathbf{I}(\omega t) \tag{1.15}$$

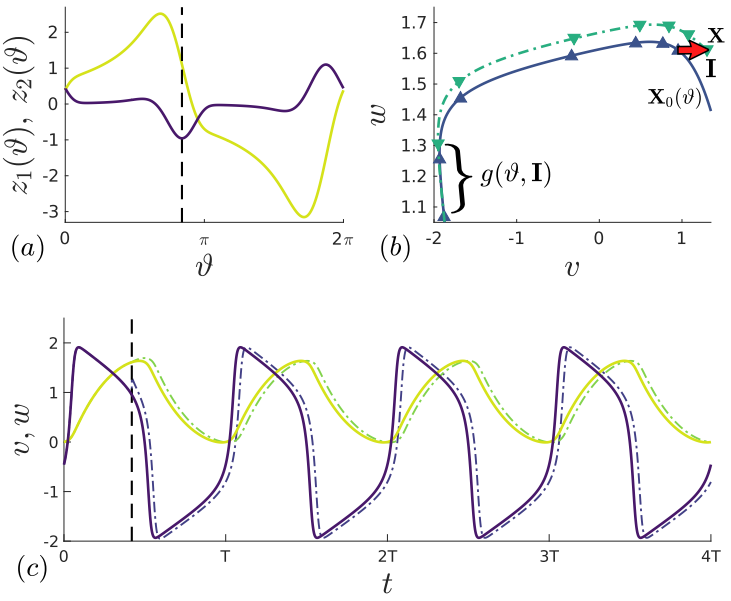

Figure 1.3 Phase response of an oscillating FHN neuron to a perturbative impulse. The phase and time of the perturbation is indicated by the vertical dashed lines. The perturbed trajectories are depicted in dash-dotted lines. (a) The phase response curve (PRC) components $z_1(\vartheta)$ (purple) and $z_2(\vartheta)$ (yellow) corresponding to the voltage v and recovery variable w of an oscillating FHN neuron. The impulse coincides with the minimum of the PRC in order to cause a maximal delay in the oscillation. (b) The impulse $\mathbf{I}$ (red arrow) applied to the membrane potential v kicks the state of the neuron out of the limit cycle $\mathcal{L}$ and results in a new state $\mathbf{X} = \mathbf{X}_0(\vartheta) + \mathbf{I}$, which eventually converges back to $\mathcal{L}$ with a phase shift $g(\vartheta, \mathbf{I})$. The triangle symbols mark the phase in equal time intervals. (c) The response of the voltage v (purple) and recovery variable w (yellow) to the external stimulus.

to obtain

$$\dot{\vartheta} = \omega_0 + \mathbf{z}(\vartheta) \cdot \mathbf{I}(\omega t), \tag{1.16}$$

where ω_0 is the natural frequency of the neuron, ω is the frequency of the external current.

Similarly, this scheme can be applied to describe the phase dynamics of a weakly coupled network of N neurons:

$$\dot{\mathbf{X}}_i = \mathbf{\Phi}_i(\mathbf{X}_i) + \sum_{j=1}^{N} \mathbf{H}_{ij}(\mathbf{X}_i, \mathbf{X}_j), \tag{1.17}$$

where $\mathbf{H}_{ij}(\mathbf{X}_i, \mathbf{X}_j)$ describes the effect of neuron j on neuron i. If the differences between the neurons are small, we can express the dynamics of each neuron as

$$\mathbf{\Phi}_i(\mathbf{X}_i) = \mathbf{\Phi}(\mathbf{X}_i) + \mathbf{f}_i(\mathbf{X}_i), \tag{1.18}$$

where $\mathbf{f}_j$ is a small individual heterogeneity. This system can be reduced to the following phase model:

$$\dot{\vartheta}_i = \omega_0 + \mathbf{z}_i(\vartheta_i) \cdot \left[\mathbf{f}_i(\mathbf{X}_i(\vartheta_i)) + \sum_{j=1}^{N} \mathbf{H}_{ij}(\mathbf{X}_i(\vartheta_i), \mathbf{X}_j(\vartheta_j)) \right]. \tag{1.19}$$

If the effect of the coupling and the heterogeneity between neurons is sufficiently small, the above expression may be further simplified. By separating the relatively fast neural oscillations from the slow drift caused by the interaction and differences between neurons, and averaging over the period of the limit cycle, we obtain

$$\dot{\vartheta}_i = \omega_i + \sum_{j=1}^{N} \Gamma_{ij}(\vartheta_i - \vartheta_j), \tag{1.20}$$

where ω_i is the new individual natural frequency and Γ_{ij} is the *phase coupling function*.

Note that in some cases the external current may be applied to only a subset of the neurons. If we only care about the collective phase dynamics, we can consider the network an nN-dimensional system, in which case the network

equations reduce to a single equation of the collective phase. Then the effective PRC of the network is the sum of the PRCs of the stimulated neurons [82]:

$$\dot{\vartheta} = \omega_0 + \sum_{i=1}^{M} \mathbf{z}_i(\vartheta) \cdot \mathbf{I}_i(\omega t), \tag{1.21}$$

here ϑ is the collective phase, i is the index of M stimulated neurons in a network of N cells. See Chapter 3 for more details.

Synchronization

In this section we will briefly discuss the main terminology of synchronization of phase oscillators. For simplicity, we will consider a general system of two phase oscillators

$$\dot{\vartheta}_1 = f_1(\vartheta_1, \vartheta_2), \tag{1.22a}$$
$$\dot{\vartheta}_2 = f_2(\vartheta_1, \vartheta_2), \tag{1.22b}$$

where f_1 and f_2 are some positive functions, but the definitions can be extended to more dimensions as needed.

Since the phase is defined on the circle $\mathbb{S}^1$, the state space of two coupled oscillators is the 2-torus $\mathbb{T}^2 = \mathbb{S}^1 \times \mathbb{S}^1$. Various modes of synchronization are therefore defined as flows on the surface of this torus. If there exists a periodic trajectory on the 2-torus in which ϑ_1 performs p rotations and ϑ_2 performs q rotations, where p and q are relatively prime integers, the oscillators are said to exhibit *p*:*q frequency-locking*. A 1:1 frequency locking is called *entrainment*. If two oscillators are frequency-locked and the difference $q\vartheta_1 - p\vartheta_2$ is constant, the oscillators are said to be *phase-locked*. Depending on the value of this constant, in-phase, anti-phase or out-of-phase locking can occur. We will call 1:1 phase-locking *synchronization*.

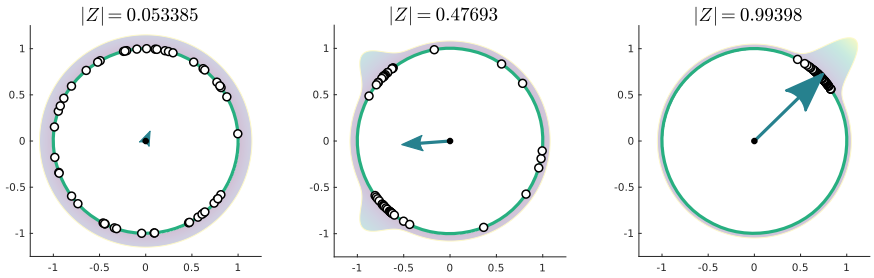

Figure 1.4 The Kuramoto synchronization index for different orders of synchronization in a network of phase oscillators. The phases of individual oscillators are depicted as dots on the unit circle. The complex-valued order parameter Z as a vector and its corresponding absolute value is shown for three cases (left to right): an incoherent network, a partially synchronized and a fully synchronized state.

In a network of N oscillators we can define the complex-valued *Kuramoto synchronization index* or *order parameter* [83]

$$Z = \frac{1}{N} \sum_{j=1}^{N} \exp\left(\mathrm{i}\vartheta_j\right). \tag{1.23}$$

A synchronized state of the network corresponds to $|Z| \approx 1$. When $|Z| \approx 0$, two cases are possible: either the network is incoherent, or there exist several synchronized clusters of neurons, evenly spaced on the phase circle. Intermediate values of $|Z|$ correspond to a partially synchronized state. A graphical representation of these possibilities is shown in Fig. 1.4.

1.3 Mean-field reduction

Recent advances in dynamical systems theory have allowed us to better understand the effects of synchronization in large-scale oscillatory networks. A major breakthrough in these studies was achieved by Ott and Antonsen [84], who showed that the microscopic model equations of globally coupled heterogeneous phase oscillators (Kuramoto model) can be reduced to a low-dimensional system

of ordinary differential equations that accurately describe the macroscopic evolution of the system in the infinite-size (thermodynamic) limit. Later this approach was extended to a particular class of heterogeneous neural networks composed of all-to-all pulse-coupled quadratic integrate-and-fire (QIF) neurons [85], which are the normal form of class I neurons [73]. In the thermodynamic limit, a low-dimensional system of mean-field equations was derived for biophysically relevant macroscopic quantities: the firing rate and the mean membrane potential. The approach has been further developed in recent publications to analyze the occurrence of synchronized macroscopic oscillations in networks of QIF neurons with a realistic synaptic coupling [86], in the presence of a delay in couplings [87–89], in the presence of noise [90], in the presence of electrical coupling [91] and in the case of two interacting populations [92, 93].

In this section we will describe the derivation of firing-rate equations for networks of heterogeneous, all-to-all networks of QIF neurons, originally presented in [85].

The QIF neuron model describes the dynamics of the membrane potentials V_j, $(j = 1, \ldots, N)$:

$$\dot{V}_j = V_j^2 + \eta_j + Js(t) + I_j, \quad \text{if } V_j \geq V_p, \quad \text{then } V_j \leftarrow V_r, \tag{1.24}$$

where the last three terms define the input currents: η_j is the heterogeneous parameter of excitability, $s(t)$ is the synaptic activation function with weight J, and $I(t)$ is a common time-varying component. For simplicity, the membrane time for all neurons is assumed to be unity. The isolated neurons ($J = 0$, $I_j = 0$) with the negative value of the parameter $\eta_j < 0$ are at rest, while the neurons with the positive value of the parameter $\eta_j > 0$ generate instantaneous spikes. Each time a potential V_j reaches the threshold value V_p, it is reset to the value V_r, and the neuron emits an instantaneous spike which contributes to the network mean firing rate

$$s(t) = \frac{1}{N} \sum_{j=1}^{N} \sum_{k \setminus t_j^k < t} \delta(t - t_j^k), \tag{1.25}$$

where t_j^k is the moment of the k-th spike of the j-th neuron and $\delta(t)$ is the Dirac delta function. Because of the quadratic nonlinearity, V_j reaches infinity in a finite time, and this allows us to choose the threshold parameters as $V_p = -V_r = \infty$. With this choice, the QIF neuron can be transformed into a theta neuron. This choice is also crucial for the derivation of the reduced mean-field equations in an infinite size limit [85].

We take the limit as $N \to \infty$ and define the conditional voltage density function $\rho(V|\eta, t)\,\mathrm{d}V$ which gives the fraction of neurons with voltages between V and $V + \mathrm{d}V$. In the limit the excitability parameter η is a continuous random variable with some distribution function $g(\eta)$. Because the number of neurons is conserved, we arrive at the continuity equation

$$\frac{\partial \rho}{\partial t} + \frac{\partial [\rho(V^2 + \eta + Js + I)]}{\partial V} = 0. \tag{1.26}$$

The main idea of [85], designated the Lorentzian ansatz, is that the solutions to (1.26) converge to a Lorentzian function with half-width $x(\eta, t)$ and center $y(\eta, t)$:

$$\rho(V|\eta, t) = \frac{1}{\pi} \frac{x(\eta, t)}{(V - y(\eta, n))^2 + x^2(\eta, t)}. \tag{1.27}$$

From the QIF model definition and the two previous equations it is possible to obtain the expressions for the macroscopic observable variables, the firing rate $r(t)$ and mean membrane potential $v(t)$, in terms of $x(\eta, t)$ and $y(\eta, t)$. The firing rate for each η can be calculated by taking the limit of the probability flux $\rho\dot{V}$ as $V \to \infty$ to directly obtain $r(\eta, t) = x(\eta, t)/\pi$. The total firing rate can then be expressed as

$$r(t) = \int_{-\infty}^{\infty} x(\eta, t) g(\eta)\,\mathrm{d}\eta\,, \tag{1.28}$$

where $g(\eta)$ once again is the probability distribution function of η.

Similarly, because the Lorentz distribution is symmetric, the location parameter $y(\eta, t)$ is the mean membrane potential for every η:

$$y(\eta, t) = \text{p.v.} \int_{-\infty}^{\infty} \rho(V|\eta, t) V\,\mathrm{d}V\,, \tag{1.29}$$

where p.v. denotes the Cauchy principal value. The mean membrane potential is then expressed as

$$v(t) = \int_{-\infty}^{\infty} y(\eta, t) g(\eta)\, \mathrm{d}\eta\,. \tag{1.30}$$

The Lorentzian ansatz holds and Eqs. (1.28) and (1.30) are valid for arbitrary distributions $g(\eta)$, but it is particularly convenient to invoke the Lorentz distribution again (which is unrelated to the previous assumption on the distribution of membrane potentials V). If the excitability parameter is assumed to be distributed according to the Lorenz distribution centered at $\bar{\eta}$ with half-width Δ

$$g(\eta) = \frac{1}{\pi} \frac{\Delta}{(\eta - \bar{\eta})^2 + \Delta^2}, \tag{1.31}$$

the integrals (1.28) and (1.30) can be evaluated using contour integration and the Cauchy residue theorem to obtain a system of firing rate equations in two dimensions [85]:

$$\dot{r} = \Delta/\pi + 2rv, \tag{1.32a}$$

$$\dot{v} = v^2 + \bar{\eta} + Jr + I(t) - \pi^2 r^2. \tag{1.32b}$$

Other distributions $g(\eta)$ yield qualitatively similar network dynamics, but the dimension reduction is greatest with the Lorentzian function. If $g(\eta)$ has $2n$ poles off the real axis, it is possible to derive an n-dimensional system of complex firing-rate equations. Furthermore, the Lorentzian ansatz is also valid for distributions that do not satisfy this condition, e.g. the normal and the uniform distributions.

If we combine the mean firing rate and mean membrane potential into one complex firing-rate quantity $W = \pi r + \mathrm{i}v$, for a Lorentzian distribution $g(\eta)$, W relates in a natural way to the Kuramoto order parameter (1.23):

$$Z = \frac{1 - W^*}{1 + W^*} \quad \longleftrightarrow \quad W = \frac{1 - Z^*}{1 + Z^*}, \tag{1.33}$$

where the superscript asterisk denotes the complex conjugate.

Eqs. (1.32) will serve as an example for the minimum-charge entrainment algorithm (Section 3.3.3). We will also analyze the effect of high-frequency

stimulation to a generalization of this model for two interacting populations of excitatory and inhibitory populations of QIF neurons (Chapter 4).

1.4 Pontryagin's maximum principle

Let us consider a dynamical system of the form

$$\dot{\mathbf{x}} = \mathbf{f}(\mathbf{x}, \mathbf{u}, t), \quad \mathbf{x}(t_0) = \mathbf{x_0}. \tag{1.34}$$

Here $\mathbf{x} \in \mathbb{R}^n$ is the system state, $t \in \mathbb{R}$ is the time, t_0 is the initial time and $\mathbf{x}_0$ is the initial state. We assume that the dynamics of the system can be influenced by a *control* $\mathbf{u} \in \mathcal{U} \subseteq \mathbb{R}^m$. The set of *admissible controls* $\mathcal{U}$ is the set of all bounded piecewise continuous functions, everywhere equal to either their right- or left-sided limits. Let $\mathcal{L}(\mathbf{x}, \mathbf{u}, t)$ be a real-valued *running cost* function, also called the *Lagrangian*. We assume that the components of $\mathbf{f}(\mathbf{x}, \mathbf{u}, t)$ and the Lagrangian are continuous in x and u and continuously differentiable with respect to $x^1, \ldots, x^n$ and t. Depending on the problem, the final state $\mathbf{x}_1$ and time t_1 can be fixed, free, or restricted to some set. Let us introduce the *target set* $S = S_1 \times [t_0, \infty)$ to account for all the above possibilities; here $S_1 \subseteq \mathbb{R}^n$.

Fundamental problem of optimal control. *Among all admissible controls* $\mathbf{u} \in \mathcal{U}$*, which transfer the state of the system* (1.34) *from the initial point* $\mathbf{x}_0$ *at time* t_0 *to the target set S, find the control* $\mathbf{u}^*$ *for which the* objective functional

$$J = \int_{t_0}^{t_1} \mathcal{L}(\mathbf{x}(t), \mathbf{u}(t), t)\, \mathrm{d}t \tag{1.35}$$

takes on the least possible value.

We will state the necessary conditions for optimality for the autonomous free-time variable-endpoint control problem. The case of time-dependent system state and Lagrangian can be reduced to the autonomous case by a change of variables.

Pontryagin's maximum principle. *Let* $\mathbf{u}^*(t)$ *be the optimal control and let* $\mathbf{x}^*(t)$ *be the corresponding optimal trajectory. Then there exists a function* $\boldsymbol{\psi}^*(t)$ *called the* adjoint *or* costate *satisfying the following conditions:*

1. $\mathbf{x}^*$ *and* $\boldsymbol{\psi}^*$ *satisfy the canonical equations*

$$\dot{\mathbf{x}}^*(t) = \frac{\partial \mathcal{H}}{\partial \boldsymbol{\psi}} \left[\mathbf{x}^*(t), \mathbf{u}^*(t), \boldsymbol{\psi}^*(t)\right], \tag{1.36}$$

$$\dot{\boldsymbol{\psi}}^*(t) = -\frac{\partial \mathcal{H}}{\partial \mathbf{x}} \left[\mathbf{x}^*(t), \mathbf{u}^*(t), \boldsymbol{\psi}^*(t)\right], \tag{1.37}$$

   with boundary conditions $\mathbf{x}^*(t_0) = \mathbf{x}_0$ *and* $\mathbf{x}^*(t_1) \in S$*, where* $\mathcal{H}$ *is the* Hamiltonian function *defined as*

$$\mathcal{H}(\boldsymbol{\psi}, \mathbf{x}, \mathbf{u}) = \boldsymbol{\psi} \cdot \mathbf{f}(\mathbf{x}, \mathbf{u}) - \mathcal{L}(\mathbf{x}, \mathbf{u}). \tag{1.38}$$

2. *The Hamiltonian has a global maximum at* $\mathbf{u} = \mathbf{u}^*(t)$ *for all* $t \in [t_0, t_1]$*:*

$$\mathcal{H}(\mathbf{x}^*(t), \mathbf{u}^*(t), \boldsymbol{\psi}^*(t)) = \max_{\mathbf{u} \in \mathcal{U}} \mathcal{H}(\mathbf{x}^*(t), \mathbf{u}, \boldsymbol{\psi}^*(t)). \tag{1.39}$$

3. *If the final time* t_1 *is free, the Hamiltonian vanishes for all* $t \in [t_0, t_1]$*:*

$$\mathcal{H}(\mathbf{x}^*(t), \mathbf{u}^*(t), \boldsymbol{\psi}^*(t)) \equiv 0. \tag{1.40}$$

   If t_1 *is fixed,* $\mathcal{H}(\mathbf{x}^*(t), \mathbf{u}^*(t), \boldsymbol{\psi}^*(t)) = const.$

4. $\boldsymbol{\psi}^*(t_1)$ *is orthogonal to the tangent space* $T_{\mathbf{x}^*(t_1)}$ *of* S_1 *at* $\mathbf{x}^*(t_1)$*:*

$$\boldsymbol{\psi}^*(t_1) \cdot \mathbf{v} = 0, \quad \textit{for all} \quad \mathbf{v} \in T_{\mathbf{x}^*(t_1)}. \tag{1.41}$$

The final condition is called the transversality condition. If the endpoint is not restricted to a subset of the state space (i.e. $S_1 = \mathbb{R}^n$), the transversality condition reduces to $\boldsymbol{\psi}^*(t_1) = \mathbf{0}$. If the endpoint $\mathbf{x}_0$ is fixed, the tangent space is 0 and no conditions are placed on $\boldsymbol{\psi}^*(t_1)$.

For the proof of the Maximum principle, refer to the original publication [94].

Chapter 2

Optimal waveform for entrainment of a spiking neuron with minimum stimulating charge

In this chapter, we consider an optimal control problem for a single neuron. We set out to find an optimal waveform of a periodic stimulus that ensures an entrainment of a neuron to the stimulation frequency with the minimum mean absolute value of the applied current or, equivalently, with the minimum integral charge transferred to the model neuron in both directions during the stimulation period. For brevity, we refer to this problem as a *minimum-charge* control. We assume that the stimulating current satisfies the charge-balance requirement and is bounded from above and below. We also suppose that the stimulating current is sufficiently weak, so that the phase reduction theory [73, 81, 95] can be applied to the model neuron. To determine an optimal waveform we apply Pontryagin's maximum principle [94, 96].

Note, a similar performance measure, proportional to a mean absolute value of a control variable, is used in an optimal space navigation problem when seeking to transfer a spacecraft from an initial state to a desired target with the minimum expenditure of fuel [96]. Such a *minimum-fuel* transfer problem leads to a *bang-off-bang* waveform of the control variable. We will see that our minimum-charge entrainment problem also results in a bang-off-bang waveform, which consists of two repetitive time-separated positive and negative

rectangular pulses, generally of different widths and amplitudes. We also refer to relevant publications [97–99], where the authors introduce a general form of a functional and consider the problem of maximizing the width of the entrainable frequency detuning of a spiking neuron for the fixed value of the functional. The relation and the difference between that and our problem will be discussed in Sec. 2.5.1.

The chapter is organized as follows. In Sec. 2.1 we formulate the optimization problem and in Sec. 2.2 present its solution. An algorithm of constructing the minimum-charge waveform is demonstrated analytically and graphically for a simple example of a Stuart-Landau oscillator in Sec. 2.3. The performance of the minimum-charge waveform is compared with that of other different waveforms including a minimum-power waveform. In Sec. 2.4 we consider the simplified version of the optimization theory when the frequency mismatch between the neuron and external current is small. This theory is then demonstrated for an oscillator defined by a randomly generated phase response curve [97] as well as the classical Hodgkin-Huxley [74] neuron model in Sec. 2.5. We finish the chapter with a discussion of possible clinical applications and conclusions presented in Sec. 2.6.

2.1 Problem formulation

We consider a general Hodgkin-Huxley-type neuron model under periodic stimulation

$$C_m \dot{v} = F(v, \mathbf{w}) + I(\omega t), \tag{2.1a}$$

$$\dot{\mathbf{w}} = \mathbf{G}(v, \mathbf{w}). \tag{2.1b}$$

Here C_m is the membrane capacitance and v is the membrane potential. The function $F(v, \mathbf{w})$ describes the sum of currents flowing through the ion channels. $I(\omega t)$ is a periodic stimulating current that satisfies $I(\omega t + 2\pi) = I(\omega t)$, where ω is the stimulation frequency and $T = 2\pi/\omega$ is the period of stimulation. Equation (2.1b) describes the dynamics of a recovery variable $\mathbf{w}$ that generally is a vector variable, $\mathbf{w} = (w_1, \ldots, w_n)$. The function $\mathbf{G}(v, \mathbf{w})$ represents the

ionic channel dynamics. The dimension n of the vector variable $\mathbf{w}$ as well as the functions F and $\mathbf{G}$ are defined by the specific neuron model.

We assume that without stimulation [$I(\omega t) = 0$] the neuron generates periodic spikes with a period T_0. Then for sufficiently small stimulating current $I(\omega t)$ we can apply the phase reduction method [73, 81, 95] and reduce Eqs. (2.1) to a single scalar phase equation

$$\dot{\vartheta} = \omega_0 + z(\vartheta) I(\omega t), \tag{2.2}$$

where ϑ is the phase, $\omega_0 = 2\pi/T_0$ is the spiking frequency of a free neuron and $z(\vartheta)$ is the 2π-periodic phase response curve (PRC). The PRC is derived from a free neuron model; it contains all necessary information about the neuron's response to any weak external forcing.

The main purpose of this chapter is to derive the optimal waveform of the stimulating current $I(\omega t)$ that ensures an entrainment of a given isolated neuron (i.e., not coupled to other neurons) to the frequency of stimulation with the minimum mean absolute value of the current injected into the neuron. Specifically, we are going to minimize the following functional:

$$\mathcal{J}[I] = \frac{1}{T} \int_0^T |I(\omega t)| \, \mathrm{d}t \, . \tag{2.3}$$

We require that the stimulating current never exceeds some predefined minimal $I_- < 0$ and maximal $I_+ > 0$ values, i.e.,

$$I_- \le I(\omega t) \le I_+ \tag{2.4}$$

for any time. In addition, we introduce a clinically mandatory charge-balance condition $\int_0^T I(\omega t) \, \mathrm{d}t = 0$. The charge q satisfies the differential equation

$$\dot{q} = I(\omega t) \tag{2.5}$$

and thus the charge-balance condition can be alternatively written as

$$q(0) = 0, \quad q(T) = 0. \tag{2.6}$$

The entrainment takes place if the system (2.2) admits a solution with the boundary conditions

$$\vartheta(0) = 0, \quad \vartheta(T) = 2\pi. \tag{2.7}$$

To summarize, in order to find the optimal waveform of the stimulating current we need to minimize the functional (2.3) with the variables ϑ and q satisfying differential Eqs. (2.2) and (2.5) with the boundary conditions (2.6) and (2.7). We also have to take into account the limitation of the amplitude (2.4) of the stimulating current.

2.2 Solving the optimization problem

To solve the above formulated optimization problem, we make use of the Pontryagin maximum principle [94, 96] similarly as it has been done in Refs. [34, 40, 41] for finding the minimum-power waveform of the stimulating current. Here we minimize the mean absolute value of the stimulating current defined by the functional (2.3). To this end, we introduce the Lagrangian as $\mathcal{L}(I) = |I|$ and define the Hamiltonian of the system as $\mathcal{H}(q, \vartheta, I, p, \mu) = p(t)\dot{\vartheta} + \mu(t)\dot{q} - \mathcal{L}$ or

$$\mathcal{H}(\vartheta, I, p, \mu) = [\omega_0 + z(\vartheta)I]p + \mu I - |I| \tag{2.8}$$

Here we have omitted the variable q from the list of arguments of the Hamiltonian function, since it does not depend explicitly on this variable. Within this formalism, the Euler equations that define the minimum of the functional (2.3) coincide with the Hamiltonian equations:

$$\dot{\vartheta} = \frac{\partial \mathcal{H}}{\partial p}, \quad \dot{q} = \frac{\partial \mathcal{H}}{\partial \mu}, \quad \dot{p} = -\frac{\partial \mathcal{H}}{\partial \vartheta}, \quad \dot{\mu} = -\frac{\partial \mathcal{H}}{\partial q}. \tag{2.9}$$

In a mechanical interpretation, $p(t)$ and $\mu(t)$ define the components of the momentum while in the Eulerian formalism they are the Lagrange multipliers. The first two Hamiltonian equations are equivalent respectively to Eqs. (2.2) and (2.5), the third equation defines the dynamics of the Lagrange multiplier $p(t)$: $\dot{p}(t) = -z'(\vartheta)I(\omega t)p(t)$, and the last equation gives $\dot{\mu} = 0$, since the Hamiltonian function does not depend on q. Thus, the Lagrange multiplier μ is

independent of time and the Hamiltonian function can be presented in the form

$$\mathcal{H}(\vartheta, I, p, \mu) = \begin{cases} \omega_0 p + [z(\vartheta)p + \mu - 1]I, & \text{if} \quad I \geq 0, \\ \omega_0 p + [z(\vartheta)p + \mu + 1]I, & \text{if} \quad I \leq 0, \end{cases} \tag{2.10}$$

with a constant parameter $\mu = const$ and a time-dependent Lagrange multiplier $p(t)$.

The Pontryagin maximum principle provides a necessary condition for the optimal control. For our problem, it states that the Hamiltonian function (2.10) on the optimal trajectory is maximal and time-independent. We introduce a switching function

$$\psi(t) = z(\vartheta(t))p(t) + \mu \tag{2.11}$$

and rewrite Eq. (2.10) as

$$\mathcal{H}(\vartheta, I, p, \mu) = \begin{cases} \omega_0 p(t) + [\psi(t) - 1]I, & \text{if} \quad I \geq 0, \\ \omega_0 p(t) + [\psi(t) + 1]I, & \text{if} \quad I \leq 0. \end{cases} \tag{2.12}$$

Applying Pontryagin's maximum principle to this equation, we can derive an expression for the optimal current $I^* = I^*(\vartheta(t))$, which we denote by an asterisk and express its dependence on time through the phase variable ϑ. The Hamiltonian (2.12) reaches its maximum, when the current I is maximally positive for $\psi(t) > 1$, maximally negative for $\psi(t) < -1$ and equal to zero for $-1 < \psi(t) < 1$:

$$I^*(\vartheta(t)) = \begin{cases} I_+ & \text{for} \quad \psi(t) > 1, \\ I_- & \text{for} \quad \psi(t) < -1, \\ 0 & \text{for} \quad -1 < \psi(t) < 1. \end{cases} \tag{2.13}$$

Now we use the requirement that the Hamiltonian is time independent on the optimal trajectory. We denote the maximum constant value of the Hamiltonian on the optimal trajectory as ω_0/z_0, i.e.,

$$\mathcal{H}(\vartheta(t), I^*(\vartheta(t)), p(t), \mu) = \frac{\omega_0}{z_0} = \text{ const.} \tag{2.14}$$

Here z_0 is a yet unknown constant. In time intervals where $I^*(\vartheta(t))$ is zero, from Eq. (2.12) we have $\mathcal{H}(\vartheta, I^*, p, \mu) = \omega_0 p(t)$. Substituting this into Eq. (2.14), we obtain $p(t) = 1/z_0$ and from Eq. (2.11) we get $\psi(t) = z(\vartheta(t))/z_0 + \mu$. Thus, the third condition $-1 < \psi(t) < 1$ in Eq. (2.13) can be rewritten as $-1 - \mu < z(\vartheta(t))/z_0 < 1 - \mu$. The first and the second conditions can be rewritten in a similar way and then the expression for the optimal current becomes:

$$I^*(\vartheta) = \begin{cases} I_+ & \text{for} \quad \frac{z(\vartheta)}{z_0} > 1 - \mu, \\ I_- & \text{for} \quad \frac{z(\vartheta)}{z_0} < -1 - \mu, \\ 0 & \text{for} \quad -1 - \mu < \frac{z(\vartheta)}{z_0} < 1 - \mu. \end{cases} \tag{2.15}$$

This expression contains two so far unknown parameters z_0 and μ. It is convenient to replace these two parameters (z_0, μ) with another pair of parameters (z_1, z_2) using the following transformation:

$$z_1 = -z_0(\mu + 1), \tag{2.16a}$$

$$z_2 = \ z_0(1 - \mu). \tag{2.16b}$$

For any given values of the new parameters $z_1 \neq z_2$, the initial parameters can be rebuilt from the unambiguous backward transformation $z_0 = (z_2 - z_1)/2$, $\mu = (z_1 + z_2)/(z_1 - z_2)$. With the new parameters, the expression for the optimal current can be written as

$$I^*(\vartheta) = \begin{cases} I_+ & \text{for} \quad \operatorname{sgn}(z_2 - z_1) z(\vartheta) > z_2, \\ I_- & \text{for} \quad \operatorname{sgn}(z_2 - z_1) z(\vartheta) < z_1, \\ 0 & \text{for} \quad z_1 < \operatorname{sgn}(z_2 - z_1) z(\vartheta) < z_2, \end{cases}$$

or equivalently

$$I^*(\vartheta) = I_+ H[z(\vartheta) - z_2] + I_- H[z_1 - z(\vartheta)], \quad \text{if} \quad z_2 > z_1,$$
$$I^*(\vartheta) = I_- H[z(\vartheta) - z_1] + I_+ H[z_2 - z(\vartheta)], \quad \text{if} \quad z_2 < z_1,$$

where $H(\cdot)$ is the Heaviside step function. Since z_1 and z_2 are so far arbitrary parameters, we can exchange $z_1 \rightleftarrows z_2$ in the second equation and combine

these two equations into one final equation for the optimal current

$$I^*(\vartheta) = I_{\pm} H[z(\vartheta) - z_2] + I_{\mp} H[z_1 - z(\vartheta)]. \tag{2.17}$$

Here the upper and lower subscripts correspond to two different possible expressions for the optimal current. In both these expressions the parameters z_1 and z_2 satisfy the inequality $z_2 > z_1$.

Now our aim is to write down the equations for the unknown parameters z_1 and z_2. These equations are derived from the boundary conditions (2.6) and (2.7). We start from the entrainment conditions (2.7). Substituting $I(\omega t) = I^*(\vartheta(t))$ into Eq. (2.2) and using boundary conditions (2.7), we get

$$\int_0^{2\pi} \frac{\mathrm{d}\vartheta}{\omega_0 + z(\vartheta) I^*(\vartheta)} = \int_0^T \mathrm{d}t = T. \tag{2.18}$$

In order to further simplify the analysis, we assume that the boundaries I_+ and $|I_-|$ of the stimulating current are sufficiently small so that the inequalities

$$|z(\vartheta)| I_+ \ll \omega_0 \quad \text{and} \quad |z(\vartheta)||I_-| \ll \omega_0 \tag{2.19}$$

hold for all $\vartheta \in [0, 2\pi]$. Using binomial approximation, the denominator in Eq. (2.18) can then be rewritten as $[\omega_0 + z(\vartheta) I^*(\vartheta)]^{-1} \approx [1 - z(\vartheta) I^*(\vartheta)/\omega_0]/\omega_0$, and we get

$$\frac{1}{2\pi} \int_0^{2\pi} z(\vartheta) I^*(\vartheta)\, \mathrm{d}\vartheta = \omega_0^2 \left(\frac{1}{\omega_0} - \frac{T}{2\pi} \right). \tag{2.20}$$

The right-hand side of this equation is approximately equal to the frequency mismatch $\Delta\omega = \omega - \omega_0$ provided that $|\Delta\omega| \ll \omega_0$. Thus, Eq. (2.20) can be presented in the form

$$\langle z(\vartheta) I^*(\vartheta) \rangle_\vartheta = \Delta\omega, \tag{2.21}$$

where the angle brackets marked by the subscript ϑ denote the averaging of a function over the variable ϑ:

$$\langle f(\vartheta) \rangle_\vartheta \equiv \frac{1}{2\pi} \int_0^{2\pi} f(\vartheta)\, \mathrm{d}\vartheta\,. \tag{2.22}$$

Inserting Eq. (2.17) into Eq. (2.21) and using the definitions (2.30a) and (2.30b) for the auxiliary functions $M_+(\xi)$ and $M_-(\xi)$, we obtain the first equation for the parameters z_1 and z_2:

$$I_\pm M_+(z_2) + I_\mp M_-(z_1) = \Delta\omega. \tag{2.23}$$

The second equation for these parameters is obtained from the charge-balance condition:

$$\int_0^T I^*(\vartheta(t))\,\mathrm{d}t = \int_0^{2\pi} \frac{I^*(\vartheta)\,\mathrm{d}\vartheta}{\omega_0 + z(\vartheta)I^*(\vartheta)} = 0. \tag{2.24}$$

Taking into account the inequalities (2.19), this equation can be simplified to

$$\langle I(\vartheta)\rangle_\vartheta = 0. \tag{2.25}$$

Inserting Eq. (2.17) into Eq. (2.25) and using the definitions (2.30c) and (2.30d) for the auxiliary functions $N_+(\xi)$ and $N_-(\xi)$, we obtain the second equation for the parameters z_1 and z_2:

$$I_\pm N_+(z_2) + I_\mp N_-(z_1) = 0. \tag{2.26}$$

By solving the system of Eqs. (2.23) and (2.26) one can obtain the unknown parameters z_1 and z_2 and find an explicit expression for the optimal current (2.17). The analysis of these equations for specific models shows that for $\Delta\omega > 0$ the solution exists only with the upper subscript and for $\Delta\omega < 0$ only with the lower subscript.

Finally, we can compute the mean absolute value of the stimulating current on the optimal trajectory:

$$\mathcal{J}[I^*] = \frac{1}{T}\int_0^T |I^*(\vartheta(t))|\,\mathrm{d}t = \int_0^{2\pi} \frac{|I^*(\vartheta)|\,\mathrm{d}\vartheta}{\omega_0 + z(\vartheta)I^*(\vartheta)}.$$

Taking into account the inequalities (2.19), we can approximate this value as $\mathcal{J}[I^*] = \langle |I^*(\vartheta)|\rangle_\vartheta$. Then inserting $I^*(\vartheta)$ from Eq. (2.17), we obtain:

$$\mathcal{J}^* \equiv \mathcal{J}[I^*] = |I_\pm| N_+(z_2) + |I_\mp| N_-(z_1). \tag{2.27}$$

Note that we constructed the optimal waveform (2.13) without considering the possibility of a singular control [96]. The singular control implies the existence of finite time intervals (singular intervals) in which the switching function $\psi(t) \equiv 1$ or $\psi(t) \equiv -1$. For such singular intervals to exist, it is necessary that all time derivatives of the switching function in the given intervals be equal to zero: $\dot{\psi}(t) = 0$, $\ddot{\psi}(t) = 0$, ... Similarly as in Ref. [40], one can show that this requirement leads to the equality $\omega_0 + z(\vartheta)I^*(\vartheta) = 0$. In our case, this equality cannot be satisfied due to the assumption (2.19), and thus the singular control is not possible.

We can now summarize the main results. Generally, the algorithm requires the knowledge of the PRC $z(\vartheta)$ of the given neuron and the permissible limits I_- and I_+ of the stimulating current. The optimal waveform (denoted by an asterisk) is of a bang-off-bang type:

$$I^*(\vartheta) = I_\pm H[z(\vartheta) - z_2] + I_\mp H[z_1 - z(\vartheta)]. \tag{2.28}$$

where $H(\cdot)$ is the Heaviside step function. The optimal current depends on the sign of the frequency mismatch $\Delta\omega = \omega - \omega_0$. Here and below the upper and the lower subscripts correspond, respectively, to $\Delta\omega > 0$ and $\Delta\omega < 0$. The parameters z_1 and z_2 satisfy $z_1 < z_2$. They are determined from the equations

$$I_\pm M_+(z_2) + I_\mp M_-(z_1) = \Delta\omega, \tag{2.29a}$$

$$I_\pm N_+(z_2) + I_\mp N_-(z_1) = 0, \tag{2.29b}$$

which are generally different for $\Delta\omega > 0$ and $\Delta\omega < 0$. These equations contain four auxiliary functions

$$M_+(\xi) = \langle z(\vartheta)H[z(\vartheta) - \xi]\rangle_\vartheta, \tag{2.30a}$$

$$M_-(\xi) = \langle z(\vartheta)H[\xi - z(\vartheta)]\rangle_\vartheta, \tag{2.30b}$$

$$N_+(\xi) = \langle H[z(\vartheta) - \xi]\rangle_\vartheta, \tag{2.30c}$$

$$N_-(\xi) = \langle H[\xi - z(\vartheta)]\rangle_\vartheta, \tag{2.30d}$$

where the angle brackets marked by the subscript ϑ denotes the averaging of a function over the variable ϑ as defined by Eq. (2.22). The value of the functional (2.3) computed on the optimal trajectory (2.28) is given by Eq. (2.27).

To specify some general properties of the above auxiliary functions (2.30), we define the minimal and the maximal values of the PRC as z_{min} and z_{max}, respectively. Then for $\xi \leq z_{min}$, the functions (2.30b) and (2.30d) are equal to zero, $M_-(\xi) = 0$ and $N_-(\xi) = 0$, while the functions (2.30a) and (2.30c) are equal to constants, $M_+(\xi) = \langle z(\vartheta)\rangle_\vartheta$ and $N_+(\xi) = 1$. Similarly, for $\xi \geq z_{max}$, the functions (2.30a) and (2.30c) are zeros, $M_+(\xi) = 0$ and $N_+(\xi) = 0$, while the functions (2.30b) and (2.30d) are constants, $M_-(\xi) = \langle z(\vartheta)\rangle_\vartheta$ and $N_-(\xi) = 1$. In the interval $z_{min} < \xi < z_{max}$, the function $N_-(\xi)$ monotonically increases and the function $N_+(\xi)$ monotonically decreases. For the specific model, these functions will be presented analytically and graphically in the next section. The solution of Eqs. (2.29) and the construction of the optimal current (2.28) will be demonstrated analytically and graphically as well.

2.3 Analytical example: A Stuart-Landau oscillator

To get more insight into the algorithm of constructing the optimal waveform of the stimulating current, we first consider an analytically solvable example of a Stuart-Landau oscillator. This system represents a canonical model of limit cycle oscillations. In the presence of the stimulating current the model reads:

$$\dot{x} = -y + x\Big(1 - x^2 - y^2\Big) + I(\omega t), \tag{2.31a}$$

$$\dot{y} = \quad x + y\Big(1 - x^2 - y^2\Big). \tag{2.31b}$$

In the context of the neural model (2.1), we interpret the variable x as a voltage and the variable y as a recovery variable. Without stimulation, the system has the limit cycle solution $x_c = \cos(t), \quad y_c = \sin(t)$ with the frequency $\omega_0 = 1$.

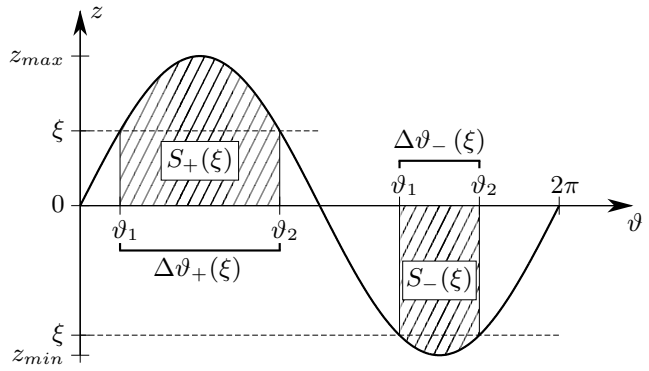

Figure 2.1 The geometrical meaning of the auxiliary functions (2.30). The solid curve represents the PRC. The shaded areas marked by $S_+(\xi)$ and $S_-(\xi)$ define the values of the functions $M_+(\xi) = S_+(\xi)/2\pi$ and $M_-(\xi) = S_-(\xi)/2\pi$. The functions $N_+(\xi) = \Delta\vartheta_+/2\pi$ and $N_-(\xi) = \Delta\vartheta_-/2\pi$ define the relative intervals of the phase variable ϑ where the PRC is above and below of the horizontal line $z = \xi$, respectively.

The analytically obtained PRC of this system is

$$z(\vartheta) = \sin(\vartheta) \tag{2.32}$$

and for weak stimulation the system (2.31) can be reduced to the following phase equation:

$$\dot{\vartheta} = 1 + \sin(\vartheta) I(\omega t). \tag{2.33}$$

The advantage of this model is that it admits a complete analytical solution of the above optimization problem. For the given PRC, the geometrical meaning of the auxiliary functions (2.30) is shown in Fig. 2.1. The functions $M_+(\xi)$ and $M_-(\xi)$ define certain areas under the PRC when intersecting it with the horizontal line $z = \xi$. The function $N_+(\xi)$ $[N_-(\xi)]$ shows the relative interval of the phase variable ϑ where the PRC is above [below] of the line $z = \xi$. Substituting Eq. (2.32) into Eqs. (2.30) and solving the corresponding integrals, we obtain the following analytical expressions for the auxiliary functions (2.30)

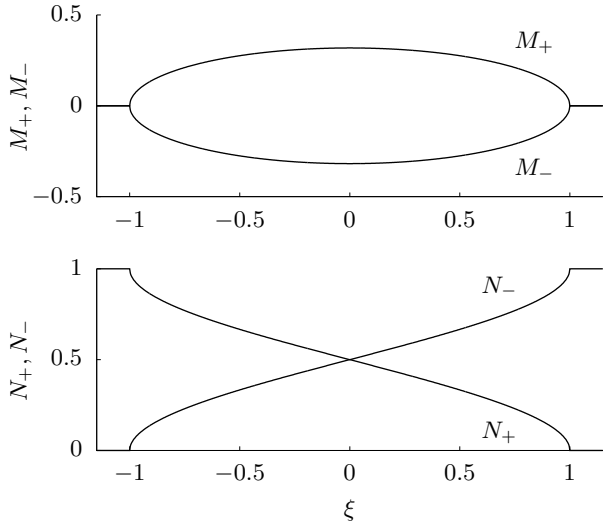

Figure 2.2 Auxiliary functions (top) $M_+(\xi)$ and $M_-(\xi)$ as well as (bottom) $N_+(\xi)$ and $N_-(\xi)$ for the Stuart-Landau oscillator.

$$M_{+,-}(\xi) = \pm\sqrt{1-\xi^2}/\pi, \tag{2.34a}$$

$$N_{+,-}(\xi) = 1/2 \mp \arcsin(\xi)/\pi, \tag{2.34b}$$

which are valid in the interval $z_{min} < \xi < z_{max}$ with $z_{min} = -1$ and $z_{max} = 1$. Outside this interval, the values of the functions are: $M_{+,-}(\xi) = 0$, $N_-(\xi) = 0$, $N_+(\xi) = 1$ for $\xi \leq -1$ and $M_{+,-}(\xi) = 0$, $N_-(\xi) = 1$, $N_+(\xi) = 0$ for $\xi \geq 1$. The functions are graphically presented in Fig. 2.2.

Since the PRC (2.32) of the Stuart-Landau oscillator is an odd function $z(-\vartheta) = -z(\vartheta)$, it is natural to choose the symmetric restriction of the stimulating current, $I_+ = -I_- \equiv I_0$. In this case, Eqs. (2.29) that define the values of the parameters z_1 and z_2 become equivalent for both positive and negative frequency mismatch $\Delta\omega$,

$$M_+(z_2) - M_-(z_1) = |\Delta\omega|/I_0, \tag{2.35a}$$

$$N_+(z_2) - N_-(z_1) = 0, \tag{2.35b}$$

and the optimal current (2.28) changes the sign when the sign of $\Delta\omega$ is changed:

$$I^*(\vartheta) = I_0\{H[z(\vartheta) - z_2] - H[z_1 - z(\vartheta)]\}\,\mathrm{sgn}(\Delta\omega). \tag{2.36}$$

Here $\mathrm{sgn}(\cdot)$ is the sign function. Finally, Eq. (2.27) can be simplified to:

$$\mathcal{J}^* = I_0[N_+(z_2) + N_-(z_1)]. \tag{2.37}$$

According to Eq. (2.34b), the functions $N_{+,-}(\xi)$ have the following symmetric relation $N_+(\xi) = N_-(-\xi)$. Thus, Eq. (2.35b), which expresses the charge-balance condition, will be automatically satisfied if we take $z_1 = -z_2$. Then the value of the parameter z_2 can be found from Eq. (2.35a), that after taking into account the symmetric relation of the functions $M_-(-\xi) = -M_+(\xi)$, transforms to

$$M_+(z_2) = |\Delta\omega|/2I_0. \tag{2.38}$$

In Fig. 2.3, we use this equation in order to demonstrate graphically the algorithm of constructing the optimal waveform of the stimulating current. For the given $\Delta\omega$ and I_0, the horizontal line $z = z_2$ has to be chosen in such a way that the shaded area satisfies $S_+(z_2) \equiv 2\pi M_+(z_2) = \pi|\Delta\omega|/I_0$. Then, by projecting the intersection points of the lines $z = z_2$ and $z = z_1 = -z_2$ with the PRC onto the ϑ axis, the bang-off-bang optimal waveform (2.36) is simply constructed as shown in the figure. The construction is demonstrated for $\Delta\omega > 0$. For $\Delta\omega < 0$, the sign of the waveform should be inverted.

Equation (2.38) with the function (2.34a) $M_+(\xi) = \sqrt{1-\xi^2}/\pi$ can be solved analytically. As a result, we obtain the following expression for the parameters $z_{1,2}$:

$$z_{1,2} = \mp\sqrt{1 - (\pi\Delta\omega/2I_0)^2}. \tag{2.39}$$

Thus Eq. (2.36) together with the Eqs. (2.32) and (2.39) provides an explicit analytical expression for the optimal stimulating current. By using Eqs. (2.34b) and (2.39), we also derive an analytical expression for the optimal value of the functional (2.37):

$$\mathcal{J}^* = \frac{2I_0}{\pi}\arcsin\left(\frac{\pi|\Delta\omega|}{2I_0}\right). \tag{2.40}$$

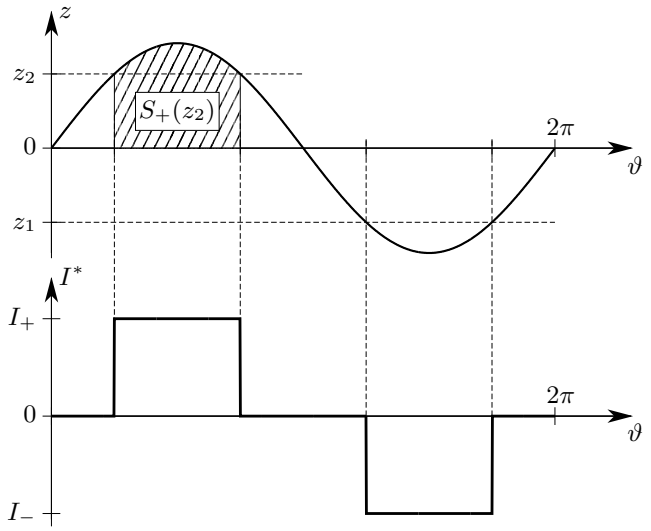

Figure 2.3 Geometrical construction of the optimal waveform of the stimulating current for the Stuart-Landau oscillator. The line $z = z_2$ is chosen such that the shaded area satisfies Eq. (2.38): $S_+(z_2) = \pi|\Delta\omega|/I_0$. The bang-off-bang optimal waveform (2.36) is constructed by projecting the intersection points of the lines $z = z_2$ and $z = z_1 = -z_2$ with the PRC onto the ϑ axis. The optimal waveform is shown for $\Delta\omega > 0$. For $\Delta\omega < 0$, its sign should be inverted.

Note, the entrainment with the waveform (2.36) is possible only in the finite frequency interval, referred to as entrainment interval:

$$|\Delta\omega| \leq 2I_0/\pi. \tag{2.41}$$

Outside this interval, the entrainment is impossible due to the requirement for restriction of the amplitude of the stimulating current.

In Fig. 2.4 the dependence of $\mathcal{J}^*$ on the frequency mismatch $\Delta\omega$ (the Arnold tongue) for $I_0 = 0.1$ is shown by a solid curve. The dots represent the Arnold tongue obtained numerically from the original system (2.31). To this end we used the following algorithm. For a given $\Delta\omega$, Eqs. (2.31) were simulated using the optimal waveform (2.36) with a greater amplitude than the given restriction, $I_0 > 0.1$, to provide an entrainment of the oscillator to the stimulating current. Then the amplitude was gradually decreased until the threshold value, when the synchronization disappeared. The value of the functional $\mathcal{J}$ [Eq. (2.3)] at the threshold amplitude gives the numerical estimate of the Arnold tongue. We see an excellent agreement of the numerical results with the theoretical curve (2.40).

2.3.1 Comparing results for different waveforms

In order to verify whether the derived waveform (2.36) is really optimal, we computed the Arnold tongues for two more waveform examples: a symmetric bang-bang waveform and a minimum-power waveform.

Symmetric bang-bang waveform

We constructed a symmetric bang-bang waveform from the optimal bang-off-bang waveform (2.36) by setting $z_2 = z_1 = 0$ and assuming that the amplitude I_0 is arbitrary:

$$I_{sb}(\vartheta) = I_0\{H[\sin(\vartheta)] - H[-\sin(\vartheta)]\}. \tag{2.42}$$

The entrainment condition for the given waveform can easily be derived from the phase Eq. (2.33). Substituting $I(\omega t) = I_{sb}(\omega t)$ into this equation and changing

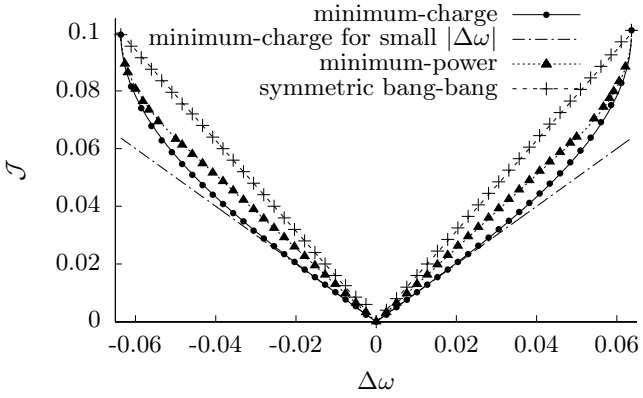

Figure 2.4 Arnold tongues for the Stuart-Landau oscillator. The mean absolute values of the stimulating current $\mathcal{J}$ [Eq. (2.3)] as functions of the frequency mismatch $\Delta\omega$ are shown for three different waveforms. The solid curve and dots correspond to the minimum-charge waveform (2.36). The dash-dot lines show the approximation (2.49). The dotted curve and triangle symbols represent the minimum-power waveform (2.46). The dashed lines and "+" symbols correspond to the symmetric bang-bang waveform (2.42).

the variable $\vartheta = \omega t + \varphi$, we get an equation $\dot{\varphi} = -\Delta\omega + \sin(\omega t + \varphi) I_{sb}(\omega t)$ for the new variable φ. Assuming that $\Delta\omega$ and I_0 are small parameters and averaging this equation over the period $T = 2\pi/\omega$ of fast oscillations, we obtain:

$$\dot{\varphi} = -\Delta\omega + \langle \sin(\vartheta + \varphi) I_{sb}(\vartheta) \rangle_\vartheta . \tag{2.43}$$

The integral in this equation can be easily solved, $\langle \sin(\vartheta + \varphi) I_{sb}(\vartheta) \rangle_\vartheta = (2I_0/\pi)\cos(\varphi)\,\mathrm{sgn}(\Delta\omega)$. It follows that the entrainment appears when the amplitude I_0 exceeds the threshold value $I_{th} = \pi|\Delta\omega|/2$. The waveform (2.42) with the threshold amplitude $I_0 = I_{th}$ is graphically presented in Fig. 2.5. Substituting Eq. (2.42) into Eq. (2.3) and taking $I_0 = I_{th}$, we get an expression for the Arnold tongue

$$\mathcal{J} = \frac{\pi}{2}|\Delta\omega| \tag{2.44}$$

of the waveform (2.42). In Fig 2.4 this result is presented by dashed lines. The symbols "+" show the same result obtained by direct numerical simulation of the original system (2.31). We see that the entrainment with the waveform

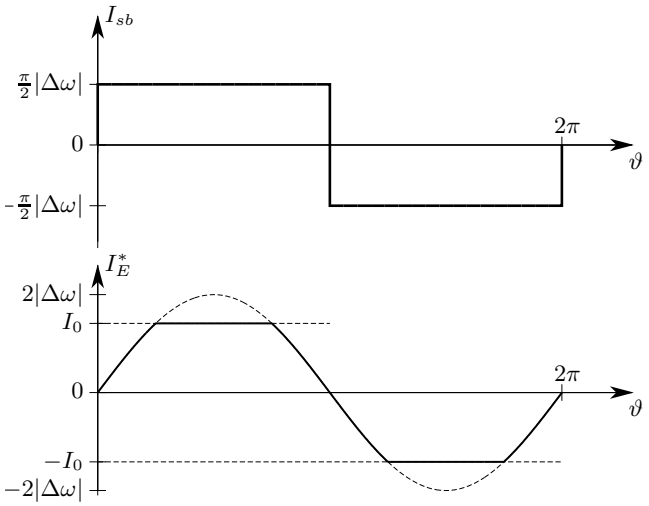

Figure 2.5 (top) Symmetric bang-bang and (bottom) minimum-power waveforms of the stimulating current applied to the Stuart-Landau oscillator. The Arnold tongues obtained with these waveforms are presented in Fig 2.4.

(2.42) appears at larger values of the functional (2.3) than that with the optimal waveform (2.36).

Minimum-power waveform

As a second example, we consider the waveform that ensures an entrainment of the oscillator with the minimum applied power. The theory of charge-balanced minimum-power control with constrained amplitude for an arbitrary PRC is presented in Ref. [41]. Here we apply this theory to obtain the minimum-power waveform for the Stuart-Landau oscillator. The minimum-power waveform is derived by the minimization of the mean energy functional $E[I] = (1/T)\int_0^T [I(\omega t)]^2\,\mathrm{d}t$ rather than the functional (2.3). If there were no amplitude restriction, the minimum-power waveform would be proportional to the PRC:

$$\tilde{I}_E(\vartheta) = 2|\Delta\omega|\sin(\vartheta). \tag{2.45}$$

In the presence of the symmetric restriction $-I_0 \le I(\omega t) \le I_0$ of the stimulating current, the minimum-power waveform $I_E^*(\vartheta)$ is the same as in Eq. (2.45) [$I_E^*(\vartheta) = \tilde{I}_E(\vartheta)$] when $2|\Delta\omega| \le I_0$, but its amplitude is truncated when

$2|\Delta\omega| \leq I_0$:

$$I_E^*(\vartheta) = \begin{cases} -I_0, & \text{if } \tilde{I}_E(\vartheta) \leq -I_0, \\ \tilde{I}_E(\vartheta), & \text{if } \left|\tilde{I}_E(\vartheta)\right| < I_0, \\ I_0, & \text{if } \tilde{I}_E(\vartheta) \geq I_0. \end{cases} \tag{2.46}$$

This waveform is graphically presented in Fig. 2.5. Substituting Eq. (2.46) into Eq. (2.3) and solving the corresponding integrals, we obtain the Arnold tongue for this waveform. For $|\Delta\omega| \leq I_0/2$, the dependence $\mathcal{J}$ vs $\Delta\omega$ is linear,

$$\mathcal{J} = \frac{4}{\pi}|\Delta\omega|, \tag{2.47}$$

while for $|\Delta\omega| > I_0/2$ it is nonlinear and determined by the following parametric equations

$$|\Delta\omega(p)| = \frac{I_0}{\pi}\left[\frac{1}{p}\arcsin(p) + \sqrt{1-p^2}\right], \tag{2.48a}$$

$$\mathcal{J}(p) = \frac{2I_0}{\pi}\left[\frac{1-\sqrt{1-p^2}}{p} + \frac{\pi}{2} - \arcsin(p)\right], \tag{2.48b}$$

where p is a parameter that varies in the interval $(0, 1)$. Due to the amplitude restriction of the waveform (2.46), the entrainment of the oscillator is possible only in the finite frequency interval $|\Delta\omega| \leq 2I_0/\pi$, which coincides with the entrainment interval (2.41) of the minimum-charge waveform (2.36).

In Fig. 2.4 the dotted curve shows the Arnold tongue plotted from Eqs. (2.47) and (2.48). The triangle symbols show the same result obtained by direct simulation of Eqs. (2.31) with the stimulating current (2.46). While the values of $\mathcal{J}$ for the minimum-power waveform (2.46) are smaller than those for the bang-bang waveform (2.42), they are greater than the values of $\mathcal{J}$ obtained with the minimum-charge waveform (2.36). These results confirm the validity of the optimization theory presented above.

2.3.2 Small frequency mismatch

As mentioned above, an entrainment of the oscillator with the minimum-charge waveform (2.36) is possible only in the finite frequency interval (entrain-

ment interval): $|\Delta\omega| \le 2I_0/\pi$. The border of the interval $2I_0/\pi$ is proportional to the permissible limit I_0 of the stimulating current. The larger the limiting amplitude I_0, the wider is the entrainment interval.

Let us consider the case of a small frequency mismatch $|\Delta\omega| \ll 2I_0/\pi$, when the amplitude restriction of the stimulating current is inconsiderable. In this case Eq. (2.40) transforms to

$$\mathcal{J}^* \approx |\Delta\omega|, \tag{2.49}$$

i.e, the Arnold tongue is defined by straight lines (see dash-dot lines in Fig. 2.4). For small $|\Delta\omega|$, these lines coincide with the curve (2.40).

It is interesting to reconsider the whole algorithm of constructing the optimal waveform for small $|\Delta\omega|$. From Eq. (2.40) we get $z_{1,2} \approx \mp[1 - (\pi\Delta\omega/2I_0)^2/2]$. Thus, for $|\Delta\omega| \to 0$, the value of the parameter z_2 tends to the maximum of the PRC, $z_2 \to \max[z(\vartheta)] = 1$, and the value of the parameter z_1 tends to the minimum of the PRC, $z_1 \to \min[z(\vartheta)] = -1$. It follows that the optimal waveform consists of two narrow rectangular pulses of height I_0, one positive and the other negative, located at the maximum and the minimum of the PRC. The width of the pulses tends to zero when $|\Delta\omega| \to 0$. Thus, the optimal waveform depends only on the shape of the PRC close to its maximum and minimum and does not depend on other details of the PRC. We exploit this finding in the next section in order to derive an algorithm for constructing the optimal waveform for arbitrary PRCs.

2.4 Optimal waveform for a small $|\Delta\omega|$ in the general case

Now we consider the optimization problem for small $|\Delta\omega|$ in a general case. We will deal with an arbitrary PRC $z(\vartheta)$ and a general nonsymmetric amplitude restriction $I_- \le I(\omega t) \le I_+$ of the stimulating current. By small $|\Delta\omega|$ we mean its smallness with respect to the entrainment interval, which is proportional to the given amplitude restrictions I_- and I_+. As mentioned above, the construction of the optimal waveform at small $|\Delta\omega|$ does not require any

detailed information on the PRC except the properties close to its maximum and minimum. The main idea of our approach is to approximate the PRC close to the extrema by parabolas and analytically solve the Eqs. (2.29).

We assume that the PRC $z(\vartheta)$ is a smooth 2π periodic function that has an absolute maximum $z_{max} > 0$ at $\vartheta = \vartheta_{max}$ and an absolute minimum $z_{min} < 0$ at $\vartheta = \vartheta_{min}$. We expect that for $|\Delta\omega| \to 0$ the solution of Eqs. (2.29) satisfies $z_1 \to z_{min}$ and $z_2 \to z_{max}$. To then solve the Eqs. (2.29) for small finite $|\Delta\omega|$ we will need information on the PRC only in the vicinity of its extrema. The PRC close to the extrema can be approximated by parabolas. Specifically, for ϑ close to ϑ_{max} we write

$$z(\vartheta) \approx z_{max} - \frac{|z''(\vartheta_{max})|}{2}(\vartheta - \vartheta_{max})^2 \tag{2.50}$$

and for ϑ close to ϑ_{min} we have

$$z(\vartheta) \approx z_{min} + \frac{z''(\vartheta_{min})}{2}(\vartheta - \vartheta_{min})^2. \tag{2.51}$$

Using these approximations, we can estimate the auxiliary functions (2.30). We need the values of functions $M_+(\xi)$ and $N_+(\xi)$ for ξ close to z_{max}. Thus, substituting Eq. (2.50) into Eqs. (2.30a) and (2.30c) and solving the corresponding integrals, we obtain:

$$M_+(\xi) \approx \frac{z_{max}}{\pi}\sqrt{\frac{2(z_{max} - \xi)}{|z''(\vartheta_{max})|}}, \tag{2.52a}$$

$$N_+(\xi) \approx \frac{1}{\pi}\sqrt{\frac{2(z_{max} - \xi)}{|z''(\vartheta_{max})|}}. \tag{2.52b}$$

We also need the values of functions $M_-(\xi)$ and $N_-(\xi)$ for ξ close to z_{min}. They are obtained in a similar way by substituting Eq. (2.51) into Eqs. (2.30b)

and (2.30d):

$$M_-(\xi) \approx \frac{z_{min}}{\pi}\sqrt{\frac{2(\xi - z_{min})}{z''(\vartheta_{min})}}, \tag{2.53a}$$

$$N_-(\xi) \approx \frac{1}{\pi}\sqrt{\frac{2(\xi - z_{min})}{z''(\vartheta_{min})}}. \tag{2.53b}$$

Now we are ready to solve Eqs. (2.29). We demonstrate this solution only for $\Delta\omega > 0$ while for $\Delta\omega < 0$ simply write out the result. Taking into account Eqs. (2.52) and (2.53), the system (2.29) for $\Delta\omega > 0$ can be written as

$$I_+\frac{z_{max}}{\pi}\sqrt{\frac{2\delta z_2}{|z''(\vartheta_{max}|}} + I_-\frac{z_{min}}{\pi}\sqrt{\frac{2\delta z_1}{z''(\vartheta_{min})}} = \Delta\omega,$$
$$I_+\frac{1}{\pi}\sqrt{\frac{2\delta z_2}{|z''(\vartheta_{max})|}} + I_-\frac{1}{\pi}\sqrt{\frac{2\delta z_1}{z''(\vartheta_{min})}} = 0.$$

where $\delta z_1 = z_1 - z_{min} > 0$ and $\delta z_2 = z_{max} - z_2 > 0$. The solution of these equations with respect to the parameters δz_1 and δz_2 gives the following relations:

$$\frac{I_+}{\pi}\sqrt{\frac{2\delta z_2}{|z''(\vartheta_{max})|}} = -\frac{I_-}{\pi}\sqrt{\frac{2\delta z_1}{z''(\vartheta_{min})}} = \frac{\Delta\omega}{z_{max} - z_{min}}. \tag{2.54}$$

Substituting Eq. (2.50) into Eq. (2.28) and using the above relations, we can write the optimal current for $\Delta\omega > 0$ as

$$I^*(\vartheta) = I_+\Pi\left(\frac{\vartheta - \vartheta_{max}}{\Delta\vartheta_+}\right) + I_-\Pi\left(\frac{\vartheta - \vartheta_{min}}{\Delta\vartheta_-}\right), \tag{2.55}$$

where $\Pi(x)$ is the rectangular function that satisfies $\Pi(x) = 1$ for $|x| < 1/2$ and $\Pi(x) = 0$ for $|x| > 1/2$. Thus, the waveform defined by Eq. (2.55) consists of two rectangular pulses, one positive located at ϑ_{max} and the other negative located at ϑ_{min}. The height of the positive (negative) pulse is I_+ (I_-) and its

width is $\Delta\vartheta_+$ ($\Delta\vartheta_-$). The widths $\Delta\vartheta_{+,-}$ are defined as

$$\Delta\vartheta_{+,-} = \frac{2\pi\Delta\omega}{I_{+,-}(z_{max} - z_{min})}. \tag{2.56}$$

Similarly, one can show that the optimal current for $\Delta\omega < 0$ is

$$I^*(\vartheta) = I_-\Pi\left(\frac{\vartheta - \vartheta_{max}}{\Delta\vartheta_-}\right) + I_+\Pi\left(\frac{\vartheta - \vartheta_{min}}{\Delta\vartheta_+}\right). \tag{2.57}$$

Substituting Eqs. (2.52b) and (2.53b) into Eq. (2.27) and using the relations (2.54), we can determine the optimal value of the functional $\mathcal{J}^*$. Here we present the result in the form valid for both the positive and negative $\Delta\omega$:

$$\mathcal{J}^* = \frac{2|\Delta\omega|}{z_{max} - z_{min}}. \tag{2.58}$$

From Eqs. (2.55), (2.56), and (2.57) we see that the construction of the optimal waveform requires the knowledge of only two parameters of the PRC, namely, the distance $\vartheta_{max} - \vartheta_{min}$ between its extrema and the amplitude of the PRC $z_{max} - z_{min}$. Though the parameters ϑ_{max} and ϑ_{min} come separately in Eqs. (2.55) and (2.57), we need to know only the difference $\Delta\vartheta_z = \vartheta_{max} - \vartheta_{min}$, because the effect of entrainment does not depend on the initial phase of the stimulating current. By shifting the initial phases in Eqs. (2.55) and (2.57) in such a way as to locate the positive pulse in both of them at $\vartheta = 0$, we can rewrite these equations in the form

$$I^*(\vartheta) = I_+\Pi\left(\frac{\vartheta}{\Delta\vartheta_+}\right) + I_-\Pi\left(\frac{\vartheta \pm \Delta\vartheta_z}{\Delta\vartheta_-}\right), \tag{2.59}$$

where the upper and lower sign in the argument of the second function correspond, respectively, to $\Delta\omega > 0$ and $\Delta\omega < 0$.

In the following, we numerically verify the theoretical results presented in this section. First, we make sure that the theory works for the Stuart-Landau oscillator considered in the previous section. For this oscillator, the PRC is defined by Eq. (2.32) and its amplitude is $z_{max} - z_{min} = 2$. From Eq. (2.58) it follows that the Arnold tongue of the system is $\mathcal{J}^* = |\Delta\omega|$. This coincides with

Eq. (2.49) derived from the general expression (2.40) in the limit $|\Delta\omega| \to 0$. In the next section, we apply this theory for more sophisticated models, namely a randomly generated phase response curve introduced in Ref. [97] and the Hodgkin-Huxley neuron model.

2.5 Numerical examples

2.5.1 A randomly generated phase response curve

First, we verify the above theory for a randomly generated PRC

$$\begin{aligned} z(\vartheta) = {} & 0.745705\cos(\vartheta) - 0.666276\sin(\vartheta) \\ & - 0.134064\cos(2\vartheta) - 0.940493\sin(2\vartheta) \\ & - 0.222622\cos(3\vartheta) + 0.768401\sin(3\vartheta) \end{aligned} \tag{2.60}$$

introduced in Ref. [97]. The PRC contains higher harmonics as usually observed in real-world models. The values of the parameters that define the optimal waveform (2.59) for this PRC are $\Delta\vartheta_z = \vartheta_{max} - \vartheta_{min} \approx 1.3660$ and $z_{max} - z_{min} \approx 4.1367$.

Based on the optimal waveform (2.59), we construct a trial stimulating current function consisting of two rectangular positive and negative pulses

$$I(\vartheta) = a\left[\Pi\left(\frac{s\vartheta}{l}\right) - \frac{1}{s}\Pi\left(\frac{\vartheta + d}{l}\right)\right] \tag{2.61}$$

separated by a distance d. Here the parameter s defines the asymmetry of the pulses, so the positive pulse of the width l/s and the amplitude a is located at $\vartheta = 0$, while the negative pulse of the width l and the amplitude a/s is located at $\vartheta = -d$. The trial function (2.61) coincides with the optimal waveform (2.59), $I(\vartheta) = I^*(\vartheta)$, provided that its parameters accord with the optimal values defined by Eqs. (2.56) and (2.59), i.e., $l = \Delta\vartheta_- = 2\pi|\Delta\omega|/sI_+(z_{max} - z_{min})$, $a = I_+$ and $d = \Delta\vartheta_z = \vartheta_{max} - \vartheta_{min}$ for $\Delta\omega > 0$ and $d = -\Delta\vartheta_z$ for $\Delta\omega < 0$. In the following we vary the parameters l and d of the trial function and compute the threshold value of the amplitude $a = a_{th}$ at which the entrainment of

the oscillations occurs. The value of the functional (2.3) at the entrainment condition is:

$$\mathcal{J}_{th} = a_{th} l/s\pi. \tag{2.62}$$

Our aim is to verify whether the value of J_{th} is minimal when the parameters l and d of the trial function coincide with the optimal values $l = \Delta_-$ and $d = \pm\Delta\vartheta_z$ as well as whether the minimum of $\mathcal{J}_{th}$ coincides with the theoretical optimal value $\mathcal{J}^*$ defined by Eq. (2.58).

In order to obtain the threshold amplitude a_{th}, we proceed similarly as in Sec. 2.3.1. We introduce the phase difference $\varphi = \vartheta - \omega t$ and, using Eq. (2.2), derive for this variable the averaged equation

$$\dot{\varphi} = -\Delta\omega + \langle z(\vartheta + \varphi) I(\vartheta)\rangle_\vartheta. \tag{2.63}$$

Then we define an auxiliary function

$$\begin{aligned}\Phi(\varphi|s,l,d) &= \frac{1}{a}\langle z(\vartheta+\varphi)I(\vartheta)\rangle_\vartheta \\ &= \frac{1}{2\pi}\int_{\varphi-l/2s}^{\varphi+l/2s} z(\vartheta)\,\mathrm{d}\theta - \frac{1}{2\pi s}\int_{\varphi+d-l/2}^{\varphi+d+l/2} z(\vartheta)\,\mathrm{d}\theta\,,\end{aligned} \tag{2.64}$$

which allows us to estimate the threshold amplitude as

$$a_{th} = \Delta\omega \begin{cases} 1/\max\limits_{\varphi}[\Phi(\varphi|s,l,d)] & \text{for} \quad \Delta\omega > 0, \\ 1/\min\limits_{\varphi}[\Phi(\varphi|s,l,d)] & \text{for} \quad \Delta\omega < 0. \end{cases} \tag{2.65}$$

Now, using Eqs. (2.60), (2.62), (2.64) and (2.65), we can study the dependence of the functional (2.62) on the parameters l, d, and $\Delta\omega$. First, we assume that the width of the negative pulse is optimal $l = \Delta\vartheta_- = 2\pi|\Delta\omega|/sI_+(z_{max} - z_{min})$ and analyze the dependence of $\mathcal{J}_{th}$ on $\Delta\omega$ (the Arnold tongues). We note that the optimal width $\Delta\vartheta_-$ is proportional to $|\Delta\omega|$. To completely specify the dependence $\Delta\vartheta_-$ on $|\Delta\omega|$, we take $I_+ = 1$ and $s = 2$. The value of the latter parameter means that the positive pulse is two times higher and two times narrower than the negative pulse. Several examples of the Arnold tongues, corresponding to the different distances

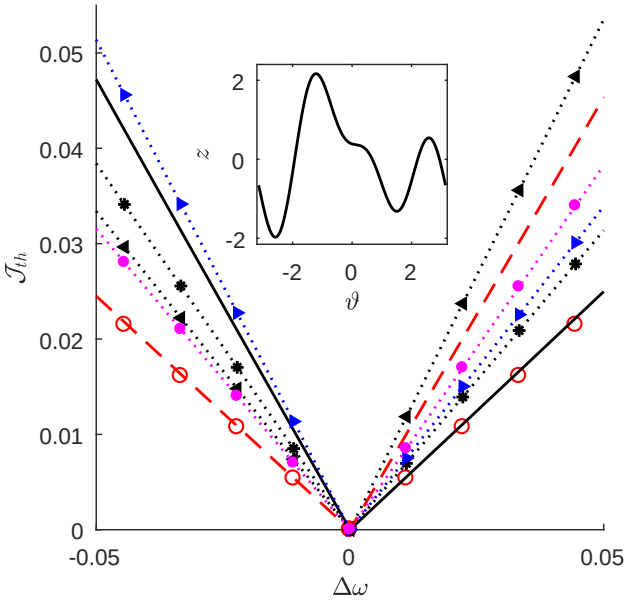

Figure 2.6 Arnold tongues for the oscillator defined by the PRC (2.60). The mean absolute values of the stimulating current $\mathcal{J}_{th}$ [Eq. (2.62)] as functions of the frequency detuning $\Delta\omega$ are shown for the trial waveform (2.64) with the fixed parameters $s = 2$ and $I_+ = 1$ and different values of parameter d that defines the distance between the negative and positive pulses: $d = -2$ (black dotted lines marked by asterisks), $d = -\Delta\vartheta_z \approx -1.3660$ (black solid lines), $d = -0.7$ (blue dotted lines marked by right-pointing triangles), d=0.7 (black dotted lines marked by left-pointing triangles), $d = \Delta\vartheta_z$ (red dashed lines) and $d = 2$ (magenta dotted lines marked by filled circles). Empty red circles show theoretical optimal values of the functional $\mathcal{J}^*$ defined by Eq. (2.58). The inset shows the graphic of the PRC (2.60).

$d = (-2, -\Delta\vartheta_z, -0, 7, 0.7, \Delta\vartheta_z, 2)$ between the negative and positive pulses, are presented in Fig. 2.6. Here the values $d = -\Delta\vartheta_z$ and $d = \Delta\vartheta_z$ define the theoretical optimal distances for $\Delta\omega > 0$ and $\Delta\omega < 0$, respectively. As is seen from the figure, they represent the lowest Arnold tongues (the black solid line for $\Delta\omega > 0$ and the dashed red line for $\Delta\omega < 0$). In addition, we see that the lowest Arnold tongues agree well with the theoretical optimal values of the functional $\mathcal{J}^*$ defined by Eq. (2.58), which are depicted by the red circles.

In the second numerical experiment, we fix the width l of the negative pulse and compute the values of the functional $\mathcal{J}_{th}$ under continuous variation of the

distance d between the pulses in the whole admissible interval $d \in [-\pi, \pi]$ (we exclude from this interval the distances that lead to the overlap of the pulses). From Eq. (2.64), we see that for a fixed l the auxiliary function $\Phi(\varphi|s, l, d)$ is independent of $\Delta\omega$. Then from Eqs. (2.65) and (2.62), it follows that a_{th} and $\mathcal{J}_{th}$ are proportional to $\Delta\omega$. Thus, it is convenient to consider the dependence $\mathcal{J}_{th}/|\Delta\omega|$ vs d. In Fig. 2.7, we plot such a dependence for different fixed widths $l = (0.1, 0.2, 0.4, 0.8)$ of the negative pulse. The value of the parameter that defines the asymmetry between the pulses is taken the same as in the previous example, $s = 2$. We see that all curves $\mathcal{J}_{th}/|\Delta\omega|$ vs d, corresponding to different values of l, reach the *absolute minimum* at the theoretical optimal distance, i.e., at $d = -\Delta\vartheta_z \approx -1.3660$ for $\Delta\omega > 0$ and at $d = \Delta\vartheta_z$ for $\Delta\omega < 0$. The optimal distances $\pm\Delta\vartheta_z$ are shown in the figure by the dashed vertical lines. Note that the maximal width $l = 0.8$ of the negative pulse considered here is comparable with the optimal distance $\Delta\vartheta_z$ between the pulses. Furthermore, the value of the functional $\mathcal{J}_{th}$ at the absolute minimum is close to the theoretical optimal value $\mathcal{J}^*$ (the red circle), defined by Eq. (2.58) if the width of the negative pulse is not too large. Numerical experiments with different values of the parameter s that defines the asymmetry of the pulses lead to a similar outcome (not shown here).

Thus, this example confirms the general theoretical result that the distance between the pulses in the optimal waveform is equal to the distance between the maximum and the minimum of the PRC and is independent of the pulses' widths and their asymmetry. The sequence of the positive and negative pulses, however, depends on the sign of the frequency detuning $\Delta\omega$ between the oscillator and the forcing. For $\Delta\omega > 0$, this sequence should be such that the positive pulse hits the oscillator at the timing of the maximum of PRC while the negative pulse hits the oscillator at the timing of the minimum of PRC. This results in the maximal phase advance in the oscillator during the one period of the forcing. For $\Delta\omega < 0$, the most effective is the inverse sequence of the pulses, i.e., the positive pulse should hit the oscillator at the minimum of the PRC while the negative pulse should hit the oscillator at the maximum of the PRC in order to provide the maximum phase delay of the oscillator.

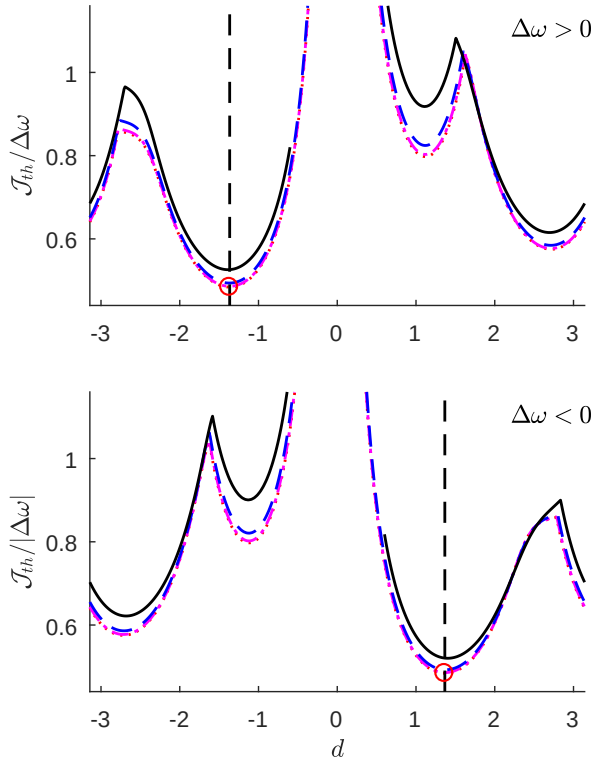

Figure 2.7 Dependence of $\mathcal{J}_{th}/|\Delta\omega|$ vs d for the oscillator defined by the PRC (2.60). Here d is the distance between the negative and positive pulses in the trial waveform (2.64). The top and the bottom graphs correspond to $\Delta\omega > 0$ and $\Delta\omega < 0$, respectively. The pulses' asymmetry parameter is fixed at $s = 2$. Different curves correspond to different fixed values of the width l of the negative pulse: $l = 0.1$ (red dotted curves), $l = 0.2$ (magenta dash-dotted curves), $l = 0.4$ (blue dashed curves) and $l = 0.8$ (black solid curves) The dashed vertical lines show the theoretical optimal distances between the pulses: $d = -\Delta\vartheta_z \approx -1.3660$ for $\Delta\omega > 0$ and at $d = \Delta\vartheta_z$ for $\Delta\omega < 0$. The red circles mark the theoretical optimal values $\mathcal{J}^*$, defined by Eq. (2.58).

As indicated in the Introduction, we now discuss the optimization problem considered in Refs [97–99]. Here we mainly refer to Tanaka's paper [97], where he first formulated the problem. Tanaka introduced a general form of the functional $M[I] = \langle |I(\vartheta)|^p \rangle_\vartheta^{1/p}$ with an arbitrary parameter $p \geq 1$. For $p = 1$, this functional coincides with our functional $J[I]$ defined in Eq. (2.3). However, the mathematical formulation of the optimization problem as well as the derived optimal waveforms differ from ours. The main difference in the problem formulation is that, Tanaka maximizes the width of the Arnold tongue (the frequency-locking range) for a fixed $M[I]$, while we minimize $J[I]$ for a fixed frequency detuning $\Delta\omega$. Tanaka's formulation produces an optimal waveform that does not depend on $\Delta\omega$ in the whole frequency-locking range, including both $\Delta\omega < 0$ and $\Delta\omega > 0$, while our optimal waveform does depend on $\Delta\omega$, especially on the sign of $\Delta\omega$. In our optimal waveform, the sequence of the positive and negative pulses is inverted with the inversion of the sign of $\Delta\omega$. For the oscillator defined by the PRC (2.60), Tanaka has derived an optimal solution in the form of two narrow symmetric rectangular pulses, the one positive and the other negative. Formally this solution is similar to our optimal waveform in the case of symmetric amplitude restriction, $I_- = -I_+$. However, the distance between the pulses in Tanaka's waveform differs from the distance between the maximum and the minimum of the PRC. Such a disagreement between Tanaka's and our optimal waveforms is natural, because we solve different optimization problems.

2.5.2 A Hodgkin-Huxley neuron model

Now we verify our theory for the classical Hodgkin-Huxley neuron model [74]. For the model definition see page 2.

We apply a direct current $I_d = 20\ \mu\text{A/cm}^2$ in order to induce self-sustained periodic spiking of the neuron. The action potential in the absence of stimulation [$I(\omega t) = 0$] is shown in Fig. 2.8 (top). The neuron fires with the period $T_0 \approx 11.5654356$ ms or angular frequency $\omega_0 = 2\pi/T_0 \approx 0.5432727$ rad/ms. In the same figure (bottom), we show the PRC of the neuron and the optimal waveform (2.55) for $I_+ = -I_- = 1\ \mu\text{A/cm}^2$ and $\Delta\omega = 0.01$ rad/ms. The optimal waveform is constructed by using only two parameters of the PRC:

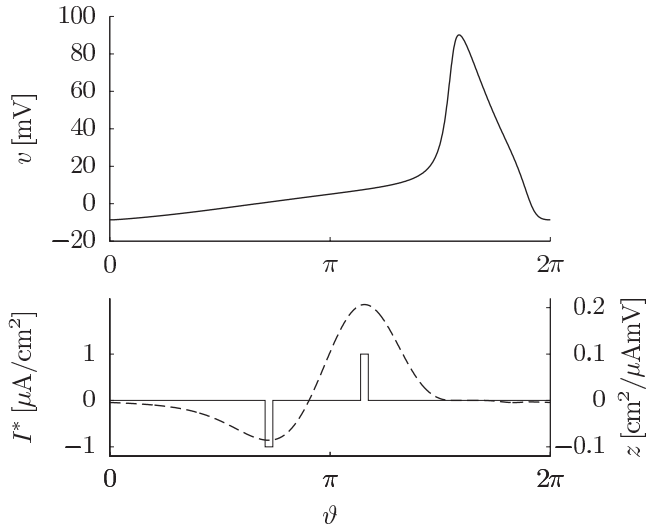

Figure 2.8 (Top) Membrane potential of the spiking Hodgkin-Huxley neuron for a direct current $I_d = 20$ μA/cm^2. (Bottom) The PRC (dashed) and the optimal waveform [Eq. (2.55)] (solid) for $I_+ = -I_- = 1$ μA/cm^2 and $\Delta\omega = 0.01$ rad/ms.

the distance between the extrema $\vartheta_{max} - \vartheta_{min} \approx 1.3667$ and the amplitude $z_{max} - z_{min} \approx 0.1591$ cm$^2/\mu$Ams.

Figure 2.9 shows the Arnold tongues for the Hodgkin-Huxley neuron obtained with different waveforms of the stimulating current. The solid lines represent the analytical expression (2.58). The dots show the Arnold tongue obtained by direct numerical simulation of the HH Eqs. (1.1) with the optimal current defined by Eqs. (2.55), (2.56) and (2.57). We see a good agreement between the theoretical and numerical results.

For comparison, in Fig. 2.9 we present the Arnold tongues for two more waveforms. One of them is the symmetric bang-bang waveform (2.42). The results for this waveform derived from the phase Eq. (2.2) are shown by dashed lines and those obtained by direct numerical simulation of the HH Eqs. (1.1) by "+" signs. Another waveform is constructed as an asymmetric charge-balanced bang-bang function

$$I_{ab}(\vartheta) = I_0 \begin{cases} 1, & \text{if} \quad 0 \le \vartheta \le \vartheta_0, \\ -\vartheta_0/(2\pi - \vartheta_0), & \text{if} \quad \vartheta_0 < \vartheta < 2\pi, \end{cases} \tag{2.66}$$

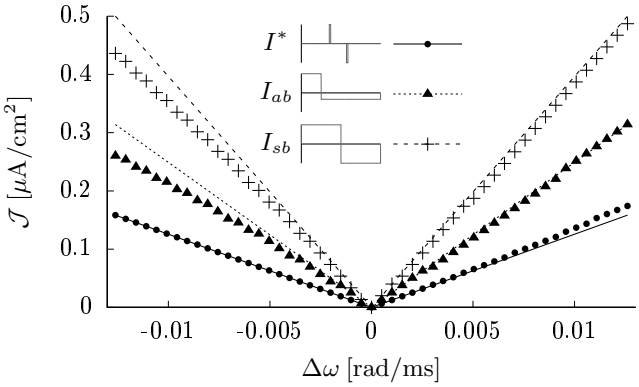

Figure 2.9 Arnold tongues for the Hodgkin-Huxley neuron model. The mean absolute values of the stimulating current $\mathcal{J}$ [Eq. (2.3)] as functions of the frequency mismatch $\Delta\omega$ are shown for three different waveforms. The solid lines and dots correspond to the optimal waveform defined by Eqs. (2.55), (2.56), and (2.57). The dotted lines and triangle symbols represent the asymmetric bang-bang waveform (2.66). The dashed lines and "+" symbols correspond to the symmetric bang-bang waveform (2.42).

with $\vartheta_0 = \pi/2$. The results for this waveform derived from the phase Eq. (2.2) are shown by dotted lines, and the results obtained by integration of the HH Eqs. (1.1) by triangle symbols. We see that the entrainment with both waveforms is attained at larger mean absolute values of the stimulating current than with the optimal waveform defined by Eqs. (2.55), (2.56) and (2.57). This confirms the validity of our general theory presented in the previous section.

2.6 Summary

We considered the problem of optimal entrainment of a spiking neuron to a periodic external stimulation using the mean absolute value of the stimulating current as a performance measure to be minimized. The choice of such a performance measure is motivated by the desire to minimize the damage to nervous tissue under stimulation. We refer to this problem as a minimum-charge control problem, since it provides the minimum integral charge transferred to the model neuron in both directions during the stimulation period. We took into account the clinically relevant charge-balance condition and the

amplitude limitation of the stimulating current. Using the phase reduction theory and Pontryagin's maximum principle, we derived an algorithm for constructing the optimal waveform that provides the entrainment of a spiking neuron to the stimulating current with the conditions mentioned above. The optimal waveform is of the bang-off-bang type: it consists of two rectangular pulses, one positive and the other negative, located at the extrema of the phase response curve of the neuron. The widths and the amplitudes of the pulses can be generally different, since our optimization problem takes into account an asymmetric amplitude restriction of the stimulating current. In previous theoretical considerations [40, 41, 97], only symmetric amplitude restriction was considered. Searching for asymmetric optimal waveforms is very important, since stimulation protocols in animal experiments and, especially, in clinical applications typically employ positive and negative pulses that are not symmetric [45, 100–102]. We confirmed the validity of our optimization theory by an analytically solvable Stuart-Landau oscillator, a randomly generated phase response curve and a classical Hodgkin-Huxley neuron model.

The minimum-charge control problem analyzed here differs from typical optimization problems considered before. Usually, the problem of optimal entrainment of a spiking neuron is considered as a minimum-power control problem and deals with the minimization of a mean energy functional [34–43]. The energy delivered to the neuron is proportional to the square of the stimulating current rather than to its absolute value. The minimum-charge waveform derived here by the minimization of the mean absolute value of the stimulating current differs significantly from the minimum-power waveform.

Along with the minimization of tissue damage, the minimum-charge control algorithm has another practical advantage over the minimum-power control approach. For a small frequency mismatch, the minimum-power waveform is proportional to the phase response curve of the neuron, and thus its construction requires the knowledge of the whole PRC. On the contrary, the minimum-charge waveform is of the bang-off-bang type and depends only on a few parameters. Theoretically, the values of these parameters are determined only by the distance between absolute extrema of the PRC and the PRC amplitude.

In a real experiment, the parameters of the optimal bang-off-bang waveform can hopefully be estimated empirically by trial and error, without recourse to the neuron model and the phase reduction theory.

To cause a phase reset of populations of oscillatory neurons, brief high-frequency pulse trains, i.e. trains of charge-balanced pulses with intraburst frequency greater than 100 Hz, were used [13, 100–103]. On the one hand, brief high-frequency pulse trains enable one to safely convey larger amounts of charge to brain tissue (see, e.g, Ref [103]). On the other hand, in animal experiments [104] as well as computational studies [13] it was shown that the brief high-frequency pulse train can reset the phase of neuronal populations.

Bang-off-bang waveforms for optimal entrainment might have several clinical applications. For instance, it was shown that brief high-frequency pulse trains delivered at low frequencies, may cause a tremor phase entrainment during DBS electrode implantation [103]. This technique might provide significant additional information to anatomical information, obtained with CT and/or MRI, and functional information, achieved by high-frequency test stimulation and recording methods, required for precise DBS electrode implantation [105–107].

For CR-DBS sequences of brief high-frequency pulse trains are delivered through N, say four, stimulation sites, equidistantly spaced within a stimulation period T_{stim} [13, 100–102]. So far, different variants of CR stimulation were tested. The sequence of stimulation contact activation can be fixed [108]. In this case, the stimulation basically aims at a phase entrainment of different neuronal subpopulations, with phase shifts between the different stimulation sites. In the case of CR stimulation with slowly varying sequences, the sequence is kept constant for a larger number of stimulation periods, e.g. 100, until the next sequence is randomly drawn [109]. In both cases, with constant and with slowly varying sequences, one might use an optimal bang-off-bang waveform instead of delivering brief high-frequency pulse trains at a low frequency. However, in most of the pre-clinical [100, 101] and clinical studies [102] performed to date, the sequence of stimulation sites activation was randomly varied from one cycle to the other. Obviously, in this case no phase-shifted entrainment of different subpopulations is induced. The mechanism of action

of standard high-frequency DBS is not yet sufficiently understood [9, 110–114]. However, optimized stimulus trains might possibly also help to establish DBS as treatment for medically refractory epilepsy [115], in particular, in the context of closed-loop stimulation approaches employing seizure prediction algorithms [116] or aiming at preventive effects [117].

Mechanisms and effects of standard high-frequency DBS might be diverse and not restricted to desynchronization [9, 110–114]. From a computational standpoint, there are different approaches to desynchronization, employing high-frequency DBS or short high-frequency pulse trains. For instance, permanent high-frequency stimulation may cause a desynchronization when delivered predominantly to excitatory structures [118]. High-frequency stimulation may cause desynchronizing effects when using optimal waveforms [119]. High-frequency DBS may have pronounced desynchronizing effects with amplitudes modulated by linear or nonlinear delayed feedback delivered through one [120, 121] or several [122] stimulation sites. Desynchronization by means of CR stimulation means to deliver brief high-frequency pulse trains at different sites at different times [13]. The aforementioned different approaches require different optimal waveforms. However, motivated by achieving CR-DBS-induced long-lasting desynchronization and therapeutic effects in Parkinsonian monkeys [100, 101] and PD patients [102], we are aiming at a spatially separate entrainment of different subpopulations, as required for CR stimulation during time epochs when the CR sequence is fixed [108] or slowly varying [109]; see above. As a first step toward this goal, we consider the optimal entrainment of a single (isolated) spiking neuron which generates periodic spikes in the absence of stimulation. In the next chapter we will consider the impact of optimal waveform stimuli on interacting model neurons. To this end, we will use a recently developed phase reduction theory for a network of coupled dynamical elements [82] as well as exact macroscopic equations derived in the thermodynamic limit for networks of spiking neurons [85, 86, 92]. Such models admit a description of the collective behavior of heterogeneous networks of coupled neurons in terms of a single phase equation. Although the optimal control theory is developed here for a single neuron, it can be directly applied to such complex systems.

Chapter 3

Entrainment of a network of interacting neurons with minimum stimulating charge

The synchronization of coupled dynamical elements is of great interest to the physical, chemical, and biological sciences [73, 83, 123, 124]. In the nervous system, synchronization processes play an important role, as they are responsible for information processing and motor control. However, pathological, excessive synchronization can severely impair brain function and is characteristic of several neurological disorders [9, 125]. Thus, the control of synchronization processes in neural systems is a demanding clinical problem. Over the past three decades, several control methods have been developed and applied. High-frequency (> 100 Hz) deep brain stimulation (DBS) [25–28] is an established and powerful therapeutic tool for the treatment of patients with Parkinson's disease, essential tremor, dystonia and even psychiatric disorders [29–33]. Conventional DBS has only acute effects, i.e. neither clinical [126] nor electrophysiological [127] effects persist after switching off conventional DBS.

The computationally developed method of coordinated reset (CR)-DBS [13, 128] is characterized by long-lasting, sustained effects, which persist after cessation of stimulation [100–102]. Standard DBS, CR-DBS as well as theta burst DBS, i.e. the delivery of periodic sequences of electrical bursts, recently

tested in a short-term trial [129], employ periodic pulse train stimulation. For all of these approaches, it is desirable to achieve a therapeutic effect with minimal interference with nerve tissue. To avoid side effects, it is crucial to achieve therapeutic effects with minimal stimulation current [21, 56, 130]. This raises the problem of finding the optimal waveform for stimulation.

In the field of theoretical and computational neuroscience, the problem of optimal synchronization is usually formulated as a control with minimal energy [34–43]. The goal is to obtain the optimal waveform of a periodic stimulation current to entrain a given spiking neuron with minimal stimulation energy. Another approach for optimal synchronization was developed in Refs. [97–99]. The authors introduced a general form of a functional and considered the problem of maximizing the width of the entrainable frequency detuning (the width of the Arnold tongue) of a spiking neuron for the fixed value of the functional. This approach can be applied to an ensemble of non-interacting neurons with distributed frequencies.

The minimum-energy control strategies reduce the energy consumption of an implantable pulse generator but do not guarantee minimal damage to the neural tissue. In Chapter 2 we considered an alternative, minimum-charge control strategy, which aims at reducing damage to neural tissue [63]. Neurological stimulation protocols typically use periodic, charge-balanced, biphasic stimuli, usually asymmetrical in shape [45]. Typically, the first phase of the stimulus depolarizes the cell membrane and the second pulse brings the net charge balance in the electrode back to zero [54]. One of the important factors on which the threshold for tissue damage depends is the charge per phase of a stimulus pulse [50, 51]. The magnitude of charge is defined by the product of the amplitude and width of the pulse. For the periodic charge-balanced stimulation, this quantity is proportional to the mean absolute value of the stimulating current. The latter was chosen as a performance measure in our control algorithm in order to minimize the integral charge transferred to the neuron in both directions during the stimulation period. The consideration in Chapter 2 was limited to a single neuron. In this chapter, we apply this approach to a network of interacting neurons exhibiting collective periodic oscillations. We use the results of a recently developed phase reduction theory

for arbitrary networks of coupled heterogeneous dynamical elements [82]. We also apply our approach to a large-scale heterogeneous network of globally coupled quadratic integrate-and-fire (QIF) neurons, which can be reduced to an exact low-dimensional macroscopic model in the infinite-size limit [85, 86]. The reduced equations allow us to simply compute a macroscopic phase response curve (PRC) of the network [131, 132] and use it to build the optimal waveform.

The chapter is organized as follows. In Sec. 3.1 we formulate the problem, and in Sec. 3.2 we give a general expression for the optimal waveform, which ensures the minimum charge entrainment of any network of interacting neurons to the frequency of stimulating current. This general theoretical result is then numerically demonstrated for small-scale networks of synaptically and electrically coupled FitzHugh-Nagumo (FHN) neurons as well as for a large-scale network of QIF neurons in Sec. 3.3. We finish the chapter with a discussion and conclusions presented in Sec. 3.4

3.1 Problem formulation

We consider a general heterogeneous network of N coupled Hodgkin-Huxley-type neurons under periodic stimulation

$$\dot{v}_i = F_i(v_i, \mathbf{w}_i) + \sum_{j=1}^{N} H_{ij}(v_i, v_j) + I_i(\omega t), \tag{3.1a}$$

$$\dot{\mathbf{w}}_i = \mathbf{G}_i(v_i, \mathbf{w}_i), \quad (i = 1, \ldots, N). \tag{3.1b}$$

Here the scalar v_i and the vector $\mathbf{w}_i \in \mathbb{R}^n$ are the membrane potential and the gating variable of the ith neuron, respectively. The function $F_i(v_i, \mathbf{w}_i)$ describes the sum of currents flowing through the ion channels of the ith neuron and the function $H_{ij}(v_i, v_j)$ defines the coupling between the ith and jth neuron. $I_i(\omega t)$ is a periodic stimulating current applied to the ith neuron. It satisfies $I(\omega t + 2\pi) = I(\omega t)$, where ω is the stimulation frequency and $T = 2\pi/\omega$ is the period of stimulation. Equation (3.1b) describes the dynamics of the gating variable $\mathbf{w}_i$, where the function $\mathbf{G}_i(v_i, \mathbf{w}_i)$ represents the ionic channel

dynamics. The dimension n of the vector variable $\mathbf{w}_i$ as well as the functions F_i and $\mathbf{G}_i$ are defined by the specific neuron model.

We assume that without stimulation [$I_i(\omega t) = 0$] the entire network exhibits stable collective limit cycle oscillations with a period T_0 and a frequency $\omega_0 = 2\pi/T_0$. Our goal is to find the optimal waveform for the stimulating currents $I_i(\omega t)$, which ensures the entrainment of the network to the stimulation frequency ω with minimum integral charge transferred to neurons in both directions during the stimulation period. For a single neuron, such a problem was considered in Chapter 2. Below we will show that, under certain assumptions, the results can be adapted to a network of interacting neurons.

For sufficiently small stimulating currents $I_i(\omega t)$, the phase reduction method [73, 83, 95] can be applied to reduce Eqs. (3.1) to a single scalar phase equation. Our equations represent a particular case of equations considered in a recent publication [82] for which such a reduction has been performed, and thus we can directly use these results to write down the reduced equations for our problem. The dynamics of the $(n+1)N$ dimensional system of ordinary differential Eqs. (3.1) can be approximated by the phase equation

$$\dot{\vartheta} = \omega_0 + \sum_{i=1}^{N} z_i(\vartheta) I_i(\omega t) \tag{3.2}$$

for the collective phase $\vartheta(t)$. Here $z_i(\vartheta)$ is the 2π-periodic phase response curve (PRC) of the ith neuron.

The PRCs are derived from a free [$I_i(\omega t) = 0$] network model. It is convenient to introduce $(n+1)$-dimensional vectors

$$\mathbf{X}_i = \begin{pmatrix} v_i \\ \mathbf{w}_i \end{pmatrix}, \quad \mathbf{\Phi}_i(\mathbf{X}_i) = \begin{pmatrix} F_i(v_i, \mathbf{w}_i) \\ \mathbf{G}_i(v_i, \mathbf{w}_i) \end{pmatrix} \tag{3.3}$$

and rewrite the free network Eqs. (3.1) in the form

$$\dot{\mathbf{X}}_i = \mathbf{\Phi}_i(\mathbf{X}_i) + \mathbf{k} \sum_{j=1}^{N} H_{ij}(v_i, v_j), \quad (i = 1, \ldots, N), \tag{3.4}$$

where $\mathbf{k}$ is a $(n+1)$ dimensional unit vector with the first component equal to one and all other components equal to zero. We denote the T_0 periodic stable limit-cycle solution of the free network (3.4) as

$$\mathbf{X}_i^{(0)}(t) = \mathbf{X}_i^{(0)}(t + T_0), \quad (i = 1, \ldots, N). \tag{3.5}$$

Generally, the PRCs of the system (3.4) are the $(n+1)$ dimensional 2π-periodic vectors

$$\mathbf{Q}_i(\vartheta) = [Q_i^{(1)}, \ldots, Q_i^{(n+1)}]^T, \quad (i = 1, \ldots, N). \tag{3.6}$$

However, since the stimulating currents $I_i(\omega t)$ in the system (3.1) perturb only membrane potentials of neurons [Eq. (3.1a)], their contribution to the phase dynamics in the Eq. (3.2) is determined by the first components $Q_i^{(1)}(\vartheta)$ of the vectors $\mathbf{Q}_i(\vartheta)$, which in Eq. (3.2) are denoted as

$$z_i(\vartheta) \equiv Q_i^{(1)}(\vartheta). \tag{3.7}$$

Although we only need the first components of the PRC vectors to find them, we have to solve the system of adjoint equations for the full PRCs vectors [82]:

$$\begin{aligned} \omega_0 \frac{d}{d\vartheta}\mathbf{Q}_i(\vartheta) = &- A_i^T(\vartheta)\mathbf{Q}_i(\vartheta) - \mathbf{k}\sum_{j=1}^{N} M_{ij}(\vartheta) z_i(\vartheta) \\ &- \mathbf{k}\sum_{j=1}^{N} N_{ji}(\vartheta) z_j(\vartheta), \quad (i = 1, \ldots, N), \end{aligned} \tag{3.8}$$

where $A_i(\vartheta) = \partial\mathbf{\Phi}_i(\mathbf{X}_i)/\partial\mathbf{X}_i$, $M_{ij}(\vartheta) = \partial H_{ij}(v_i, v_j)/\partial v_i$ and $N_{ij}(\vartheta) = \partial H_{ij}(v_i, v_j)/\partial v_j$ are Jacobian matrices of $\mathbf{\Phi}_i$ and partial derivatives of the scalar coupling functions H_{ij} evaluated at $\mathbf{X}_i^{(0)}(\vartheta) = \mathbf{X}_i^{(0)}(\omega_0 t)$, respectively. The superscript T denotes the matrix transpose. The PRCs have to satisfy the normalization condition

$$\sum_{i=1}^{N} \mathbf{Q}_j(\vartheta) \cdot \frac{\mathrm{d}\mathbf{X}_i^{(0)}(\vartheta)}{\mathrm{d}\vartheta} = 1. \tag{3.9}$$

Thus, for a specific neural network model (3.1), PRCs $z_i(\vartheta)$ can be found by numerically solving the Eqs. (3.8) for vectors $\mathbf{Q}_i(\vartheta)$ with the normalization condition (3.9).

3.2 Optimal waveform for entrainment of a network of interacting neurons

In what follows, we assume that the subset $i \in \{i_k\} \equiv \{i_1, i_2, \ldots, i_M\}$ of $M \leq N$ network neurons are stimulated by the same current $I(\omega t)$, while other neurons remain free from stimulation, i.e. we set

$$I_i(\omega t) = \begin{cases} I(\omega t) & \text{for } i \in \{i_1, i_2, \ldots, i_M\}, \\ 0, & \text{otherwise.} \end{cases} \tag{3.10}$$

Then the phase Eq. (3.2) simplifies to

$$\dot{\vartheta} = \omega_0 + z(\vartheta) I(\omega t), \tag{3.11}$$

where

$$z(\vartheta) = \sum_{k=1}^{M} z_{i_k}(\vartheta). \tag{3.12}$$

This assumption allows us to adapt the results presented in the previous chapter, where a minimum-charge control strategy for a single neuron was developed. The phase Eq. (3.11) has the same form as in the case of a single neuron, with the only difference that $z(\vartheta)$ is now the sum of PRCs of stimulated neurons [Eq. (3.12)] in a connected network, rather than the PRC of a single neuron. Thus, we can use the optimal waveform derived for the single neuron by replacing the PRC of a single neuron with an effective network's PRC defined by the Eq. (3.12).

Following Chapter 2, we briefly describe the minimum-charge control strategy for our network. The aim of the strategy is to minimize the integral charge transferred to the neurons in both directions during the stimulation period. We look for the optimal waveform $I(\omega t) = I^*(\omega t)$ that ensures an

entrainment of a connected network (3.1) to the frequency of stimulation with the minimum mean absolute value of the current injected into neurons:

$$\mathcal{J}[I] = \frac{1}{T}\int_0^T |I(\omega t)|\,\mathrm{d}t\,. \tag{3.13}$$

We minimize the functional (3.13) with two additional, clinically relevant, conditions. We require that the stimulating current never exceeds some predefined minimal $I_- < 0$ and maximal $I_+ > 0$ values, i.e.,

$$I_- \le I(\omega t) \le I_+ \tag{3.14}$$

for any time and introduce a clinically mandatory charge-balance condition

$$\int_0^T I(\omega t)\,\mathrm{d}t = 0. \tag{3.15}$$

For a sufficiently small frequency detuning

$$\Delta\omega = \omega - \omega_0, \tag{3.16}$$

the optimization problem defined by Eqs. (3.11), (3.13), (3.14), and (3.15) leads to the following optimal waveform [63]

$$I^*(\vartheta) = I_+\Pi\left(\frac{\vartheta}{\Delta\vartheta_+}\right) + I_-\Pi\left(\frac{\vartheta \pm \Delta\vartheta_z}{\Delta\vartheta_-}\right), \tag{3.17}$$

which is a 2π-periodic function $I^*(\vartheta) = I^*(\vartheta + 2\pi)$ of the bang-off-bang type. Here $\Pi(x)$ is the rectangular function that satisfies $\Pi(x) = 1$ for $|x| < 1/2$ and $\Pi(x) = 0$ for $|x| > 1/2$, and

$$\Delta\vartheta_z = \vartheta_{max} - \vartheta_{min} + \pi \pmod{2\pi} - \pi \tag{3.18}$$

is the phase difference between the location of the absolute maximum ϑ_{max} and the location of the absolute minimum ϑ_{min} of PRC (3.12) reduced to the interval $\Delta\vartheta_z \in [-\pi, \pi]$. The upper and lower signs in the argument of the second function in Eq. (3.17) correspond to $\Delta\omega > 0$ and $\Delta\omega < 0$, respectively.

Thus, the waveform (3.17) consists of two rectangular pulses, one positive located at $\vartheta = 0$, and the other negative located at $\vartheta = -\Delta\vartheta_z$ for $\Delta\omega > 0$ or at $\vartheta = \Delta\vartheta_z$ for $\Delta\omega < 0$. The height of the positive (negative) pulse is I_+ (I_-) and its width is $\Delta\vartheta_+$ ($\Delta\vartheta_-$). The widths $\Delta\vartheta_{+,-}$ are defined as

$$\Delta\vartheta_{+,-} = \frac{2\pi\Delta\omega}{I_{+,-}(z_{max} - z_{min})}, \tag{3.19}$$

where $z_{max} = z(\vartheta_{max})$ and $z_{min} = z(\vartheta_{min})$ are the absolute maximum and absolute minimum of PRC (3.12), respectively, therefore $z_{max} - z_{min}$ is the amplitude of the PRC. The network (3.1) of interacting neurons oscillating with a frequency of ω_0 is synchronized with the optimal stimulating current $I^*(\omega t)$ of a frequency of ω at a minimum value of the functional (3.13) equal to [63]:

$$\mathcal{J}^* = \frac{2|\Delta\omega|}{z_{max} - z_{min}}. \tag{3.20}$$

Summing up, in order to build the optimal waveform (3.17) only limited information on the PRC (3.12) of the network is required, namely the phase difference $\Delta\vartheta_z$ between its absolute maximum and minimum, and the amplitude $z_{max} - z_{min}$. The optimal waveform $I^*(\vartheta)$ is of the bang-off-bang type with periodically repeated positive and negative rectangular pulses separated by the distance $\Delta\vartheta_z$. The pulse sequence depends on the sign of the frequency detuning $\Delta\omega$. For $\Delta\omega > 0$, this sequence is such that the positive pulse hits the network at the timing of the maximum of PRC while the negative pulse hits the network at the timing of the minimum of PRC. As a result, the maximum phase advancement occurs in the network during one period of the forcing. For $\Delta\omega < 0$, the reverse pulse sequence is optimal. The maximum phase delay of the network is achieved when the positive pulse hits the network at the minimum of the PRC, and the negative pulse hits the network at the maximum of the PRC. The amplitudes of the positive and negative pulses are equal to the permissible limits I_+ and I_- of the stimulating current, respectively. The width of the positive $\Delta\vartheta_+$ (negative $\Delta\vartheta_-$) pulse is proportional to the frequency detuning $\Delta\omega$ and inversely proportional to the permissible limit I_+ (I_-). It

follows that the areas under the positive and negative pulses are equal to each other, so that the condition of charge-balance is satisfied.

In the next section, we will numerically verify the general theoretical results derived above for specific network models.

3.3 Numerical examples

To check whether the waveform (3.17) provides an entrainment of a specific network with a minimum value of the functional (3.13), we use a trial function consisting of two rectangular positive and negative pulses [63]

$$I(\vartheta) = a\left[\Pi\left(\frac{s\vartheta}{l}\right) - \frac{1}{s}\Pi\left(\frac{\vartheta + d}{l}\right)\right], \tag{3.21}$$

separated by a distance $d \in [-\pi, \pi]$. Here l is the width of the negative pulse and a is the amplitude of the positive pulse. The parameter s defines the asymmetry of the pulses. The width of the positive pulse is l/s and the amplitude of the negative pulse is a/s, so that the charge balance condition (3.15) is satisfied. The trial function (3.21) coincides with the optimal waveform (3.17), $I(\vartheta) = I^*(\vartheta)$, provided that its parameters accord with the optimal values defined by Eqs. (3.18) and (3.19), i.e., $l = \Delta\vartheta_-$, $a = I_+$ and $d = \Delta\vartheta_z$ for $\Delta\omega > 0$ and $d = -\Delta\vartheta_z$ for $\Delta\omega < 0$. For any fixed values of the parameters l and d of the trial function, we can compute the threshold value of the amplitude $a = a_{th}$ at which the entrainment of the oscillations occurs. The value of the functional (3.13) at the entrainment condition is:

$$\mathcal{J}_{th} = a_{th} l/s\pi. \tag{3.22}$$

Thus we can verify whether the value of $\mathcal{J}_{th}$ is minimal when the parameters l and d of the trial function coincide with the optimal values $l = \Delta\vartheta_-$ and $d = \pm\Delta\vartheta_z$.

Below we estimate the threshold amplitude a_{th} using two different methods: (i) by directly integrating the nonlinear system (3.1) and (ii) using the approximate phase Eq. (3.11). The first method is straightforward. For given

fixed values of the parameters s, l and d, we vary the amplitude a of the trial signal (3.21) and find the minimum a at which the entrainment in Eqs. (3.1) appears. We interpret this minimum value of a as a threshold amplitude a_{th}. In the second method, we introduce the phase difference $\varphi = \vartheta - \omega t$ and, using Eq. (3.11), we derive the averaged equation for this variable:

$$\dot{\varphi} = -\Delta\omega + \frac{1}{2\pi}\int_{-\pi}^{\pi} z(\vartheta+\varphi)I(\vartheta)\,\mathrm{d}\vartheta\,. \tag{3.23}$$

Then we define an auxiliary function

$$\Phi(\varphi|s,l,d) = \frac{1}{2\pi a}\int_{-\pi}^{\pi} z(\vartheta+\varphi)I(\vartheta)\,\mathrm{d}\vartheta \tag{3.24}$$

and estimate the threshold amplitude as

$$a_{th} = \Delta\omega \begin{cases} 1/\max\limits_{\varphi}[\Phi(\varphi|s,l,d)] & \text{for} \quad \Delta\omega > 0, \\ 1/\min\limits_{\varphi}[\Phi(\varphi|s,l,d)] & \text{for} \quad \Delta\omega < 0. \end{cases} \tag{3.25}$$

We see that the threshold amplitude a_{th} is proportional to the frequency detuning $\Delta\omega$, and therefore $\mathcal{J}_{th}$ is also proportional to $\Delta\omega$. The natural characteristic for analysis is $\mathcal{J}_{th}/|\Delta\omega|$. We fix the parameters s and l and analyze the dependence of this characteristic on the distance d between the positive and negative pulses. We check if $\mathcal{J}_{th}/|\Delta\omega|$ reaches an absolute minimum at $d = \Delta\vartheta_z$ ($d = -\Delta\vartheta_z$) for $\Delta\omega > 0$ ($\Delta\omega < 0$). We also check whether the values of these minima coincide with the theoretical optimal value $\mathcal{J}^*/|\Delta\omega|$ defined by the Eq. (3.20). We emphasize that the optimal value depends only on the amplitude of the PRC, $\mathcal{J}^*/|\Delta\omega| = 2/(z_{max} - z_{min})$, and does not depend on any parameters of the control algorithm, such as admissible limits I_- and I_+ of the stimulating current.

Now we present the results of the above analysis for two small-scale FitzHugh-Nagumo neuron networks with synaptic and electric couplings, as well as a large-scale network of synaptically coupled quadratic integrate-and-fire neurons.

3.3.1 A network of synaptically coupled FHN neurons

First, we verify the theoretical results presented in Sec. 3.2 for a network of synaptically coupled FitzHugh-Nagumo neurons. The gating (recovery) variable w_i of the FHN neuron is a scalar variable, and the functions on the right side of the Eq. (3.1) are as follows

$$F_i(v_i, w_i) = v_i - v_i^3/3 - w_i + \gamma_i, \tag{3.26a}$$

$$G_i(v_i, w_i) = \delta(\alpha + v_i - \beta w_i), \tag{3.26b}$$

$$H_{ij}(v_i, v_j) = K_{ij} S_j(v_j). \tag{3.26c}$$

The schematic diagram of the network considered here is shown in Fig. 3.1. It consists of $N = 5$ neurons with identical parameters $\alpha = 0.7$, $\beta = 0.8$, and $\delta = 0.08$ for all neurons. The parameters γ_i, which determine the type of isolated neurons, are not identical. Depending on this parameter, the neuron may be oscillatory or excitable. The values of these parameters are $\gamma_i = 0.8$ for the first three neurons, $i = 1, 2, 3$, which exhibit self-oscillatory dynamics, and $\gamma_i = 0.2$ for the last two neurons, $i = 4, 5$, which demonstrate excitable dynamics.

We assume that synaptic dynamics are fast, and the synaptic current induced by the jth presynaptic neuron to the ith postsynaptic neuron can be written by Eq. (3.26c), where K_{ij} is the coupling strength between the jth and ith neuron, and $S_j(v_j)$ describes the synaptic spike generated by the jth presynaptic neuron. We simulate the dependence of this spike on the voltage v_j of the presynaptic neuron using the sigmoid function

$$S_j(v_j) = p_j \left[1 + \exp\left(-\frac{v_j - v_{th}}{\sigma}\right)\right]^{-1}, \tag{3.27}$$

where v_{th} and σ are the characteristic parameters of the synapse and the parameter p_j determines the sign of the synaptic spike: $p_j = +1$ for excitatory neurons and $p_j = -1$ for inhibitory neurons. We assume that the oscillating neurons are excitatory ($p_j = +1$ for $j = 1, 2, 3$) and excitable neurons are inhibitory ($p_j = -1$ for $j = 4, 5$). Synaptic parameters are $v_{th} = 1.5$ and $\sigma = 0.5$. Elements K_{ij} of the coupling matrix are randomly and independently

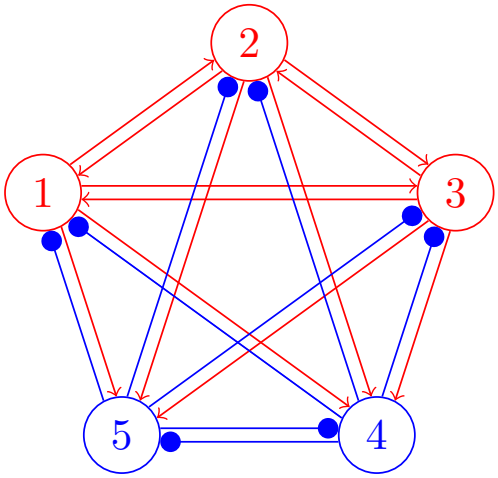

Figure 3.1 Schematic diagram of a network of five synaptically coupled FHN neurons. Red circles with numbers 1, 2 and 3 are excitatory neurons and blue circles with numbers 4 and 5 are inhibitory neurons. Red lines ending with arrows indicate excitatory couplings and blue lines ending with filled circles indicate inhibitory couplings. Excitatory neurons are oscillating ($\gamma_i = 0.8$ for $i = 1, 2, 3$), and inhibitory neurons are excitable ($\gamma_i = 0.2$ for $i = 4, 5$).

taken from a uniform distribution $[0, 0.5]$. Below we present the results for a specific realization of a randomly generated matrix:

$$K = \begin{pmatrix} 0 & 0.4710 & 0.2769 & 0.4334 & 0.2007 \\ 0.0855 & 0 & 0.3400 & 0.2034 & 0.4167 \\ 0.4693 & 0.2260 & 0 & 0.0563 & 0.2018 \\ 0.2952 & 0.4198 & 0.1196 & 0 & 0.1951 \\ 0.2203 & 0.2663 & 0.2895 & 0.1501 & 0 \end{pmatrix}. \tag{3.28}$$

The zero diagonal elements mean that self-coupling is excluded. For given parameter values, the free network demonstrates collective limit-cycle oscillations with a period $T_0 \approx 35.159894$. The dynamics of the membrane potentials $v_j(t)$ and the spike variables $S_j(v_j(t))$ for all neurons are shown in Fig. 3.2. Figure 3.3 shows the corresponding PRCs $z_j(\vartheta)$ obtained by solving the Eqs. (3.8).

The network architecture shown in Fig. 3.1, mimics the architecture of the neural network of the subthalamic nucleus (STN) and the external segment of

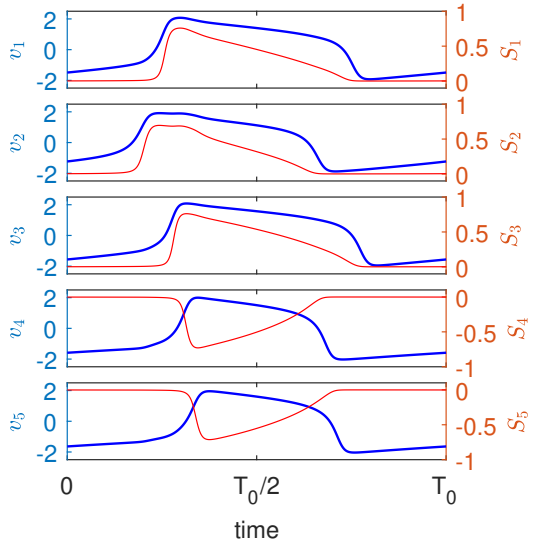

Figure 3.2 Dynamics of membrane potentials v_j (bold blue curves) and synaptic variables S_j (thin red curves) of a network of synaptically coupled FHN neurons in the absence of stimulation.

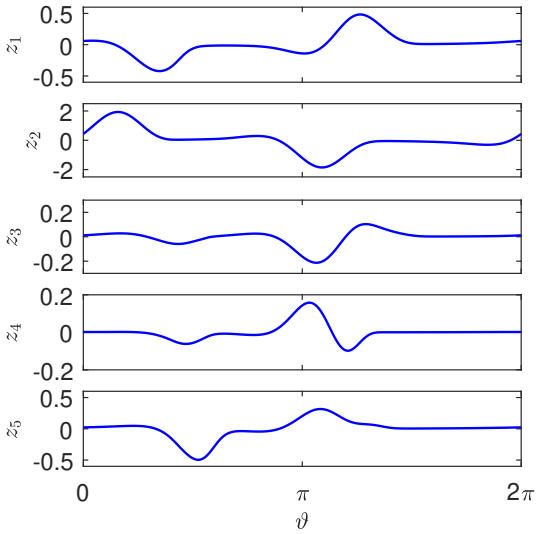

Figure 3.3 Phase response curves of a network of synaptically coupled FHN neurons.

the globus pallidus (GPe), which is often used to model Parkinson's disease (cf., e.g., Ref. [133]). STN is a network of oscillating excitatory neurons (in our case, the first three neurons), and GPe consists of excitable inhibitory neurons (in our case, the last two neurons). Using the calculated PRCs, we can build the optimal waveform for various stimulation protocols.

Below we consider two options for stimulation: (i) only oscillating excitatory neurons with indexes $j = 1, 2, 3$ are stimulated. Here the effective PRC is $z = z_1 + z_2 + z_3$; (ii) only excitable inhibitory neurons with indexes $j = 4, 5$ are stimulated. Here the effective PRC is $z = z_4 + z_5$. The corresponding effective PRC and dependence of $\mathcal{J}_{th}/|\Delta\omega|$ on the distance d between the pulses of the trial waveform (3.21) for (i) and (ii) stimulation protocols are shown in Fig. 3.4 and 3.5, respectively. Other parameters of the trial waveform are fixed, $l = 0.2$ and $s = 2$. The solid blue curves show the results obtained by the averaged phase Eq. (3.23) for positive frequency detuning $\Delta\omega > 0$, and the thin red curves show the same results for negative frequency detuning $\Delta\omega < 0$. For sufficiently small values of $|\Delta\omega|$, the curves $\mathcal{J}_{th}/|\Delta\omega|$ vs d are independent of $\Delta\omega$. In numerical experiments with FHN networks here and below, we took the values $|\Delta\omega|$ of order 10^{-3}. Symbols denote the results obtained by integrating a system of nonlinear Eqs. (3.1). Theoretical optimal distances $d = \pm\Delta\vartheta_z$ between positive and negative pulses are shown by vertical dashed lines. Open circles indicate the theoretical optimal value (3.20) of the functional (3.13), normalized to the frequency detuning $|\Delta\omega|$.

In both cases, the solution of the averaged phase Eq. (3.23) and the direct simulation of a nonlinear system of Eqs. (3.1) confirm the theoretical results presented in the Sec. 3.2. For $\Delta\omega > 0$, the absolute minimum of the functional (3.13) is attained when the distance d between the positive and negative pulses of the trial waveform (3.21) coincides with distance $\Delta\vartheta_z$ between the absolute maximum and the absolute minimum of the corresponding PRC. For $\Delta\omega < 0$, the absolute minimum is attained at $d = -\Delta\vartheta_z$. The values of these minima are in good agreement with the theoretically predicted value (3.20). Also note the good agreement between the results obtained from the averaged phase Eq. (3.23) and the nonlinear system (3.1) when calculating the dependence $\mathcal{J}_{th}/|\Delta\omega|$ vs. d in the entire interval $d \in [-\pi, \pi]$.

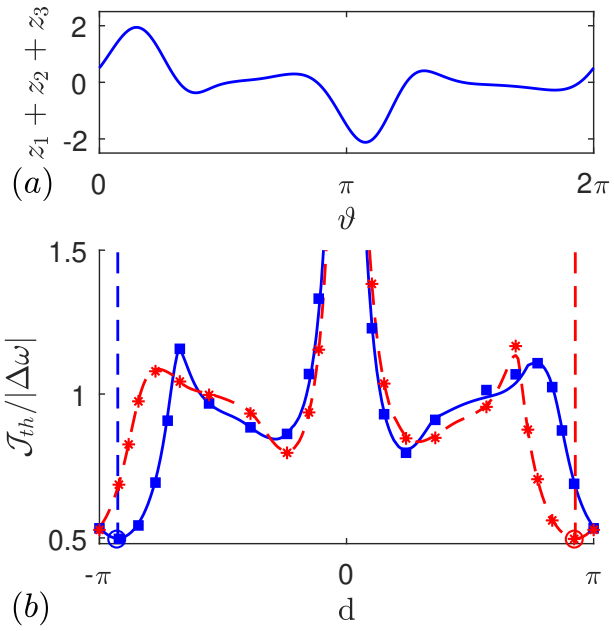

Figure 3.4 Testing the minimum-charge control theory for a network of five synaptically coupled FHN neurons in the case of stimulation of only oscillating excitatory neurons with the indexes $j = 1, 2, 3$. (a) Effective PRC $z = z_1+z_2+z_3$. The phase distance between the maximum and the minimum is $\Delta\vartheta_z = -2.9084$, and the amplitude of the PRC is $z_{max} - z_{min} = 4.0634$. (b) Threshold value $\mathcal{J}_{th}$ of the functional (3.13), normalized to the frequency detuning $|\Delta\omega|$, as a function of the distance d between positive and negative pulses of the trial waveform (3.21) for the fixed parameters $l = 0.2$ and $s = 2$. The bold blue curve and the thin red curve show the results obtained from the averaged phase Eq. (3.23) for $\Delta\omega > 0$ and $\Delta\omega < 0$, receptively. Blue squares and red stars denote the corresponding results obtained by integrating a system of nonlinear Eqs. (3.1). The dashed vertical lines show the theoretical optimal distances $d = \pm\Delta\vartheta_z$. Open circles indicate the optimal theoretical value (3.20).

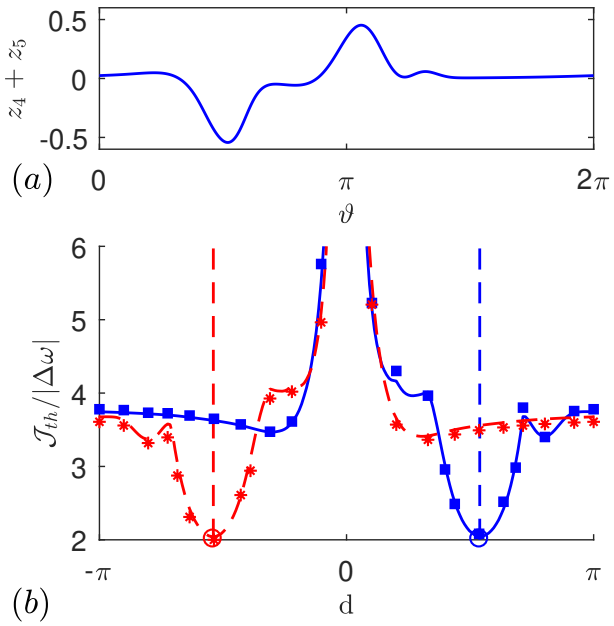

Figure 3.5 The same as in Fig. 3.4, but for the case of stimulation of only excitable inhibitory neurons with the indexes $j = 4, 5$. The effective PRC is $z = z_4 + z_5$. The phase distance between the maximum and the minimum is $\Delta\vartheta_z = 1.6935$, and the amplitude of the PRC is $z_{max} - z_{min} = 0.9949$. The remaining parameters are the same as in Fig. 3.4.

From a physical point of view, an interesting result is that the first stimulation protocol is more effective than the second. For the first protocol, the total charge delivered to each neuron during the stimulation period is four times less. This is due to the fact that oscillating excitatory neurons are more sensitive to external perturbations than excitable inhibitory neurons. It can be seen from the effective PRCs of these two subsystems shown in the Figs. 3.4(a) and 3.5(a). The amplitudes of these PRCs differ four times. The optimal value of the functional (3.20) is inversely proportional to the amplitude of the PRC and, therefore, for the first stimulation protocol is four times less than for the second. We also note that the optimal distance between the positive and negative pulses of the stimulation current is different for these two stimulation protocols, because the distance between the maximum and the minimum of the corresponding effective PRCs is different.

3.3.2 A network of electrically coupled FHN neurons

As a second example, we consider the network of electrically coupled FHN neurons introduced in Ref. [82]. The network size $N = 10$ is two times larger than in the previous example. As before, the functions $F_i(v_i, w_i)$ and $G_i(v_i, w_i)$ are defined by the Eqs. (3.26a) and (3.26b), respectively, and the function $H_{ij}(v_i, v_j)$ is now described by an electric coupling of the form

$$H_{ij}(v_i, v_j) = K_{ij}(v_j - v_i). \tag{3.29}$$

As in the previous example, the parameters $\alpha = 0.7$, $\beta = 0.8$, and $\delta = 0.08$ are the same for all neurons, and the parameters γ_i are not identical. The values of these parameters are $\gamma_i = 0.2$ for the neurons $i = 1, \ldots, 7$, which exhibit excitable dynamics, and $\gamma_i = 0.8$ for the neurons $i = 8, \ldots, 10$, which demonstrate self-oscillatory dynamics. The elements K_{ij} of the 10×10 coupling matrix are generated randomly. Here we use the specific realization of this matrix presented in Ref. [82]. For the above parameter values, the free $[I_i(\omega t) = 0]$ network demonstrates collective limit-cycle oscillations in the 20-dimensional state space with the period $T_0 \approx 75.709874$. The dynamics of

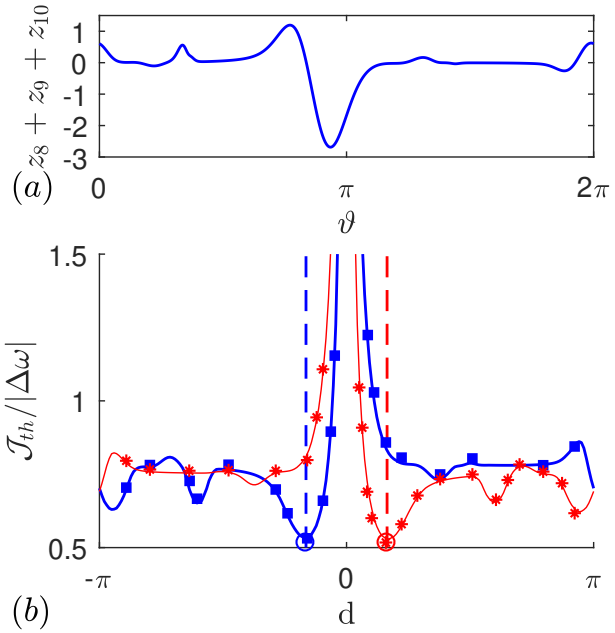

Figure 3.6 Testing the minimum-charge control theory for a network of ten electrically coupled FHN neurons in the case of stimulation of only oscillating neurons with the indexes $j = 8, 9, 10$. (a) Effective PRC $z = z_8 + z_9 + z_{10}$. The phase distance between the maximum and the minimum is $\Delta\vartheta_z = -0.5154$, and the amplitude of the PRC is $z_{max} - z_{min} = 3.8814$. (b) The dependence $\mathcal{J}_{th}/|\Delta\omega|$ vs. d for the fixed parameters $l = 0.2$ and $s = 2$. Marking of curves and symbols is the same as in Fig. 3.4.

the variables $v_i(t)$ and the PRCs $z_i(\vartheta)$ for all neurons are graphically presented in Ref. [82].

In Fig. 3.6, we show the results for the stimulation protocol, when only oscillating neurons with indexes $i = 8, 9, 10$ are stimulated. The effective PRC of the network, $z = z_8 + z_9 + z_{10}$ [Fig. 3.6(a)] is now more complex than in previous examples; it has more extrema. This leads to a more complex dependence of $\mathcal{J}_{th}/|\Delta\omega|$ on d [Fig. 3.6(b)], which also has more extrema. However, as in previous examples, the absolute minimum of this dependence is located at $d = \vartheta_z$ for $\Delta\omega < 0$ and at $d = -\vartheta_z$ for $\Delta\omega < 0$, where $\vartheta_z \approx -0.5154$ is the distance between the absolute maximum and the absolute minimum of the PRC. The absolute minimum value of $\mathcal{J}_{th}/|\Delta\omega|$ is consistent with the

Eq. (3.20). Therefore, the more complex network model discussed here also confirms the general theory presented in the Sec. 3.2.

3.3.3 A large-scale network of synaptically coupled quadratic integrate-and-fire neurons

As a final example, we consider a heterogeneous network with a large number N of all-to-all synaptically coupled QIF neurons. The microscopic state of the network is determined by the set of neurons' membrane potentials v_i, which satisfy the following equations [80]:

$$\dot{v}_i = v_i^2 + \eta_i + S(t) + I(\omega t), \quad (i = 1, \ldots, N). \tag{3.30}$$

Here, the constants η_i specify the behavior of individual neurons, $S(t)$ denotes the synaptic current and the last term $I(\omega t)$ represents a periodic stimulating current. We assume that all neurons are stimulated by the same external signal. The QIF neuron model does not contain a gating (recovery) variable. Recovery is described by an instantaneous reset of the membrane potential. Every moment when the membrane potential v_i reaches the peak value v_{peak} its voltage is reset to the value v_{reset}. To simplify the analysis, we set $v_{peak} = -v_{reset} \to \infty$. With this assumption, a QIF neuron can be transformed to a theta neuron. This assumption is also crucial for the analytical treatment of a network model in an infinite size limit [85]. We also assume that the synaptic dynamics is fast, and synaptic current can be written as [86]:

$$S(t) = J\frac{v_{th}}{N}\sum_{j=1}^{N} H(v_j(t) - v_{th}). \tag{3.31}$$

Here J represents the coupling strength, $H(\cdot)$ is the Heaviside step function, and v_{th} is the threshold potential. The positive and negative signs of J correspond to the excitatory and inhibitory interactions, respectively. At time t, only those neurons contribute to the synaptic current, whose membrane potential $v_j(t)$ exceeds the threshold value v_{th}. In fact, the v_{th} parameter determines the width and height of the synaptic pulses. When the jth neuron spikes, the therm

$v_{th}H(v_j(t) - v_{th})$ generates a rectangular pulse of height v_{th}. The pulse width for large v_{th} can be approximated as $1/v_{th}$ [86]. When $v_{th} \to \infty$, the pulse turns into a zero-width Dirac delta spike. The case of interaction with instantaneous Dirac delta pulses was considered in Ref. [85], and macroscopic limit cycle oscillations were not found in such a model. The finite width of synaptic pulses is a crucial factor for the occurrence of macroscopic self-sustained oscillations [86].

The isolated $[S(t) = 0, I(\omega t) = 0]$ QIF neuron is the canonical model for the class I neurons near the spiking threshold [73]. Spiking instability in such neurons is manifested through bifurcation of the saddle node on the invariant curve (SNIC). The system following this scenario exhibits excitability before the bifurcation. For the QIF neuron, this scenario is provided by the bifurcation parameter η_i. For $\eta_i < 0$, the neuron is in the excitable mode and for $\eta_i > 0$ it is in the spiking mode. We assume that the values of the parameters η_i are distributed in accordance with a bell-shaped probability density function, which can be approximated by the Lorentzian distribution:

$$g(\eta) = \frac{1}{\pi} \frac{\Delta}{(\eta - \bar{\eta})^2 + \Delta^2}, \tag{3.32}$$

where Δ and $\bar{\eta}$ are the width and the center of the distribution, respectively.

The advantage of this model is that it allows an exact low-dimensional reduction of system equations in the thermodynamic limit of infinite number of neurons, $N \to \infty$. In this limit, one can derive the closed system of two ordinary differential equations for biophysically relevant macroscopic quantities, the mean membrane potential $v(t)$ and the firing rate $r(t)$ [86]:

$$\dot{v} = \bar{\eta} + v^2 - \pi^2 r^2 + S(v, r) + I(\omega t), \tag{3.33a}$$

$$\dot{r} = \Delta/\pi + 2rv. \tag{3.33b}$$

Here, the synaptic current $S = S(v, r)$ is a function of the variables v and r of the following form:

$$S(v, r) = J \frac{v_{th}}{\pi} \left[\frac{\pi}{2} - \arctan\left(\frac{v_{th} - v}{\pi r} \right) \right]. \tag{3.34}$$

The low-dimensional macroscopic model greatly simplifies the task of finding an effective PRC for the original microscopic model determined by a large system of Eqs. (3.30). For large N, the macroscopic model (3.33) approximates well the solutions of the microscopic model (3.30), and therefore the PRC for the microscopic model can be obtained from the above system of Eqs. (3.33). Consider the case when the free $[I(\omega t) = 0]$ system (3.33) has a limit cycle solution $[v^{(0)}(t), r^{(0)}(t)] = [v^{(0)}(t + T_0), r^0(t + T_0)]$ with the period T_0. Then the PRC $\mathbf{Q} = [Q^{(1)}, Q^{(2)}]^T$ of the reduced system (3.33) satisfies the adjoint equation:

$$\omega_0 \frac{\mathrm{d}}{\mathrm{d}\vartheta}\mathbf{Q}(\vartheta) = -A^T(\vartheta)\mathbf{Q}(\vartheta), \tag{3.35}$$

where $\omega_0 = 2\pi/T_0$ and

$$A(\vartheta) = \begin{pmatrix} \partial S(v,r)/\partial v + 2v & \partial S(v,r)/\partial r - 2\pi^2 r \\ 2r & 2v \end{pmatrix} \tag{3.36}$$

is the Jacobian matrix of the system (3.33) evaluated at $[v^{(0)}(\vartheta), r^{(0)}(\vartheta)] = [v^{(0)}(\omega_0 t), r^0(\omega_0 t)]$.

To summarize, solving the adjoint Eq. (3.35), we can find the PRC $\mathbf{Q}(\vartheta)$ of the reduced system (3.33). The first component of this PRC $z(\vartheta) = Q^{(1)}(\vartheta)$ can be used to describe the phase dynamics of the original large-scale system (3.30) in the presence of a weak stimulation current $I(\omega t)$. This dynamics is described by the phase Eq. (3.11), which is the basis for the optimal theory presented in the Sec. 3.2. Thus, the results of this theory are applicable to a large-scale network (3.30) of QIF neurons with an effective PRC $z(\vartheta)$ defined by a simple adjoint Eq. (3.35). Below we support this statement with a specific numerical example.

We consider the network of $N = 10^4$ QIF neurons with parameter values $v_{th} = 50$, $J = 30$, $\Delta = 1$ and $\bar{\eta} = 0$. Choosing a zero value for the parameter $\bar{\eta}$ means that half of the neurons in the network are oscillating and the other half are excitable. For these parameter values, the macroscopic model (3.33) shows limit cycle oscillations with a period of $T_0 \approx 1.130132$. The dynamics of the mean membrane potential $v(t)$ and the spiking rate $r(t)$ during one

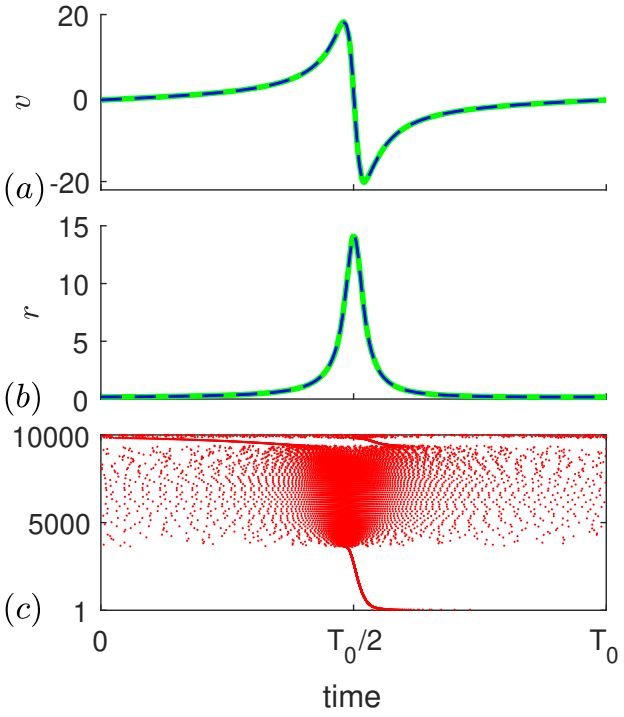

Figure 3.7 Dynamics of a heterogeneous network of 10^4 synaptically coupled QIF neurons in the absence of stimulation for parameter values $v_{th} = 50$, $J = 30$, $\Delta = 1$ and $\bar{\eta} = 0$. (a) The evolution of the mean membrane potential $v(t)$ and (b) the spiking rate $r(t)$. The thin dashed blue curves show the solutions of the reduced system of Eqs. (3.33), and the bold solid green curves show the results of direct numerical simulation of a microscopic model of Eqs. (3.38) for $N = 10^4$ neurons. (c) The raster plot. Here the dots show the spike moments for each neuron, where the vertical axis indicates neuron numbers.

oscillation period are shown by thin dashed blue curves in Fig. 3.7(a) and 3.7(b), respectively.

Numerical simulation of the microscopic model (3.30) is more convenient after changing the variables

$$v_i = \tan(\theta_i/2) \tag{3.37}$$

that turn QIF neurons into theta neurons. Such a transformation of variables avoids the problem associated with jumps of infinite size (from $+\infty$ to $-\infty$) of the membrane potential v_i of the QIF neuron at the moments of firing.

The phase θ_i of the theta neuron simply crosses the value of $\theta_i = \pi$ at these moments. For theta neurons, the Eqs. (3.30) are transformed into

$$\dot{\theta}_i = 1 - \cos\theta_i + (1 + \cos\theta_i)\left[\eta_i + S(t) + I(\omega t)\right], \tag{3.38}$$

where the synaptic current $S(t)$ is determined by the Eqs. (3.31) and (3.37). These equations were integrated by the Euler method with a time step of $dt = 10^{-4}$. The population of $N = 10^4$ theta neurons with the Lorentzian distribution (3.32) were deterministically generated using $\eta_j = \bar{\eta} + \Delta\tan\left[(\pi/2)(2j - N - 1)/(N + 1)\right]$, where $j = 1, \ldots, N$, $\Delta = 1$ and $\bar{\eta} = 0$. Such a numbering of neurons means that free neurons with the indexes $j = 1, \ldots, 5000$ are excitable and neurons with the indexes $j = 5001, \ldots, 10000$ are oscillating. More information on numerical modeling of Eqs. (3.38) can be found in Ref. [86]. To compare the results obtained from the microscopic model (3.38) with the solutions of the reduced system (3.33), we calculate the Kuramoto order parameter [83]

$$Z = \frac{1}{N}\sum_{j=1}^{N}\exp\left(i\theta_j\right) \tag{3.39}$$

and use the relationship between Z and the macroscopic parameters v and r [85]:

$$v = \mathrm{Im}\left(\frac{1 - Z^*}{1 + Z^*}\right), \quad r = \frac{1}{\pi}\,\mathrm{Re}\left(\frac{1 - Z^*}{1 + Z^*}\right), \tag{3.40}$$

where Z^* means complex conjugate of Z. The dynamics of the mean membrane potential $v(t)$ and the spiking rate $r(t)$ estimated from the microscopic model of Eqs. (3.38), (3.39) and (3.40) are shown by bold solid green curves in Figs. 3.7(a) and 3.7(b), respectively. These solutions are in excellent agreement with the solutions of the macroscopic model (3.33), shown by thin dashed blue curves. Note that, in contrast to the macroscopic model, the variables $v(t)$ and $r(t)$ obtained from the microscopic model are not exactly periodic. Their period fluctuates around a mean value of $T_0 \approx 1.1348$ with a standard deviation of about half a percent. These fluctuations are related to the finite size of the network. The microscopic dynamics of the network is quite complex. This can

be seen from the raster plot shown in Fig. 3.7(c), where dots indicate the spike moments of each neuron.

Despite the complex microscopic dynamics of the network, its macroscopic behavior is well described by the reduced system of Eqs. (3.33). The effective PRC of the network obtained from the simple adjoint Eq. (3.35) is shown in Fig. 3.8(a). The PRC parameters needed to design the optimal waveform are $\Delta\vartheta_z = 2.5832$ and $z_{max} - z_{min} = 1.7696$. As in the previous examples, the Fig. 3.8(b) shows the dependence of $\mathcal{J}_{th}/|\Delta\omega|$ on the distance d between the positive and negative pulses of the trial waveform (3.21) for the fixed parameters $l = 0.2$ and $s = 2$. Bold blue and thin red curves are obtained from the phase Eq. (3.11) for $\Delta\omega > 0$ and $\Delta\omega < 0$, respectively. Symbols show the results obtained from the microscopic model. Threshold entrainment amplitudes a_{th} were found by solving the system of 10^4 Eqs. (3.38) with a trial signal (3.21). Here in numerical simulations we took $|\Delta\omega| = 0.2$. We see that both results are in good agreement with each other. They show that the minimum of $\mathcal{J}_{th}/|\Delta\omega|$ is attained at $d = \vartheta_z$ for $\Delta\omega > 0$ and at $d = -\vartheta_z$ for $\Delta\omega < 0$, where $\vartheta_z \approx 2.5832$ is the distance between the maximum and the minimum of the PRC. The minimum value of $\mathcal{J}_{th}/|\Delta\omega|$ is consistent with the theoretically predicted optimal value (3.20). Thus, the minimum charge control theory presented in Sec. 3.2 works well not only for small neural networks, but also for a large-scale network of interacting QIF neurons, the collective behavior of which exhibits periodic macroscopic oscillations.

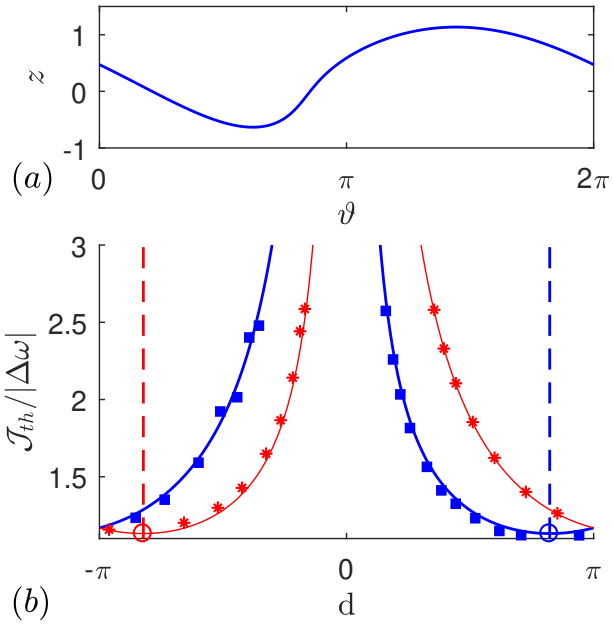

Figure 3.8 Testing the minimum-charge control theory for a network of 10^4 synaptically coupled QIF neurons. (a) Effective PRC of the network in the case of homogeneous stimulation of all neurons. The PRC is obtained from a simple adjoint Eq. (3.35). The phase distance between the maximum and the minimum is $\Delta\vartheta_z = 2.5832$, and the amplitude of the PRC is $z_{max} - z_{min} = 1.7696$. (b) Dependence $\mathcal{J}_{th}/|\Delta\omega|$ vs. d for fixed parameters $l = 0.2$ and $s = 2$. Bold blue and thin red curves are obtained in the same way as in Fig. 3.4, but using the PRC shown in panel (a) of this figure. Symbols are obtained by solving a system of 10^4 microscopic Eqs. (3.38) with a stimulation current (3.21).

3.4 Summary

We examined the problem of optimal entrainment of a network of interacting neurons by an external stimulus when an unperturbed network exhibits collective periodic oscillations. The general expression for the optimal waveform, which provides network entertainment with a minimum mean absolute value of the periodic stimulating current, is presented. This optimization is clinically relevant because it aims to reduce damage to nerve tissue by minimizing the integral charge transferred to neurons in both directions during the stimulation period. Our optimal waveform satisfies the clinically mandatory requirements: the charge-balance condition and the amplitude limitation.

The research presented in this chapter builds upon the previous chapter, where we considered a similar problem for the case of a single neuron. We obtained the optimal waveform under the assumption of a small frequency detuning, when the equations of the neuron model can be reduced to a simple scalar equation for the phase. Here we showed that, under certain assumptions, network equations can also be reduced to the same phase equation as for a single neuron. The only difference is that the phase response curve of a single neuron is replaced by an effective phase response curve of the network. This allowed us to adapt the results of the minimum charge control theory developed in Ref. [63]. As well as for a single neuron, the optimal waveform of the network is of the bang-off-bang type with periodically repeated positive and negative rectangular pulses, generally of different amplitudes and widths. However, the parameters of the optimal waveform are now determined by the parameters of the effective PRC of a network rather than the PRC of a single neuron. The distance d between positive and negative pulses is determined by the distance $\Delta\vartheta_z$ between the absolute maximum and the absolute minimum of the effective PRC of a network. For the positive frequency detuning, the optimal distance between the pulses is $d = \Delta\vartheta_z$, and for the negative frequency detuning, $d = -\Delta\vartheta_z$.

We confirmed the theoretical results with three numerical examples: two small-scale networks consisting of (i) five synaptically coupled FHN neurons, (ii) ten electrically coupled FHN neurons, and (iii) a large-scale network with

10^4 synaptically coupled QIF neurons. In the first example, the network architecture mimics the network architecture of the STN-GPe model [133], which consists of oscillating excitatory (STN) and excitable inhibitory (GPe) neurons. Two stimulation protocols were considered. In the first protocol, only oscillating excitatory neurons were stimulated, and in the second — only excitable inhibitory neurons. Our results showed that the first stimulation protocol is more effective. For the first protocol, the entrainment of the network by an external stimulus was achieved with a four time lower mean absolute value of the stimulating current than for the second. The second example demonstrated the validity of our theory for the network of electrically coupled oscillating and excitable FHN neurons introduced in Ref. [82]. Finally, in the third example, we used the QIF neural network model, which allows an exact low-dimensional reduction of system equations in the thermodynamic limit of an infinite number of neurons [85, 86]. Based on the reduced macroscopic model, we derived a simple adjoint equation for the phase response curve, which is necessary to construct the optimal waveform for a large-scale network. The validity of the optimal waveform was confirmed by direct numerical simulation of a network consisting of 10^4 synaptically interacting QIF neurons. Although we presented the results for the case when all neurons of the network are stimulated by the same external current, our approach can be extended to the case of heterogeneous stimulation. In this case, the macroscopic model obtained in the thermodynamic limit will have a higher dimension.

Chapter 4

Suppression of synchronous spiking in two interacting populations of excitatory and inhibitory quadratic integrate-and-fire neurons

In this chapter, we demonstrate that mean-field equations are useful not only for understanding the occurrence of collective oscillations in large-scale neural networks, but also for understanding the effect of stimulation on synchronization processes. As an example, we consider a network of two interacting populations of excitatory and inhibitory QIF neurons. We show that HF stimulation of the inhibitory population is very effective in suppressing the collective synchronous spiking in both populations. The suppression mechanism is explained by the stabilization of the unstable incoherent state of the network. We also explain the oscillation suppression effect caused by an inhibitory pulse applied to the excitatory population.

This chapter is organized as follows. In Sec. 4.1 we describe a microscopic model of two interacting populations of QIF neurons and present the reduced mean-field equations for this model. Section 4.2 is devoted to bifurcation

analysis of the mean-field equations without stimulation. The effects of HF stimulation of the inhibitory population, as well as the inhibitory pulse applied to the excitatory population, are discussed in Sec. 4.3. In Sec. 4.4, we present the results of numerical simulations of the microscopic model and compare them with the results obtained from the mean-field equations. The conclusions and discussion are presented in Sec. 4.5.

4.1 The model

4.1.1 Microscopic description

We consider a heterogeneous network of two interacting populations of excitatory and inhibitory quadratic integrate-and-fire neurons, which are the canonical representatives for class I neurons near the spiking threshold [73]. The microscopic state of the network is determined by the set of $2N$ neurons' membrane potentials $\{V_j^{(E,I)}\}_{j=1,\dots,N}$, which satisfy the following system of $2N$ ordinary differential equations [80]:

$$\begin{aligned} \tau \dot{V}_j^{(E,I)} &= (V_j^{(E,I)})^2 + \eta_j^{(E,I)} + \mathcal{I}_j^{(E,I)}, \\ &\text{if } V_j^{(E,I)} \geq V_p \text{ then } V_j^{(E,I)} \leftarrow V_r. \end{aligned} \tag{4.1}$$

Here, τ is the membrane time constant and $V_j^{(E,I)}$ is the membrane potential of neuron j in either the excitatory (E) or the inhibitory (I) population. For simplicity, we set the number of neurons N and the time constant τ the same for both populations. The heterogeneous parameter of excitability $\eta_j^{(E,I)}$ is a current that specifies the behavior of each isolated neuron and the term $\mathcal{I}_j^{(E,I)}$ defines the synaptic coupling between neurons as well as external stimulation. The isolated neurons ($\mathcal{I}_j^{(E,I)} = 0$) with the negative value of the parameter $\eta_j^{(E,I)} < 0$ are at rest, while the neurons with the positive value of the parameter $\eta_j^{(E,I)} > 0$ generate instantaneous spikes, which are approximated by the Dirac delta function. The spikes are emitted at the moments when the membrane potential $V_j^{(E,I)}$ reaches a peak value V_p. Immediately after the spike emission the membrane potential is reset to a value V_r. Thereafter, we assume

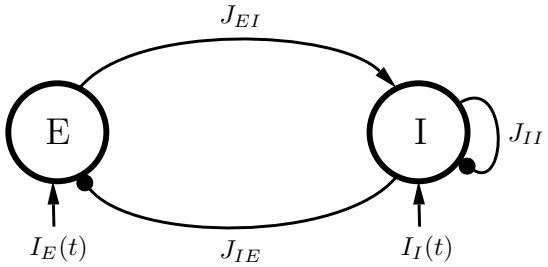

Figure 4.1 Symbolic depiction of a network of two neural populations. The large circles labeled "E" and "I" represent populations of excitatory and inhibitory neurons, respectively. The curve ending in an arrow shows excitatory coupling between populations E and I. J_{EI} is the coupling strength. Curves ending in solid circles indicate inhibitory couplings between populations I and E, as well as within population I. J_{IE} and J_{II} are the corresponding coupling strengths. The vertical arrows labeled $I_E(t)$ and $I_I(t)$ show the external stimulation currents applied to populations E and I.

$V_p = -V_r \to \infty$. With this assumption, a QIF neuron can be transformed into a theta neuron. This assumption is also crucial for the analytical treatment of the Eqs. (4.1) in an infinite size limit $N \to \infty$ [85]. The values of the heterogeneous parameter $\eta_j^{(E,I)}$ for both populations are independently taken from the Lorentzian distributions:

$$g_{E,I}(\eta) = \frac{1}{\pi} \frac{\Delta_{E,I}}{(\eta - \bar{\eta}_{E,I})^2 + \Delta_{E,I}^2}, \tag{4.2}$$

where $\Delta_{E,I}$ and $\bar{\eta}_{E,I}$ are respectively the width and the center of the distribution for the excitatory (E) and inhibitory (I) populations.

Finally, we discuss the last term $\mathcal{I}_j^{(E,I)}$ in Eqs. (4.1), which describes synaptic coupling and an external stimulation. For the excitatory and inhibitory populations this term respectively is

$$\mathcal{I}_j^{(E)} = -J_{IE} S_I(t) + I_E(t), \tag{4.3a}$$

$$\mathcal{I}_j^{(I)} = J_{EI} S_E(t) - J_{II} S_I(t) + I_I(t). \tag{4.3b}$$

Here, $S_E(t)$ and $S_I(t)$ determine the mean synaptic activation of E and I populations:

$$S_{E,I}(t) = \frac{\tau}{N} \sum_{j=1}^{N} \sum_{k \setminus (t_j^k)_{E,I} < t} \delta(t - (t_j^k)_{E,I}), \tag{4.4}$$

where $(t_j^k)_{E,I}$ is the time of the kth spike of the jth neuron in either E or I population and $\delta(t)$ is the Dirac delta function. The positive parameters J_{EI}, J_{IE} and J_{II} define synaptic weights. The current $-J_{IE}S_I(t)$ inhibits E neurons due to synaptic activity of I population, while the current $J_{EI}S_E(t)$ excites I neurons due to synaptic activity of E population. The term $-J_{II}S_I(t)$ determines recurrent inhibition of neurons within I population. For simplicity, we do not consider recurrent excitation within the E population, since it is not essential for the emergence of collective oscillations. The currents $I_E(t)$ and $I_I(t)$ represent external homogeneous stimulation of the excitatory and the inhibitory populations, respectively. Below we will consider stimulation protocols when either only inhibitory ($I_E(t) = 0$, $I_I(t) \neq 0$) or only excitatory ($I_E(t) \neq 0$, $I_I(t) = 0$) population is stimulated.

Note that the dynamics of a single population of QIF neurons interacting via instantaneous Dirac delta pulses was studied in detail in Ref. [85] and macroscopic limit cycle oscillations were not found in such a model. Macroscopic synchronized oscillations can occur in a single population when there is a delay in couplings [87–89] or when the finite width of synaptic pulses is taken into account [86]. However, two coupled populations of excitatory and inhibitory QIF neurons can generate macroscopic oscillations even when the interaction is provided by instantaneous Dirac delta pulses [93], and therefore we restrict our consideration to the simpler case of instantaneous interaction, as in the original paper [85].

The network architecture shown in Fig. 4.1, mimics the architecture of the neural network of the subthalamic nucleus (STN) and the external segment of the globus pallidus (GPe), which is often used to model Parkinson's disease (cf., e.g., Ref. [133]). STN is a network of excitatory neurons (in our case E population), and GPe consists of inhibitory neurons (in our case I population).

4.1.2 Macroscopic description: Low-dimensional mean-field equations in the limit $N \to \infty$

The advantage of the network model Eqs. (4.1) is that it allows one to derive precise low-dimensional mean-field equations in the thermodynamic limit of an infinite number of neurons, $N \to \infty$. We characterize the macroscopic dynamics of the network by four biophysically relevant quantities

$$v_{E,I} = \frac{1}{N}\sum_{j=1}^{N} V_j^{(E,I)}, \quad r_{E,I} = \tau \frac{M^{(E,I)}(\Delta t)}{N\Delta t}, \tag{4.5}$$

which represent the mean membrane potentials of the excitatory (E) and the inhibitory (I) populations and the dimensionless firing rates of E and I populations (the dimensional firing rates are $r_{E,I}/\tau$), respectively. Here, $M^{(E,I)}(\Delta t)$ is the number of spikes emitted in a small time window Δt in E and I populations. In the limit $N \to \infty$, the quantities $r_{E,I}(t)$ and $v_{E,I}(t)$ satisfy the exact system of four ordinary differential equations [85]:

$$\tau \dot{r}_E = \Delta_E/\pi + 2r_E v_E, \tag{4.6a}$$
$$\tau \dot{v}_E = \bar{\eta}_E + v_E^2 - \pi^2 r_E^2 - J_{IE} r_I + I_E(t), \tag{4.6b}$$
$$\tau \dot{r}_I = \Delta_I/\pi + 2r_I v_I, \tag{4.6c}$$
$$\tau \dot{v}_I = \bar{\eta}_I + v_I^2 - \pi^2 r_I^2 + J_{EI} r_E - J_{II} r_I + I_I(t). \tag{4.6d}$$

These low-dimensional mean-field equations greatly simplify the analysis of different network dynamics modes depending on system parameters, as well as the effect of stimulating current on network dynamics.

4.2 Network dynamics without stimulation

First, we analyze the dynamics of the network without stimulation, $I_E(t) = I_I(t) = 0$. An unperturbed network exhibits synchronized oscillations over a wide range of parameters. An example of network oscillations obtained by solving the Eqs. (4.6) for the set of parameters $\Delta_E = 0.05$, $\bar{\eta}_E = 0.5$, $\Delta_I = 0.5$,

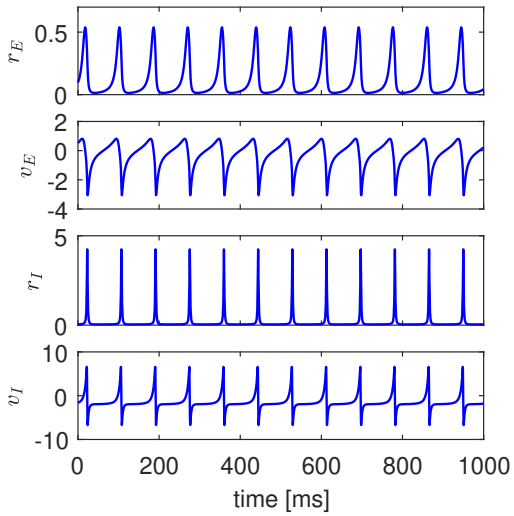

Figure 4.2 Dynamics of network macroscopic variables $r_E(t)$, $v_E(t)$, $r_I(t)$ and $v_I(t)$ obtained by solving the Eqs. (4.6) without stimulation, $I_E(t) = I_I(t) = 0$. The values of the parameters are: $\Delta_E = 0.05$, $\bar{\eta}_E = 0.5$, $\Delta_I = 0.5$, $\bar{\eta}_I = -4$, $J_{EI} = 20$, $J_{IE} = 5$, $J_{II} = 0.5$ and $\tau = 14$ ms.

$\bar{\eta}_I = -4$, $J_{EI} = 20$, $J_{IE} = 5$ and $J_{II} = 0.5$ is shown in Fig. 4.2. To get oscillations on a realistic time scale, we choose $\tau = 14$ ms, which corresponds to the membrane time constant of GPe neurons [134]. The oscillation period in the figure is $T_0 \approx 87$ ms.

Areas in the parameter space where network oscillations occur can be estimated using linear stability analysis of the Eqs. (4.6). Equating the right-hand side (RHS) of Eqs. (4.6) to zero, we can find the fixed points $(r_E^*, v_E^*, r_I^*, v_I^*)$ in the four dimensional phase space of the system. The problem leads to the solution of the 16th order polynomial equation

$$a_1[P(x)]^4 - (1+x)x^4[P(x)]^2 - a_2x^8 + a_3x^2[P(x)]^3 = 0 \qquad (4.7)$$

with respect to x, where

$$P(x) = a_5 + x^2 - a_4x^4 \qquad (4.8)$$

is a fourth order polynomial and the parameters a_j are:

$$a_1 = \frac{1}{\bar{\eta}_I}\left(\frac{\pi\bar{\eta}_E}{J_{IE}}\right)^2, \qquad a_2 = \frac{1}{\bar{\eta}_I}\left(\frac{J_{IE}\Delta_I}{2\pi\bar{\eta}_E}\right)^2, \qquad a_3 = \frac{\bar{\eta}_E J_{II}}{\bar{\eta}_I J_{IE}},$$
$$a_4 = \frac{1}{\bar{\eta}_E}\left(\frac{\pi\bar{\eta}_I}{J_{EI}}\right)^2, \qquad a_5 = \frac{1}{\bar{\eta}_E}\left(\frac{J_{EI}\Delta_E}{2\pi\bar{\eta}_I}\right)^2.$$

The solutions of the polynomial Eq. (4.7) are related to the coordinates of fixed points as follows:

$$r_E^* = \frac{\bar{\eta}_I}{J_{EI}}x, \qquad v_E^* = -\frac{J_{EI}\Delta_E}{2\pi\bar{\eta}_I}\frac{1}{x},$$
$$r_I^* = \frac{\bar{\eta}_E}{J_{IE}}\frac{P(x)}{x^2}, \qquad v_I^* = -\frac{J_{IE}\Delta_I}{2\pi\bar{\eta}_E}\frac{x^2}{P(x)}.$$

Numerical analysis of Eq. (4.7) shows that only one of its real-valued roots satisfies the requirement of non-negativity of spiking rates r_E^* and r_I^*, that is, the system has a single fixed point in the physically relevant region $r_E \geq 0$ and $r_I \geq 0$ of the phase space. The stability of this fixed point is determined by the eigenvalues λ of the characteristic equation

$$\det(\mathsf{J} - I\lambda) = 0, \tag{4.9}$$

where

$$\mathsf{J} = \frac{1}{\tau}\begin{pmatrix} 2v_E^* & 2r_E^* & 0 & 0 \\ -2\pi^2 r_E^* & 2v_E^* & -J_{IE} & 0 \\ 0 & 0 & 2v_I^* & 2r_I^* \\ J_{EI} & 0 & -(2\pi^2 r_I^* + J_{II}) & 2v_I^* \end{pmatrix} \tag{4.10}$$

is the Jacobi matrix of the system Eqs. (4.6) and I is the identity matrix. The fixed point is stable if the real parts of all eigenvalues λ are negative. With such parameter values, the network is at rest. At the microscopic level, neurons in this state exhibit incoherent behavior. If the real part of at least one of the eigenvalues λ is positive, then the state of rest becomes unstable. Numerical analysis shows that in this case neurons behave coherently, and periodic limit cycle oscillations appear in the network. Thus, solving the Eqs. (4.7) and (4.9)

gives us a simple sufficient condition for identifying areas in the parameter space where the network is in oscillatory mode. However, network oscillations can also occur in parameter areas where the resting state is stable. In such areas, the network demonstrates bistability. Along with a stable resting state, the network has a stable limit cycle.

The bistability regions are clearly visible in the one-parameter bifurcation diagrams shown in Fig. 4.3. These and other bifurcation diagrams presented in this chapter were built using the MatCont package [135]. Figure 4.3(a) shows change in the firing rate r_E of the excitatory population depending on the coupling strength J_{EI}. There are two bifurcation values of the coupling strength, at which the dynamics of the network changes qualitatively. At $J_{EI} \approx 12.6$, there is a limit point of cycles (LPC) bifurcation when two limit cycles, stable and unstable, collide and annihilate each other. At $J_{EI} \approx 16.35$, a subcritical Hopf (H^-) bifurcation occurs when an unstable limit cycle is absorbed by a stable spiral equilibrium. As J_{EI} increases, different dynamic modes are observed. For small values of the coupling strength $J_{EI} < 12.6$, the resting state is the only attractor. In the interval $12.6 < J_{EI} < 16.35$ between the LPC and H^- bifurcations, there are two attractors: a state of rest and a limit cycle. Finally, for $J_{EI} > 16.35$, the only attractor is the limit cycle. Figure 4.3(b) shows the evolution of network dynamics with a change in the coupling strength J_{IE}. As this parameter increases from zero, the oscillations manifest themselves through the supercritical Hopf (H^+) bifurcation at $J_{IE} \approx 0.13$. In the interval $0.13 < J_{IE} < 6.28$ between the supercritical and subcritical Hopf bifurcations, the only attractor is the limit cycle. In the interval $6.28 < J_{IE} < 7$ between the bifurcations H^- and LPC there is bistability, and for $J_{IE} > 7$ the rest state is the only attractor. Figure 4.3(c) shows that oscillations in the network occur with zero interaction within the inhibitory population, $J_{II} = 0$. As J_{II} increases, the oscillations persist until the LPC bifurcation, $J_{II} = 17.72$. At $J_{II} > 17.72$, the oscillations disappear, and the only attractor is the state of rest. The bistability is in the interval $9.3 < J_{II} < 17.72$ between the H^- and LPC bifurcations.

In Figs. 4.4(a) and 4.4(b), we present two-parameter bifurcation diagrams in the parameter planes (J_{IE}, J_{EI}) and (J_{II}, J_{EI}), respectively. The areas marked with Roman numerals represent the three different dynamic modes described

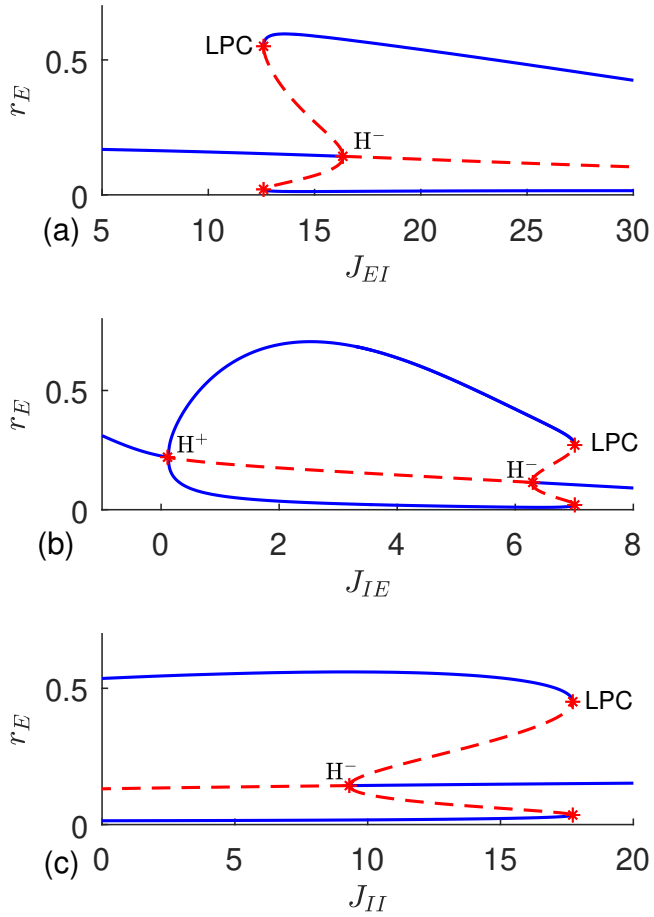

Figure 4.3 One-parameter bifurcation diagrams showing the evolution of the firing rate r_E depending on the coupling strengths (a) J_{EI}, (b) J_{IE} and (c) J_{II}. The rest of the parameters is fixed in the same way as in Fig. 4.2. The solid blue curves show the stable fixed point and the maximum and minimum of the stable limit cycle. The dashed red curves correspond to the unstable fixed point and the maximum and minimum of the unstable limit cycle. The red asterisks marked with the letters LPC, H^+ and H^- denote the limit point of cycles bifurcation, supercritical Hopf bifurcation and subcritical Hopf bifurcation, respectively.

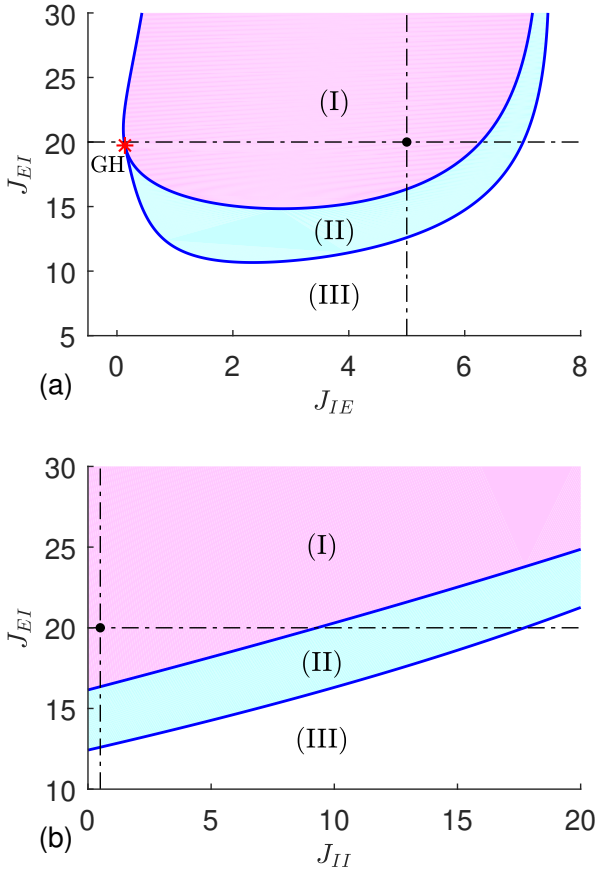

Figure 4.4 Two-parameter bifurcation diagrams in the planes of parameters (a) (J_{IE}, J_{EI}) and (b) (J_{II}, J_{EI}). Other parameters are the same as in Fig. 4.2. The areas marked with Roman numerals correspond to: (I) - the only stable limit cycle, (II) - bistability with a stable limit cycle and a stable resting state, and (III) - the only stable resting state. The red asterisk marked with letters GH denotes the generalized Hopf bifurcation point. The horizontal dash-dotted lines $J_{EI} = 20$ in (a) and (b) correspond to the one-parameter bifurcation diagrams shown in Figs. 4.3(b) and 4.3(c), respectively. The vertical dash-dotted lines $J_{IE} = 5$ in (a) and $J_{II} = 0.5$ in (b) correspond to the one-parameter bifurcation diagram shown in Fig. 4.3(a). The intersection of the horizontal and vertical lines represents the parameter values used in Fig. 4.2.

above. Specifically, in area (I) the only attractor is a limit cycle, in area (II) there is bistability with a stable limit cycle and a stable state of rest, and in area (III) the only attractor is a state of rest. We see that all modes occupy rather large areas in the parameter spaces, i.e., they are robust to parameter changes in wide intervals. Vertical and horizontal dash-dotted lines show cross-sections of two-parameter bifurcation diagrams, which correspond to one-parameter diagrams presented in Fig. 4.3 (see figure caption for details). The intersection of the horizontal and vertical lines represents the parameter values used in Fig. 4.2.

4.3 Suppressing synchronous spiking

4.3.1 High-frequency stimulation of the inhibitory population

We first show that synchronous spiking of the network can be effectively suppressed by high-frequency stimulation of the inhibitory population. We consider the network dynamics for $I_E(t) = 0$ and

$$I_I(t) = a\cos(\omega t), \tag{4.11}$$

where a is the amplitude and ω is the angular frequency of HF stimulation. The stimulation current Eq. (4.11) satisfies the clinically mandatory charge balance condition $\int_0^T I_I(t)dt = 0$, where $T = 2\pi/\omega$ is the stimulation period. We assume that the values of the parameters are chosen such that the free network has a single stable attractor of the limit cycle. We also assume that the stimulation frequency $\nu = 1/T$ is considerably greater than the frequency ν_0 of the limit cycle.

A numerical example of the effect of HF stimulation on network dynamics is shown in Fig. 4.5. The solid blue curves show the solution of the Eqs (4.6) for the same parameter values as in Fig. 4.2. For time $t < 500$ ms, the network is not perturbed and demonstrates exactly the same dynamics as in Fig. 4.2: It oscillates at a frequency of $\nu_0 = 1/T_0 \approx 11.5$ Hz. For $t \geq 500$ ms, HF

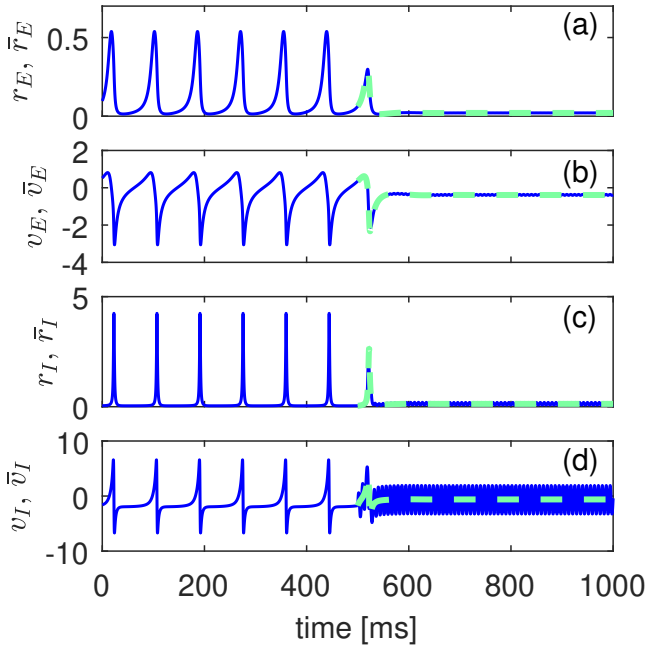

Figure 4.5 Suppression of network oscillations by HF stimulation of the inhibitory population. Thin solid blue curves show the dynamics of the variables $r_E(t)$, $v_E(t)$, $r_I(t)$ and $v_I(t)$ obtained by solving the Eqs. (4.6) for the same parameter values as in Fig. 4.2. For $t < 500$ ms, the network is not stimulated and demonstrates exactly the same dynamics as in Fig. 4.2, and at $t \geq 500$ ms, the HF stimulation of inhibitory neurons is activated with the frequency $\nu = 130$ Hz and the amplitude $a = 30$. The bold dashed green curves show dynamics of the variables $\bar{r}_E(t)$, $\bar{v}_E(t)$, $\bar{r}_I(t)$ and $\bar{v}_I(t)$ obtained by solving the averaged Eqs. (4.22).

stimulation of inhibitory neurons is activated with a frequency $\nu = 130$ Hz and an amplitude $a = 30$. We see that HF stimulation effectively suppresses synchronized spiking in the network. The spiking rates of excitatory and inhibitory neurons r_E and r_I drop to almost zero. The mean membrane potential v_E of the excitatory population becomes almost constant. The mean membrane potential v_I of the stimulated inhibitory population shows high-frequency oscillations around the resting state with a reduced amplitude.

To understand why HF stimulation of inhibitory neurons is so effective at suppressing network oscillations, we refer to the method of averaging [136], which is widely used in various fields of physics including vibrational

mechanics. This method makes it possible to explain the effect of oscillation suppression in terms of stabilizing the unstable resting state of the network. The effect is similar to stabilization of the upside-down position of a rigid pendulum by vibrating its pivot up and down at a suitably high frequency [137, 138]. A theoretical approach to solving the pendulum problem was first proposed by Kapitza [137]. It is based on dividing the dynamics of a pendulum into fast and slow motion and deriving an averaged equation for the slow dynamics of a pendulum. This approach has recently been applied to a single spiking neuron stimulated by a HF field [62]. Here, we adapt this approach to the network Eqs. (4.6).

To apply the averaging method to the Eqs. (4.6), we rewrite them in a more convenient form. We denote the dynamic variables of the first three equations, which do not contain the HF stimulation term, by a vector

$$\mathbf{q} = (r_E, v_E, r_I)^T. \tag{4.12}$$

Then the Eqs. (4.6) can be formally written as

$$\tau\dot{\mathbf{q}} = \mathbf{G}(\mathbf{q}, v_I), \tag{4.13a}$$

$$\tau\dot{v}_I = f(\mathbf{q}, v_I) + a\cos(\omega t), \tag{4.13b}$$

where $\mathbf{G}(\mathbf{q}, v_I)$ is a three-dimensional vector function defined by the RHS of the first three Eqs. (4.6a), (4.6b) and (4.6c) at $I_E(t) = 0$ and

$$f(\mathbf{q}, v_I) = \bar{\eta}_I + v_I^2 - \pi^2 r_I^2 + J_{EI} r_E - J_{II} r_I \tag{4.14}$$

is a scalar function defined by the RHS of the last Eq. (4.6d).

Our aim is to simplify the nonautonomous system Eqs. (4.13) for large frequencies ω. Using the small parameter $\varepsilon = (\omega\tau)^{-1} \ll 1$, we seek to eliminate the HF term $a\cos(\omega t)$ and obtain an autonomous system, the solutions of which approximate the original system. First, we change the

variables of the system Eqs. (4.13):

$$\mathbf{q}(t) = \mathbf{Q}(t), \tag{4.15a}$$

$$v_I(t) = V_I(t) + A\sin(\omega t) \tag{4.15b}$$

with

$$A = a/\omega\tau. \tag{4.16}$$

As in Ref [62], we assume that A is of order $O(1)$ with respect to the perturbation parameter ε. This means that we are considering the case of HF stimulation with large amplitudes, $a \sim O(\varepsilon^{-1})$. Only large amplitudes can have a noticeable effect when stimulated with frequencies significantly higher than the natural frequency of the network. The mathematical justification for this assumption can be found in the Appendix of Ref. [139]. Substituting Eqs. (4.15) into Eqs. (4.13), we derive the following equations for the new variables $\mathbf{Q}(t)$ and $V_I(t)$:

$$\tau\dot{\mathbf{Q}} = \mathbf{G}(\mathbf{Q}, V_I + A\sin(\omega t)), \tag{4.17a}$$

$$\tau\dot{V}_I = f(\mathbf{Q}, V_I + A\sin(\omega t)). \tag{4.17b}$$

By rescaling the time variable $\Theta = \omega t$ (here Θ is the "fast" time) system (4.17) can be transformed to the standard form of equations as typically used by the method of averaging [136]:

$$\frac{d\mathbf{Q}}{d\Theta} = \varepsilon\mathbf{G}(\mathbf{Q}, V_I + A\sin(\Theta)), \tag{4.18a}$$

$$\frac{dV_I}{d\Theta} = \varepsilon f(\mathbf{Q}, V_I + A\sin(\Theta)). \tag{4.18b}$$

Due to the small factor ε on the RHS of the Eqs. (4.18), the variables $\mathbf{Q}$ and V_I vary slowly, while the periodic functions in the RHS oscillate fast. In accordance with the averaging method [136], an approximate solution of the system Eqs. (4.18) can be obtained by averaging the RHS of the system over fast oscillations. Specifically, let us denote the variables of the averaged system

as $\bar{\mathbf{q}} = (\bar{r}_E, \bar{v}_E, \bar{r}_I)^T$ and $\bar{v}_I$. They satisfy the equations:

$$\frac{d\bar{\mathbf{q}}}{d\Theta} = \varepsilon \left\langle \mathbf{G}(\bar{\mathbf{q}}, \bar{v}_I + A\sin(\Theta)) \right\rangle_\Theta , \tag{4.19a}$$

$$\frac{d\bar{v}_I}{d\Theta} = \varepsilon \left\langle f(\bar{\mathbf{q}}, \bar{v}_I + A\sin(\Theta)) \right\rangle_\Theta . \tag{4.19b}$$

Here, the angle brackets denote the averaging over the period of the fast time $\langle(\cdots)\rangle_\Theta = (1/2\pi)\int_0^{2\pi}(\cdots)d\Theta$. The method of averaging states that the averaged system (4.19) approximates the solutions of the system (4.18) with the accuracy of $O(\varepsilon)$, i.e., $\mathbf{Q} = \bar{\mathbf{q}} + O(\varepsilon)$ and $V_I = \bar{v}_I + O(\varepsilon)$. After returning to the original time scale, the averaged system (4.19) takes the following form:

$$\tau\dot{\bar{\mathbf{q}}}(t) = \left\langle \mathbf{G}(\bar{\mathbf{q}}(t), \bar{v}_I(t) + A\sin(\Theta)) \right\rangle_\Theta , \tag{4.20a}$$

$$\tau\dot{\bar{v}}_I(t) = \left\langle f(\bar{\mathbf{q}}(t), \bar{v}_I(t) + A\sin(\Theta)) \right\rangle_\Theta . \tag{4.20b}$$

Here, the dot means differentiation by the original time t. Finally, the solution of the original non-autonomous system (4.13) can be expressed in terms of the solution of the averaged (autonomous) system (4.20) as follows:

$$\mathbf{q}(t) = \bar{\mathbf{q}}(t) + O(\varepsilon), \tag{4.21a}$$

$$v_I(t) = \bar{v}_I(t) + A\sin(\omega t) + O(\varepsilon). \tag{4.21b}$$

The substitution (4.15) and subsequent application of the averaging method allowed us to separate the slow and fast motion of the network and present the solution in the form of their superposition. The terms $\bar{\mathbf{q}}(t)$ and $\bar{v}_I(t)$ in the Eqs. (4.21) represent slow motion and satisfy the averaged Eqs. (4.20) while the term $A\sin(\omega t)$ describes high-frequency oscillations of the mean membrane potential of the stimulated inhibitory population.

After performing the averaging procedure in the Eqs. (4.20), we write them explicitly:

$$\tau\dot{\bar{r}}_E = \Delta_E/\pi + 2\bar{r}_E\bar{v}_E, \tag{4.22a}$$

$$\tau\dot{\bar{v}}_E = \bar{\eta}_E + \bar{v}_E^2 - \pi^2\bar{r}_E^2 - J_{IE}\bar{r}_I, \tag{4.22b}$$

$$\tau\dot{\bar{r}}_I = \Delta_I/\pi + 2\bar{r}_I\bar{v}_I, \tag{4.22c}$$

$$\tau\dot{\bar{v}}_I = \bar{\eta}_I^A + \bar{v}_I^2 - \pi^2\bar{r}_I^2 + J_{EI}\bar{r}_E - J_{II}\bar{r}_I. \tag{4.22d}$$

Formally, these equations are similar to the original Eqs. (4.6), but the HF term $I_I(t) = a\cos(\omega t)$ is excluded from the Eq. (4.6d) (recall that here we are considering the case $I_E(t) = 0$). The only difference between the Eqs (4.6) without stimulation and the averaged Eqs. (4.22) is that the parameter $\bar{\eta}_I$ is replaced by the parameter $\bar{\eta}_I^A$, whose value depends on the stimulation parameter A:

$$\bar{\eta}_I^A = \bar{\eta}_I + A^2/2. \tag{4.23}$$

In Fig. 4.5, we compare the solution of the averaged Eqs. (4.22) with the solution of the original Eqs. (4.6). For $t < 500$ ms, there is no stimulation ($a = 0$ and $A = 0$) and therefore $\bar{\eta}_I^A = \bar{\eta}_I$. In this case, the Eqs. (4.22) and (4.6) are identical and give exactly the same solution. For $t \geq 500$ ms, when stimulation is activated, the averaged Eqs. (4.22) (bold dashed green curves) also approximate well the solution of the original system Eqs. (4.6) (thin solid blue curves).

The connection of the averaged mean-field Eqs. (4.22) with the original unperturbed mean-field Eqs. (4.6) allows us to predict the effect of HF stimulation by analyzing the solutions of the unperturbed system and simply explain the oscillation suppression mechanism. According to Eq. (4.23), the effect of HF stimulation on the averaged dynamics of the network is a change in the parameter $\bar{\eta}_I$, which determines the center of the Lorentzian distribution $g_I(\eta)$ of inhibitory neurons. This center shifts to the right by a distance of $A^2/2$. As a result, the proportion of spiking neurons in the population increases, and the proportion of quenched neurons decreases. Thus, the inhibitory population becomes more active. A sufficient increase in the parameter $\bar{\eta}_I$ can lead to

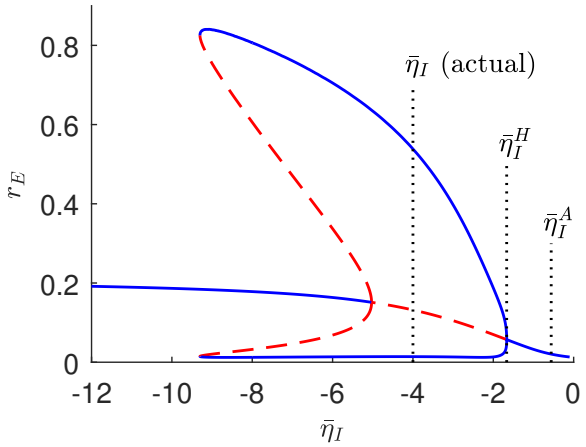

Figure 4.6 One-parameter bifurcation diagram of the unperturbed network showing the dependence of the firing rate r_E on the parameter $\bar{\eta}_I$. The rest of the parameters are fixed in the same way as in Fig. 4.2. The designations for the solid blue and dashed red curves are the same as in Fig. 4.4. Three vertical dotted lines show the actual value $\bar{\eta}_I = -4$ of the bifurcation parameter, the value $\bar{\eta}_I^H \approx -1.667$ of the supercritical Hopf bifurcation, and the value $\bar{\eta}_I^A \approx -0.559$ obtained from the Eq. (4.23) at stimulation frequency $\nu = 130$ Hz and amplitude $a = 30$.

stabilization of the initially unstable resting state of the network and, as a consequence, to the termination of oscillations.

The mechanism of stabilization of the resting state is evident from the one-parameter bifurcation diagram r_E versus $\bar{\eta}_I$ of the unperturbed system shown in Fig. 4.6. Three vertical dotted lines show the actual value $\bar{\eta}_I = -4$ of the bifurcation parameter, the value $\bar{\eta}_I^H \approx -1.667$ of the supercritical Hopf bifurcation, and the value $\bar{\eta}_I^A \approx -0.559$ obtained from Eq. (4.23) at stimulation frequency $\nu = 130$ Hz and amplitude $a = 30$. We see that the actual value of $\bar{\eta}_I$ is in the region where the limit cycle is stable, and the resting state is unstable. Due to HF stimulation, this value is shifted beyond the Hopf bifurcation point $\bar{\eta}_I^H$ to the position $\bar{\eta}_I^A$, where the resting state is stable.

In the general case, the condition for stabilization of the resting state is $\bar{\eta}_I^A > \bar{\eta}_I^H$ or $A^2 > 2(\bar{\eta}_I^H - \bar{\eta}_I)$. Taking into account the Eq. (4.16), this condition

can be written as

$$a > a_{\text{th}} \equiv 2\pi\nu\tau\sqrt{2(\bar{\eta}_I^H - \bar{\eta}_I)}, \tag{4.24}$$

where a_{th} is a threshold amplitude of the HF stimulation. When this amplitude is exceeded, the resting state of the averaged Eqs. (4.22) is stabilized, and the limit cycle oscillations in the original HF stimulated system Eqs. (4.6) are suppressed. Equation (4.24) shows that the threshold amplitude a_{th} is proportional to the stimulation frequency ν. Thus, with an increase in the frequency of stimulation, it is necessary to proportionally increase the amplitude of stimulation if we want to maintain a stable state of rest. Note that the Eq. (4.24) is only valid for sufficiently large frequencies $\nu \gg 1/2\pi\tau$. Information about the response of the network to stimulation at low frequencies, which are less or comparable to the limit cycle frequency, can be found by direct integration of the Eqs. (4.6). Figure 4.7 shows the result obtained by integrating the Eqs. (4.6) while changing both stimulation parameters, amplitude a and frequency ν. As a measure of the network's response to stimulation, we choose the standard deviation of the spiking rate of the excitatory population

$$\sigma = \sqrt{\langle [r_E(t) - \langle r_E(t)\rangle]^2\rangle}, \tag{4.25}$$

where angle brackets denote time average. Small values of this parameter correspond to a stable resting state of the network, and large values indicate oscillations of large amplitude. In Fig. 4.7, the values of σ in the parameter plane (ν, a) are shown in colors. White represents the area of suppressed oscillations. For high frequencies, the boundary of this area is in good agreement with the analytical curve of the threshold amplitude Eq. (4.24), which is shown by the solid red curve. For low frequencies, stimulation increases the oscillation amplitude. In the region $\nu < 8$ Hz, the standard deviation is significantly larger than the value of $\sigma \approx 0.15$ observed in the network without stimulation. Interestingly, the white area in Fig. 4.7 resembles an experimentally obtained area on the plane of the parameters of frequency and intensity of stimulation, where tremor in patients with Parkinson's disease was eliminated by stimulation of the ventral intermediate thalamic nucleus [25].

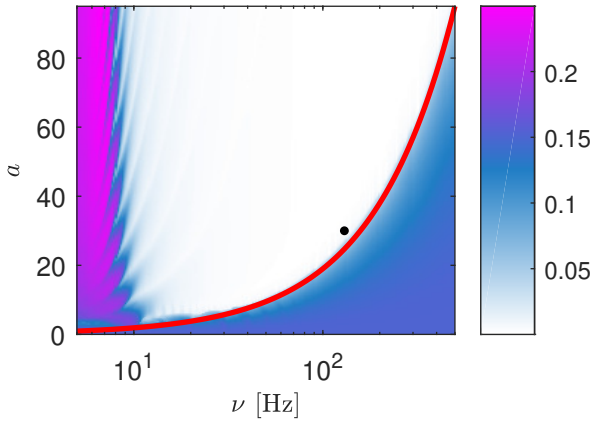

Figure 4.7 Network response to stimulation of the inhibitory population depending on the stimulation frequency ν and the amplitude a. The colors show the values of the standard deviation σ, estimated by the Eq. (4.25) using a 5000 ms time window for averaging. White represents an area of suppressed oscillations. Without stimulation ($a = 0$), the standard deviation is $\sigma \approx 0.15$. The solid red curve shows the analytical threshold amplitude Eq. (4.24). The black dot denotes the values of the (ν, a) parameters used in Fig. 4.5.

4.3.2 Suppression of oscillations by controlling the excitatory population

Next, we will consider the possibility of suppressing network oscillations by HF stimulation of the excitatory population. Now we put $I_I(t) = 0$ and

$$I_E(t) = a\cos(\omega t). \tag{4.26}$$

Applying the averaging method to the Eqs. (4.6), we can derive an autonomous system of averaged equations, similar to the Eqs. (4.22), but now the parameter $\bar{\eta}_I$ remains unchanged, and the parameter $\bar{\eta}_E$ will be modified as

$$\bar{\eta}_E \rightarrow \bar{\eta}_E^A = \bar{\eta}_E + A^2/2. \tag{4.27}$$

An increase in the $\bar{\eta}_E$ parameter means that the proportion of spiking neurons in the excitatory population increases, while the proportion of quenched neurons decreases. As a result, the excitatory population becomes more active and, in

contrast to the case of stimulation of the inhibitory population, the oscillatory effects are now enhanced. Figure 4.8 provides a graphical explanation of why the effects of HF stimulation of excitatory and inhibitory populations are different. Here, we show a two-parameter bifurcation diagram of the network without stimulation in the plane $(\bar{\eta}_I, \bar{\eta}_E)$. As in Fig. 4.4, the areas marked with Roman numerals correspond to different dynamic modes of the network: (I) – the only stable limit cycle, (II) – bistability and (III) – the only stable state of rest. The black dot in area (I) indicates the actual values of the parameters. The stimulating effect of the inhibitory population is shown by the solid horizontal arrow. As a result of stimulation, the dot showing the actual values of the parameters is shifted to the right to the region (III), where the state of rest is stable and, thus, the oscillations are suppressed. The stimulating effect of the excitatory population is shown by the dashed vertical arrow. Now the dot shifts upward and remains in area (I), where the limit cycle is the only attractor and, thus, the oscillations are preserved.

Although HF stimulation of the excitatory population is ineffective in suppressing network oscillations, in some cases we can still eliminate oscillations by applying a different type of control signal to the excitatory population. This is possible if the network parameters are in the bistable area, and the network is in the oscillatory mode. In this case, the network can be switched from stable periodic oscillations to a stable state of rest by applying a single inhibitory rectangular pulse to the excitatory population. The idea of this control algorithm is graphically illustrated in Fig. 4.8. We assume that the actual values of the parameters $(\bar{\eta}_I, \bar{\eta}_E)$ without stimulation are located in the bistable area (II). They are marked with a cross. We suppose that the network is in the oscillatory mode. We then apply a negative rectangular pulse $I_E(t)$ with amplitude $\Delta I_E < 0$ and duration Δt to the excitatory population, as shown in Fig. 4.9 (e). Since the parameters I_E and $\bar{\eta}_E$ enter into the Eq. (4.6b) as a sum, we can interpret this pulse as it applies to the $\bar{\eta}_E$ parameter not to I_E. In Fig. 4.8, we demonstrate this interpretation using the vertical double arrow connecting the cross with the square, which shows the values of the $(\bar{\eta}_I, \bar{\eta}_E)$ parameters when $I_E = \Delta I_E$. For sufficiently large pulse amplitude ΔI_E, parameter values marked with a square appear in area (III), where the

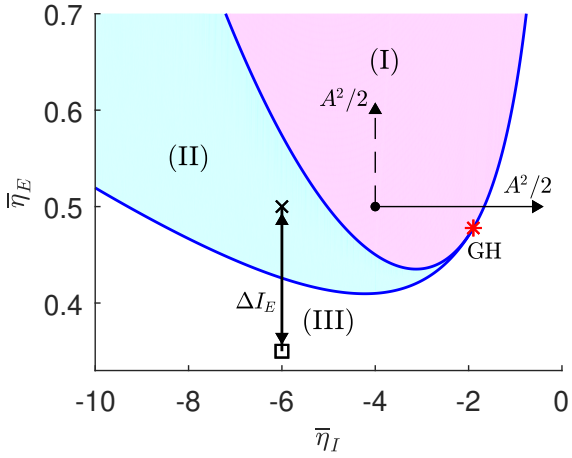

Figure 4.8 Two-parameter bifurcation diagram of the network without stimulation in the plane $(\bar{\eta}_I, \bar{\eta}_E)$. As in Fig. 4.4, the areas marked with Roman numerals correspond to different dynamic modes of the network: (I) – the only stable limit cycle, (II) – bistability with a stable limit cycle and a stable state of rest, and (III) – the only stable state of rest. The red asterisk marked with letters GH denotes the point of the generalized Hopf bifurcation. The black dot in area (I) indicates the values of the parameters used in Fig. 4.5. HF stimulating effect of the inhibitory population is shown by the solid horizontal arrow. The vertical dashed arrow shows the effect of HF stimulation of the excitatory population. The cross in area (II) indicates the values of the parameters used in Fig. 4.9. The double vertical arrow connecting the cross to the square corresponds to the inhibitory pulse applied to the excitatory population. The pulse dynamics is shown in Fig. 4.9(e).

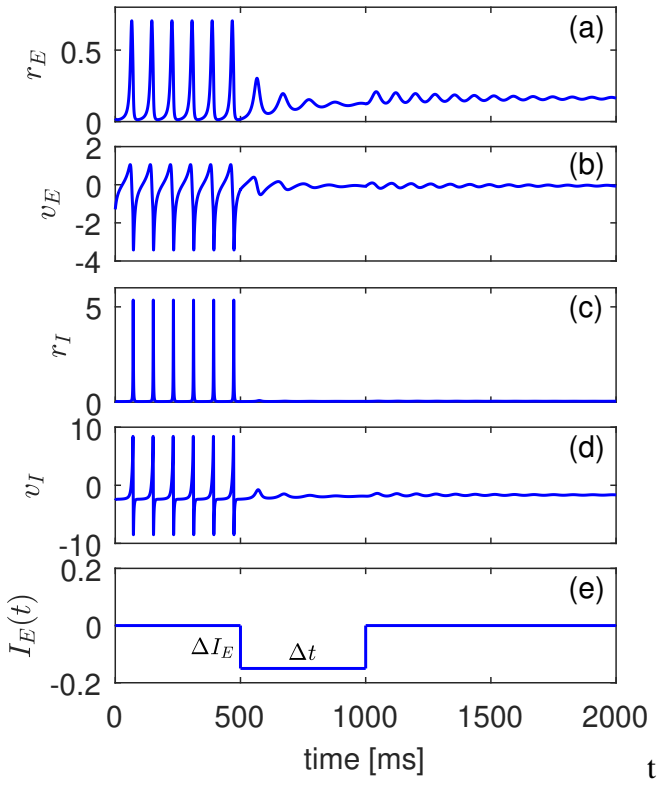

Figure 4.9 Elimination of network oscillations using an inhibitory pulse applied to the excitatory population. Dynamics of variables (a) $r_E(t)$, (b) $v_E(t)$, (c) $r_I(t)$ and (d) $v_I(t)$ obtained by solving the Eqs. (4.6) with the inhibitory pulse $I_E(t)$ shown in (e). Pulse amplitude is $\Delta I_E = -0.15$ and duration $\Delta t = 500$ ms. The parameters except for $\bar{\eta}_I = -6$ are the same as in Fig. 4.2.

fixed point is the only attractor. If the pulse duration Δt is long enough, the system will approach the fixed point. We expect that for two different values of the parameters marked with a cross ($I_E = 0$) and a square ($I_E = \Delta I_E$), the coordinates of fixed points in the phase space are close to each other, so that at the end of the pulse the state of the system will be in the basin of attraction of a fixed point corresponding to the value $I_E = 0$. Then, being in the bistable area, the system will approach a stable fixed point and remain at rest at zero stimulation current $I_E = 0$.

In Fig. 4.9, we demonstrate the efficiency of this algorithm for $\bar{\eta}_I = -6$ and other parameters such as in Fig. 4.2. This set of parameters is in the bistable area (II), as shown in Fig. 4.8. Figures 4.9(a), 4.9(b), 4.9(c) and 4.9(d) show, respectively, the dynamics of variables r_E, v_E, r_I and v_I obtained by integrating the Eqs. (4.6) with inhibitory pulse $I_E(t)$ shown in Fig. 4.9(e). As expected, this pulse stops the oscillation in the network, and the network remains at rest without further stimulation. Note that unlike the HF current Eq. (4.11), the inhibitory pulse used here does not satisfy the charge balance condition. However, this condition is not required for single pulse stimulation.

4.4 Modeling microscopic dynamics

The reduced mean-field Eqs. (4.6) are derived in the limit of an infinite-size network, while realistic networks consist of a finite number of neurons. To test if the control algorithms described above work for networks of finite size, here we perform a direct numerical simulation of the microscopic dynamics described by the Eqs. (4.1).

Numerical simulation of the Eqs. (4.1) is more convenient after changing the variables

$$V_j^{(E,I)} = \tan\left(\theta_j^{(E,I)}/2\right) \tag{4.28}$$

that turn QIF neurons into theta neurons. Such a transformation of variables avoids the problem associated with jumps of infinite size (from $+\infty$ to $-\infty$) of the membrane potential $V_j^{(E,I)}$ of the QIF neuron at the moments of firing. The phase $\theta_j^{(E,I)}$ of the theta neuron simply crosses the value of $\theta_j^{(E,I)} = \pi$ at these

moments. For theta neurons, the Eqs. (4.1) are transformed into

$$\begin{aligned}\tau\dot{\theta}_j^{(E,I)} &= 1-\cos\left(\theta_j^{(E,I)}\right)\\ &\quad+\left[1+\cos\left(\theta_j^{(E,I)}\right)\right]\left[\eta_j^{(E,I)}+\mathcal{I}_j^{(E,I)}\right].\end{aligned} \tag{4.29}$$

These equations were integrated by the Euler method with a time step of $dt = 5\times 10^{-4}$. Two populations of theta excitatory and inhibitory neurons each consisting of $N = 2000$ units with the Lorentzian distributions (4.2) were deterministically generated using $\eta_j^{(E,I)} = \bar{\eta}_{E,I} + \Delta_{E,I}\tan\left[(\pi/2)(2j-N-1)/(N+1)\right]$, $j = 1,\ldots,N$. More information on numerical modeling of Eqs. (4.29) can be found in Ref. [86]. To compare the results obtained from the microscopic model Eqs. (4.29) with the solutions of the reduced system Eqs. (4.6), we calculate the Kuramoto order parameters [83]

$$Z_{E,I} = \frac{1}{N}\sum_{j=1}^{N}\exp\left(i\theta_j^{E,I}\right) \tag{4.30}$$

for each population and use the relationship between $Z_{E,I}$ and the spiking rate $r_{E,I}$ [85]:

$$r_{E,I} = \frac{1}{\pi}\,\mathrm{Re}\left(\frac{1-Z_{E,I}^*}{1+Z_{E,I}^*}\right), \tag{4.31}$$

where $Z_{E,I}^*$ means complex conjugate of $Z_{E,I}$.

In Fig. 4.10, we show the results of HF stimulation of the inhibitory population, obtained from the Eqs. (4.29). The parameter values are the same as in Fig. 4.5. Here, as in Fig. 4.5, HF stimulation with an amplitude $a = 30$ and a frequency $\nu = 130$ Hz is activated at $t > 500$ ms. We see that the dynamics of the spiking rates of excitatory and inhibitory populations shown in Figs. 4.10(a) and 4.10(c) are similar to those shown in Figs. 4.5(a) and 4.5(c), respectively. Thus, the mean-field Eqs. (4.6) are robust, they predict well the macroscopic dynamics of a finite size network consisting of $N = 2000$ neurons in each population. Microscopic network behavior can be seen in Figs. 4.10(b) and 4.10(d), which show raster plots of 500 randomly selected neurons in populations E and I, respectively. Without stimulation ($t < 500$ ms), most

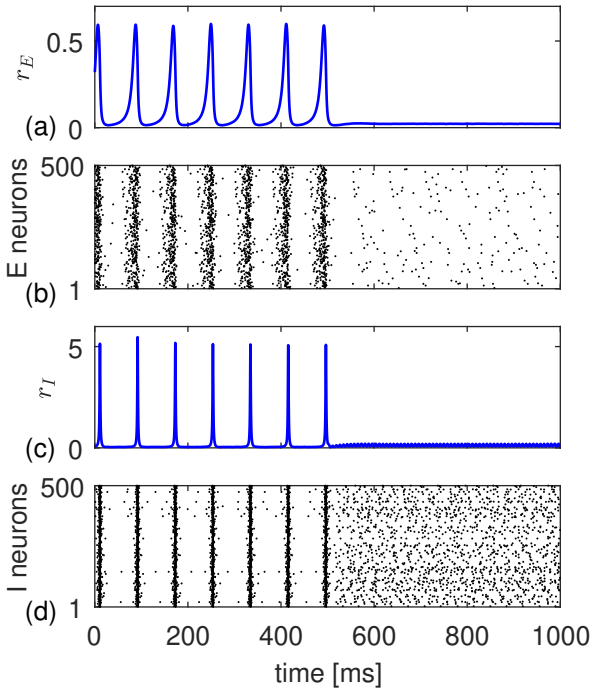

Figure 4.10 The effect of HF stimulation of the inhibitory population, obtained using the microscopic model Eqs. (4.29). The number of neurons in the excitatory and inhibitory populations is the same, $N = 2000$. All parameters are the same as in Fig. 4.5, and HF stimulation with the amplitude $a = 30$ and the frequency $\nu = 130$ Hz is also turned on at $t = 500$ ms, as in Fig. 4.5. (a) and (c) Dynamics of the spiking rates of the populations E and I, respectively. (b) and (d) Raster plots of 500 randomly selected neurons in populations E and I, respectively. Here, the dots show the spike moments for each neuron, where the vertical axis indicates neuron numbers.

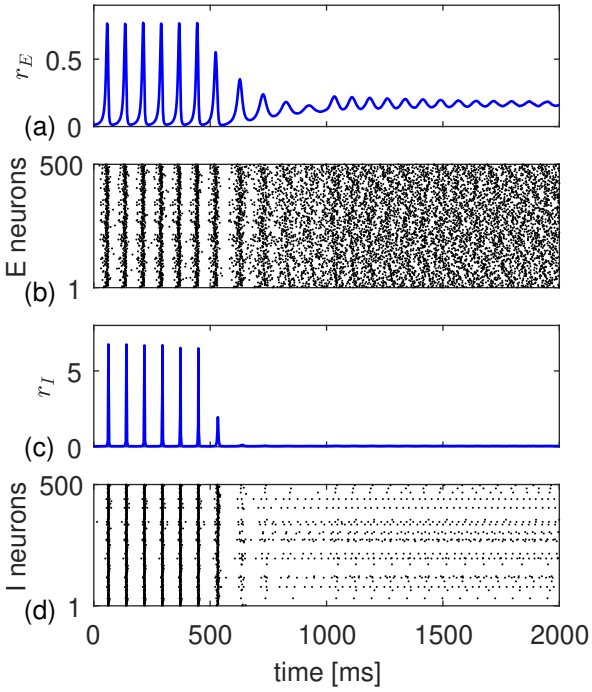

Figure 4.11 The effect of an inhibitory pulse applied to the excitatory population, obtained from the microscopic model Eqs. (4.29). The number of neurons in the excitatory and inhibitory populations is $N = 2000$. All parameters are the same as in Fig. 4.9 and the pulse shape is the same as in Fig. 4.9(e). (a) and (c) Dynamics of the spiking rates of the populations E and I, respectively. (b) and (d) Raster plots of 500 randomly selected neurons in populations E and I, respectively.

neurons in excitatory and inhibitory populations exhibit coherent behavior and produce macroscopic periodic oscillations. HF stimulation ($t > 500$ ms) increases the number of active neurons in the inhibitory population, which eliminates the coherent spiking in both populations, and the initially unstable incoherent resting state is stabilized.

Figure 4.11 shows the effect of an inhibitory pulse applied to the excitatory population, obtained from the microscopic model Eqs. (4.29). The values of the parameters are the same as in Fig. 4.9 and the pulse shape is the same as in Fig. 4.9(e). Again we see that the mean-field Eqs. (4.6) predict well

the macroscopic dynamics of a finite size network described by Eqs. (4.29). The dynamics of the spiking rates of excitatory $r_E(t)$ and inhibitory $r_I(t)$ populations shown in Figs. 4.11(a) and 4.11(c) are similar to those presented in Figs. 4.9(a) and 4.9(c), respectively. Raster plots in Figs. 4.11(b) and 4.11(d) show the microscopic network dynamics. Before the pulse ($t < 500$ ms), most neurons in the excitatory and inhibitory populations behave coherently and produce macroscopic periodic oscillations, which represent one of the two stable modes of the network. A negative pulse with amplitude $\Delta I_E = -0.15$, lasting in the interval 500 ms $< t <$ 1000 ms, transfers the system to an incoherent resting state, which is the only stable state for the given values of the parameters. For $t > 1000$ ms, when the pulse is off, the network remains in a stable incoherent resting state. Note the different point densities on raster plots of populations E and I in incoherent state. This is due to the fact that in population E, a greater proportion of neurons generates spikes than in population I.

4.5 Summary

We have analyzed the dynamics of a free and stimulated network of two globally connected neural populations consisting of excitatory and inhibitory quadratic integrate-and-fire neurons. Interaction within and between populations is provided by instantaneous pulses. Both populations are heterogeneous and contain a mixture of at-rest but excitable neurons as well as spontaneously spiking neurons. The heterogeneity is determined by the Lorentzian distribution of the excitability parameter. A model built on these assumptions has two important advantages. First, in the limit of an infinite number of neurons, an exact system of low-dimensional mean-field equations can be obtained. Second, the mean-field equations represent a universal macroscopic model for a large class of neural networks, because they are derived from the microscopic dynamics of QIF neurons, which are the normal form of class I neurons. In contrast to phenomenological neural mass models [140], the mean-field equations considered here accurately reproduce the dynamics of

spiking neurons for any degree of synchronization and can be considered as next generation neural mass models [141].

Relatively simple mean field equations make it possible to conduct a thorough bifurcation analysis of various dynamic modes of a free network and to reveal the mechanisms of action of various stimulation algorithms. We performed a bifurcation analysis of a free network depending on the coupling strengths J_{EI} and J_{IE} of the bidirectional interaction between excitatory and inhibitory populations and the coupling strength J_{II}, which determines the interaction within the inhibitory population. We also built a bifurcation diagram in the plane of the parameters $(\bar{\eta}_I, \bar{\eta}_E)$, which determine the centers of the distributions of the excitability parameter for inhibitory and excitatory populations. As a result of this analysis, three different modes were established. Depending on the values of the parameters, the system can have a single stable fixed point, a single stable limit cycle, or be in a bistable mode with these two coexisting attractors. All three modes occupy rather large areas in the parameter spaces, which means that they are robust to parameter changes in wide intervals.

As the next step in our analysis, we looked at the problem of controlling network synchronization. Pathological synchronized oscillations can be the cause of various neurological diseases, and attempts are made to suppress them using external stimulation. Some neurological diseases are successfully treated with high-frequency stimulation. Here, we tested the effectiveness of the HF algorithm for suppressing synchronous spiking in the network of excitatory and inhibitory QIF neurons. We have shown that HF stimulation of the inhibitory population is very effective, whereas HF stimulation of the excitatory population cannot suppress the oscillations. The mechanism of action of HF stimulation is explained using mean-field equations averaged over the stimulation period. The averaged mean-field equations are equivalent to the free mean-field equations, but with a modified parameter $\bar{\eta}_I$ or $\bar{\eta}_E$, depending on which inhibitory or excitatory population is stimulated. When HF stimulation is applied to the inhibitory population, changing the $\bar{\eta}_I$ parameter increases the proportion of spiking neurons in that population. This leads to the stabilization of the state of rest of the network and the termination of oscillations. The averaged mean-field

equations made it possible to obtain an analytical expression for the threshold amplitude of HF stimulation, which stabilizes the resting state. This amplitude is proportional to the frequency of stimulation.

HF stimulation of the excitatory population is ineffective, since changing the $\bar{\eta}_E$ parameter increases the proportion of spiking neurons in the excitatory population and cannot stabilize the resting state of the network. Nevertheless, stopping the network oscillation by controlling the excitatory population can still be achieved if the system parameters are in the bistable area. By applying a rectangular inhibitory pulse to this population, the network state can be switched from the stable limit cycle to the stable state of rest. Such a pulse moves the system parameters to the area where the state of rest is the only attractor, and then returns them back to the bistable area. As a result, the system approaches the stable state of rest, being in the bistable region, and remains in this state in the absence of stimulation.

To test the performance of the above stimulation algorithms for finite-size networks, we numerically simulated the equations of the microscopic model. Modeling networks with 2000 excitatory and 2000 inhibitory QIF neurons gave results that are in good agreement with the results obtained from the mean-field equations. Based on our research, we believe that mean-field equations derived from the microscopic dynamics of interacting QIF neurons can serve as an effective tool for developing various stimulation algorithms to control synchronization processes in large-scale neural networks.

Results and conclusions

1. The optimal charge-balanced waveform that ensures the entrainment of a spiking neuron to a periodic external stimulation with the minimum mean absolute value of the stimulating current is of the bang-off-bang type: it consists of two rectangular pulses, one positive and the other negative, generally of different amplitudes and widths, located at the extrema of the phase response curve of the neuron. The validity of this optimization theory is confirmed for the analytically solvable Stuart-Landau oscillator, a randomly generated phase response curve and the classical Hodgkin-Huxley neuron model.

2. Along with minimizing tissue damage, the minimum-charge control algorithm has another practical advantage: for a small frequency mismatch, in the linear part of the Arnold tongue, where the amplitude restriction is not significant, the minimum-charge waveform depends only on the distance between the absolute extrema of the PRC and the PRC amplitude. This allows estimating the stimulation parameters empirically, without recourse to the neuron model and the phase reduction theory.

3. Network equations can also be reduced to the same phase equation as for a single neuron; in this case the phase response curve of the neuron is replaced by an effective phase response curve of the network. As for a single neuron, the optimal waveform of the network is of the bang-off-bang type with periodically repeated positive and negative rectangular pulses, generally of different amplitudes and widths, determined by the distance between the absolute maximum and the absolute minimum of the effective network PRC and its amplitude.

4. The theoretical results are confirmed by three numerical examples: two small-scale networks of synaptically and electrically coupled FHN neurons, and a large-scale network of 10^4 synaptically coupled QIF neurons. In the first example, the results show that stimulating only the oscillating excitatory neurons of the network is more effective than other stimulation protocols and achieves entrainment with a four times lower mean absolute value of the stimulating current.

5. A network of two globally connected neural populations of excitatory and inhibitory quadratic integrate-and-fire neurons exhibits three possible dynamic modes: a single stable fixed point, a single stable limit cycle, or a bistable mode with these two coexisting attractors. All three modes occupy rather large areas in the parameter spaces, which means that they are robust to parameter changes in wide intervals.

6. The averaged mean-field equations over the period of HF stimulation are equivalent to the free mean-field equations but with a modified excitability parameter. Applying high-frequency stimulation to the inhibitory population increases the proportion of spiking neurons, which stabilizes the unstable incoherent resting state of the network and the termination of collective oscillations. In the HF domain the stimulation threshold amplitude is proportional to the frequency of stimulation.

7. High-frequency stimulation of the excitatory population is ineffective in suppressing network oscillation, because it increases the proportion of spiking neurons in the excitatory population. Nevertheless, stopping the network oscillation by controlling the excitatory population can still be achieved if the system parameters are in the bistable area. By applying a rectangular inhibitory pulse to this population, the system parameters move to the region where the state of rest is the only attractor and then return to the bistable area. As a result, the system approaches the stable incoherent state of rest and remains in this state in the absence of stimulation.

8. Based on the conducted research, it can be stated that mean-field equations derived from the microscopic dynamics of interacting QIF neurons can serve as an effective tool for developing various stimulation algorithms to control synchronization processes in large-scale neural networks.

Bibliography

[1] Alex Arenas, Albert Díaz-Guilera, Jurgen Kurths, Yamir Moreno, and Changsong Zhou. "Synchronization in complex networks". In: *Physics Reports* 469.3 (Dec. 2008), pp. 93–153.

[2] F. Dorfler, M. Chertkov, and F. Bullo. "Synchronization in complex oscillator networks and smart grids". In: *Proceedings of the National Academy of Sciences* 110.6 (Jan. 2013), pp. 2005–2010.

[3] M. A. Galin et al. "Synchronization of Large Josephson-Junction Arrays by Traveling Electromagnetic Waves". In: *Physical Review Applied* 9.5 (May 2018), p. 054032.

[4] Mian Zhang et al. "Synchronization of Micromechanical Oscillators Using Light". In: *Physical Review Letters* 109.23 (Dec. 2012), p. 233906.

[5] Aaron M. Hagerstrom et al. "Experimental observation of chimeras in coupled-map lattices". In: *Nature Physics* 8.9 (July 2012), pp. 658–661.

[6] Ramon Guevara Erra, Jose L. Perez Velazquez, and Michael Rosenblum. "Neural Synchronization from the Perspective of Non-linear Dynamics". In: *Frontiers in Computational Neuroscience* 11 (Oct. 2017), p. 98.

[7] Wolf Singer. "Neuronal Synchrony: A Versatile Code for the Definition of Relations?" In: *Neuron* 24.1 (Sept. 1999), pp. 49–65.

[8] Juergen Fell and Nikolai Axmacher. "The role of phase synchronization in memory processes". In: *Nature Reviews Neuroscience* 12.2 (Jan. 2011), pp. 105–118.

[9] Constance Hammond, Hagai Bergman, and Peter Brown. "Pathological synchronization in Parkinson's disease: Networks, models and treatments". In: *Trends in Neurosciences* 30.7 (July 2007), pp. 357–364.

[10] Premysl Jiruska et al. "Synchronization and desynchronization in epilepsy: Controversies and hypotheses. Synchronization in epilepsy". In: *The Journal of Physiology* 591.4 (Jan. 2013), pp. 787–797.

[11] Moritz Gerster et al. "FitzHugh–Nagumo oscillators on complex networks mimic epileptic-seizure-related synchronization phenomena". In: *Chaos: An Interdisciplinary Journal of Nonlinear Science* 30.12 (Dec. 2020), p. 123130. eprint: `https://doi.org/10.1063/5.0021420`.

[12] Peter A. Tass and Oleksandr V. Popovych. “Unlearning tinnitus-related cerebral synchrony with acoustic coordinated reset stimulation: Theoretical concept and modelling”. In: *Biological Cybernetics* 106.1 (Jan. 2012), pp. 27–36.

[13] Peter A. Tass. “A model of desynchronizing deep brain stimulation with a demand-controlled coordinated reset of neural subpopulations”. In: *Biological Cybernetics* 89.2 (Aug. 2003), pp. 81–88.

[14] Oleksandr V. Popovych and Peter A. Tass. “Control of Abnormal Synchronization in Neurological Disorders”. In: *Frontiers in Neurology* 5.268 (Dec. 2014), p. 268.

[15] Michael G. Rosenblum and Arkady S. Pikovsky. “Controlling Synchronization in an Ensemble of Globally Coupled Oscillators”. In: *Physical Review Letters* 92.11 (Mar. 2004), p. 114102.

[16] Oleksandr V. Popovych, Christian Hauptmann, and Peter A. Tass. “Effective Desynchronization by Nonlinear Delayed Feedback”. In: *Physical Review Letters* 94.16 (Apr. 2005), p. 164102.

[17] Oleksandr V. Popovych, Borys Lysyansky, Michael Rosenblum, Arkady Pikovsky, and Peter A. Tass. “Pulsatile desynchronizing delayed feedback for closed-loop deep brain stimulation”. In: *Plos One* 12.3 (Mar. 2017). Ed. by Miguel A. F. Sanjuán, e0173363.

[18] K. Pyragas, O. V. Popovych, and P. A. Tass. “Controlling synchrony in oscillatory networks with a separate stimulation-registration setup”. In: *Europhysics Letters (EPL)* 80.4 (Oct. 2007), p. 40002.

[19] Irmantas Ratas and Kestutis Pyragas. “Controlling synchrony in oscillatory networks via an act-and-wait algorithm”. In: *Physical Review E* 90.3 (Sept. 2014), p. 032914.

[20] Irmantas Ratas and Kestutis Pyragas. “Eliminating synchronization in bistable networks”. In: *Nonlinear Dynamics* 83.3 (Sept. 2015), pp. 1137–1151.

[21] Dan Wilson. “Optimal open-loop desynchronization of neural oscillator populations”. In: *Journal of Mathematical Biology* 81.1 (May 2020), pp. 25–64.

[22] Elena Adomaitienė, Skaidra Bumelienė, and Arūnas Tamaševičius. “Local control of an array of the globally coupled oscillators”. In: *Nonlinear Dynamics* 99.3 (Dec. 2019), pp. 2129–2137.

[23] Elena Adomaitienė, Skaidra Bumelienė, and Arūnas Tamaševičius. “Suppressing synchrony in an array of the modified FitzHugh–Nagumo oscillators by filtering the mean field”. In: *Journal of Applied Physics* 125.10 (Mar. 2019), p. 104902.

[24] Elena Adomaitienė, Steponas Ašmontas, Skaidra Bumelienė, and Arūnas Tamaševičius. “Quenching coupled FitzHugh-Nagumo oscillators by repulsive feedback”. In: *Physica Scripta* 95.10 (Sept. 2020), p. 105202.

[25] A.L. Benabid et al. “Long-term suppression of tremor by chronic stimulation of the ventral intermediate thalamic nucleus”. In: *The Lancet* 337.8738 (Feb. 1991), pp. 403–406.

[26] Paul Krack et al. “Five-Year Follow-up of Bilateral Stimulation of the Subthalamic Nucleus in Advanced Parkinson’s Disease”. In: *New England Journal of Medicine* 349.20 (Nov. 2003), pp. 1925–1934.

[27] Günther Deuschl et al. “A Randomized Trial of Deep-Brain Stimulation for Parkinson’s Disease”. In: *New England Journal of Medicine* 355.9 (Aug. 2006), pp. 896–908.

[28] Morten L. Kringelbach, Ned Jenkinson, Sarah L.F. Owen, and Tipu Z. Aziz. “Translational principles of deep brain stimulation”. In: *Nature Reviews Neuroscience* 8.8 (Aug. 2007), pp. 623–635.

[29] Joel S. Perlmutter and Jonathan W. Mink. “Deep Brain Stimulation”. In: *Annual Review of Neuroscience* 29.1 (July 2006), pp. 229–257.

[30] William C. Koller, Kelly E. Lyons, Steven B. Wilkinson, Alexander I. Troster, and Rajesh Pahwa. “Long-term safety and efficacy of unilateral deep brain stimulation of the thalamus in essential tremor”. In: *Movement Disorders* 16.3 (May 2001), pp. 464–468.

[31] Marie Vidailhet et al. “Bilateral Deep-Brain Stimulation of the Globus Pallidus in Primary Generalized Dystonia”. In: *New England Journal of Medicine* 352.5 (Feb. 2005), pp. 459–467.

[32] David E. Hardesty and Harold A. Sackeim. “Deep Brain Stimulation in Movement and Psychiatric Disorders”. In: *Biological Psychiatry* 61.7 (Apr. 2007), pp. 831–835.

[33] Paul Krack, Marwan I. Hariz, Christelle Baunez, Jorge Guridi, and Jose A. Obeso. “Deep brain stimulation: From neurology to psychiatry?” In: *Trends in Neurosciences* 33.10 (Oct. 2010), pp. 474–484.

[34] Jeff Moehlis, Eric Shea-Brown, and Herschel Rabitz. “Optimal Inputs for Phase Models of Spiking Neurons”. In: *Journal of Computational and Nonlinear Dynamics* 1.4 (June 2006), pp. 358–367.

[35] Takahiro Harada, Hisa-Aki Tanaka, Michael J. Hankins, and István Z. Kiss. “Optimal Waveform for the Entrainment of a Weakly Forced Oscillator”. In: *Physical Review Letters* 105.8 (Aug. 2010), p. 088301.

[36] Isuru Dasanayake and Jr-Shin Li. “Optimal design of minimum-power stimuli for phase models of neuron oscillators”. In: *Physical Review E* 83.6 (June 2011), p. 061916.

[37] Ali Nabi, Mohammad Mirzadeh, Frederic Gibou, and Jeff Moehlis. "Minimum energy desynchronizing control for coupled neurons". In: *Journal of Computational Neuroscience* 34.2 (Aug. 2012), pp. 259–271.

[38] Ali Nabi, Tyler Stigen, Jeff Moehlis, and Theoden Netoff. "Minimum energy control forin vitroneurons". In: *Journal of Neural Engineering* 10.3 (Apr. 2013), p. 036005.

[39] Jr-Shin Li, Isuru Dasanayake, and Justin Ruths. "Control and Synchronization of Neuron Ensembles". In: *IEEE Transactions on Automatic Control* 58.8 (Aug. 2013), pp. 1919–1930.

[40] Isuru S. Dasanayake and Jr-Shin Li. "Design of Charge-Balanced Time-Optimal Stimuli for Spiking Neuron Oscillators". In: *Neural Computation* 26.10 (Oct. 2014), pp. 2223–2246.

[41] Isuru S. Dasanayake and Jr-Shin Li. "Constrained charge-balanced minimum-power controls for spiking neuron oscillators". In: *Systems & Control Letters* 75 (Jan. 2015), pp. 124–130.

[42] Kestutis Pyragas and Viktor Novičenko. "Phase reduction of a limit cycle oscillator perturbed by a strong amplitude-modulated high-frequency force". In: *Physical Review E* 92.1 (July 2015), p. 012910.

[43] Amorn Wongsarnpigoon and Warren M Grill. "Energy-efficient waveform shapes for neural stimulation revealed with a genetic algorithm". In: *Journal of Neural Engineering* 7.4 (June 2010), p. 046009.

[44] Daniel R. Merrill, Marom Bikson, and John G.R. Jefferys. "Electrical stimulation of excitable tissue: Design of efficacious and safe protocols". In: *Journal of Neuroscience Methods* 141.2 (Feb. 2005), pp. 171–198.

[45] Robert J. Coffey. "Deep Brain Stimulation Devices: A Brief Technical History and Review". In: *Artificial Organs* 33.3 (Mar. 2009), pp. 208–220.

[46] S.B. Brummer and M.J. Turner. "Electrical stimulation of the nervous system: The principle of safe charge injection with noble metal electrodes". In: *Bioelectrochemistry and Bioenergetics* 2.1 (Jan. 1975), pp. 13–25.

[47] S. B. Brummer, L. S. Robblee, and F. T. Hambrecht. "Criteria For Selecting Electrodes For Electrical Stimulation: Theoretical And Practical Considerations". In: *Annals of the New York Academy of Sciences* 405.1 Cochlear Pros (June 1983), pp. 159–171.

[48] Daniel Harnack et al. "The effects of electrode material, charge density and stimulation duration on the safety of high-frequency stimulation of the subthalamic nucleus in rats". In: *Journal of Neuroscience Methods* 138.1-2 (Sept. 2004), pp. 207–216.

[49] Alexis M. Kuncel and Warren M. Grill. “Selection of stimulus parameters for deep brain stimulation”. In: *Clinical Neurophysiology* 115.11 (Nov. 2004), pp. 2431–2441.

[50] D.B. McCreery, W.F. Agnew, T.G.H. Yuen, and L. Bullara. “Charge density and charge per phase as cofactors in neural injury induced by electrical stimulation”. In: *IEEE Transactions on Biomedical Engineering* 37.10 (1990), pp. 996–1001.

[51] R.V. Shannon. “A model of safe levels for electrical stimulation”. In: *IEEE Transactions on Biomedical Engineering* 39.4 (Apr. 1992), pp. 424–426.

[52] Ulrike Gimsa et al. “Matching geometry and stimulation parameters of electrodes for deep brain stimulation experiments—Numerical considerations”. In: *Journal of Neuroscience Methods* 150.2 (Jan. 2006), pp. 212–227.

[53] Stuart F Cogan, Kip A Ludwig, Cristin G Welle, and Pavel Takmakov. “Tissue damage thresholds during therapeutic electrical stimulation”. In: *Journal of Neural Engineering* 13.2 (Jan. 2016), p. 021001.

[54] Lorenz Hofmann, Martin Ebert, Peter Alexander Tass, and Christian Hauptmann. “Modified Pulse Shapes for Effective Neural Stimulation”. In: *Frontiers in Neuroengineering* 4 (2011), p. 9.

[55] Andres M. Lozano and Hazem Eltahawy. “Chapter 78 How does DBS work?” In: *Advances in Clinical Neurophysiology, Proceedings of the 27th International Congress of Clinical Neurophysiology, AAEM 50th Anniversary and 57th Annual Meeting of the ACNS Joint Meeting*. Ed. by M. Hallett, L.H. Phillips, D.L. Schomer, and J.M. Massey. Vol. 57. Supplements to Clinical Neurophysiology. Elsevier, 2004, pp. 733–736.

[56] Andres M. Lozano et al. “Deep brain stimulation: Current challenges and future directions”. In: *Nature Reviews Neurology* 15.3 (Jan. 2019), pp. 148–160.

[57] P. Limousin et al. “Effect on parkinsonian signs and symptoms of bilateral subthalamic nucleus stimulation”. In: *The Lancet* 345.8942 (Jan. 1995), pp. 91–95.

[58] A Benazzouz et al. “Effect of high-frequency stimulation of the subthalamic nucleus on the neuronal activities of the substantia nigra pars reticulata and ventrolateral nucleus of the thalamus in the rat”. In: *Neuroscience* 99.2 (Sept. 2000), pp. 289–295.

[59] Chun-Hwei Tai et al. “Electrophysiological and metabolic evidence that high-frequency stimulation of the subthalamic nucleus bridles neuronal activity in the subthalamic nucleus and the substantia nigra reticulata”. In: *The FASEB Journal* 17.13 (Oct. 2003), pp. 1820–1830.

[60] J. O. Dostrovsky et al. “Microstimulation-Induced Inhibition of Neuronal Firing in Human Globus Pallidus”. In: *Journal of Neurophysiology* 84.1 (July 2000), pp. 570–574.

[61] Mohammed Filali, William D. Hutchison, Vanessa N. Palter, Andres M. Lozano, and Jonathan O. Dostrovsky. “Stimulation-induced inhibition of neuronal firing in human subthalamic nucleus”. In: *Experimental Brain Research* 156.3 (June 2004), pp. 274–281.

[62] Kestutis Pyragas, Viktor Novičenko, and Peter Alexander Tass. “Mechanism of suppression of sustained neuronal spiking under high-frequency stimulation”. In: *Biological Cybernetics* 107.6 (Oct. 2013), pp. 669–684.

[69] Constance Hammond. *Cellular and molecular neurophysiology*. Academic Press, 2014.

[70] B Hille. *Ion Channels of Excitable Membranes*. Sunderland, Mass., USA: Sinauer Associates, 2001.

[71] Meyer B Jackson. *Molecular and cellular biophysics*. Cambridge University Press, 2006.

[72] Daniel Johnston and Samuel Miao-Sin Wu. *Foundations of cellular neurophysiology*. MIT press, 1994.

[73] Eugene M. Izhikevich. *Dynamical Systems in Neuroscience. The Geometry of Excitability and Bursting*. The MIT Press, 2006.

[74] A. L. Hodgkin and A. F. Huxley. “A quantitative description of membrane current and its application to conduction and excitation in nerve”. In: *The Journal of Physiology* 117.4 (Aug. 1952), pp. 500–544.

[75] Richard FitzHugh. “Mathematical models of excitation and propagation in nerve”. In: *Biological engineering* (1969), pp. 1–85.

[76] Wulfram Gerstner and Werner M Kistler. *Spiking neuron models: Single neurons, populations, plasticity*. Cambridge university press, 2002.

[77] G Bard Ermentrout and Nancy Kopell. “Parabolic bursting in an excitable system coupled with a slow oscillation”. In: *SIAM journal on applied mathematics* 46.2 (1986), pp. 233–253.

[78] Frank C Hoppensteadt and Eugene M Izhikevich. *Weakly connected neural networks*. Vol. 126. Springer Science & Business Media, 1997.

[79] Bard Ermentrout. “Type I membranes, phase resetting curves, and synchrony”. In: *Neural computation* 8.5 (1996), pp. 979–1001.

[80] G. Bard Ermentrout and David H. Terman. *Mathematical Foundations of Neuroscience*. Springer New York, 2010.

[81] Viktor Novičenko and Kestutis Pyragas. “Computation of phase response curves via a direct method adapted to infinitesimal perturbations”. In: *Nonlinear Dynamics* 67.1 (Mar. 2011), pp. 517–526.

[82] Hiroya Nakao, Sho Yasui, Masashi Ota, Kensuke Arai, and Yoji Kawamura. “Phase reduction and synchronization of a network of coupled dynamical elements exhibiting collective oscillations”. In: *Chaos: An Interdisciplinary Journal of Nonlinear Science* 28.4 (Apr. 2018), p. 045103.

[83] Yoshiki Kuramoto. *Chemical Oscillations, Waves, and Turbulence*. Springer Berlin Heidelberg, 1984.

[84] Edward Ott and Thomas M. Antonsen. “Low dimensional behavior of large systems of globally coupled oscillators”. In: *Chaos: An Interdisciplinary Journal of Nonlinear Science* 18.3 (Sept. 2008), p. 037113. eprint: `https://doi.org/10.1063/1.2930766`.

[85] Ernest Montbrió, Diego Pazó, and Alex Roxin. “Macroscopic Description for Networks of Spiking Neurons”. In: *Physical Review X* 5.2 (June 2015), p. 021028.

[86] Irmantas Ratas and Kestutis Pyragas. “Macroscopic self-oscillations and aging transition in a network of synaptically coupled quadratic integrate-and-fire neurons”. In: *Physical Review E* 94.3 (Sept. 2016), p. 032215.

[87] Diego Pazó and Ernest Montbrió. “From Quasiperiodic Partial Synchronization to Collective Chaos in Populations of Inhibitory Neurons with Delay”. In: *Physical Review Letters* 116.23 (June 2016), p. 238101.

[88] Federico Devalle, Alex Roxin, and Ernest Montbrió. “Firing rate equations require a spike synchrony mechanism to correctly describe fast oscillations in inhibitory networks”. In: *PLOS Computational Biology* 13.12 (Dec. 2017). Ed. by Sonja Gruen, e1005881.

[89] Irmantas Ratas and Kestutis Pyragas. “Macroscopic oscillations of a quadratic integrate-and-fire neuron network with global distributed-delay coupling”. In: *Physical Review E* 98.5 (Nov. 2018), p. 052224.

[90] Irmantas Ratas and Kestutis Pyragas. “Noise-induced macroscopic oscillations in a network of synaptically coupled quadratic integrate-and-fire neurons”. In: *Physical Review E* 100.5 (Nov. 2019), p. 052211.

[91] Ernest Montbrió and Diego Pazó. “Exact Mean-Field Theory Explains the Dual Role of Electrical Synapses in Collective Synchronization”. In: *Physical Review Letters* 125.24 (Dec. 2020), p. 248101.

[92] Irmantas Ratas and Kestutis Pyragas. “Symmetry breaking in two interacting populations of quadratic integrate-and-fire neurons”. In: *Physical Review E* 96.4 (Oct. 2017), p. 042212.

[93] Marco Segneri, Hongjie Bi, Simona Olmi, and Alessandro Torcini. "Theta-Nested Gamma Oscillations in Next Generation Neural Mass Models". In: *Frontiers in Computational Neuroscience* 14 (May 2020), p. 47.

[94] L.S. Pontryagin. *Mathematical Theory of Optimal Processes*. Routledge, May 2018.

[95] Hiroya Nakao. "Phase reduction approach to synchronisation of nonlinear oscillators". In: *Contemporary Physics* 57.2 (Oct. 2015), pp. 188–214.

[96] Donald E. Kirk. *Optimal Control Theory: An Introduction*. Prentice Hall, Inc., New York, 1971.

[97] Hisa-Aki Tanaka. "Optimal entrainment with smooth, pulse, and square signals in weakly forced nonlinear oscillators". In: *Physica D: Nonlinear Phenomena* 288 (Nov. 2014), pp. 1–22.

[98] Hisa-Aki Tanaka. "Synchronization limit of weakly forced nonlinear oscillators". In: *Journal of Physics A: Mathematical and Theoretical* 47.40 (Sept. 2014), p. 402002.

[99] Hisa-Aki Tanaka, Isao Nishikawa, Jürgen Kurths, Yifei Chen, and István Z. Kiss. "Optimal synchronization of oscillatory chemical reactions with complex pulse, square, and smooth waveforms signals maximizes Tsallis entropy". In: *EPL (Europhysics Letters)* 111.5 (Sept. 2015), p. 50007.

[100] Peter A. Tass et al. "Coordinated reset has sustained aftereffects in Parkinsonian monkeys". In: *Annals of Neurology* 72.5 (Nov. 2012), pp. 816–820.

[101] Jing Wang et al. "Coordinated Reset Deep Brain Stimulation of Subthalamic Nucleus Produces Long-Lasting, Dose-Dependent Motor Improvements in the 1-Methyl-4-phenyl-1,2,3,6-tetrahydropyridine Non-Human Primate Model of Parkinsonism". In: *Brain Stimulation* 9.4 (July 2016), pp. 609–617.

[102] Ilya Adamchic et al. "Coordinated reset neuromodulation for Parkinson's disease: Proof-of-concept study". In: *Movement Disorders* 29.13 (June 2014), pp. 1679–1684.

[103] Utako B Barnikol et al. "Tremor entrainment by patterned low-frequency stimulation". In: *Philosophical Transactions of the Royal Society A: Mathematical, Physical and Engineering Sciences* 366.1880 (July 2008), pp. 3545–3573.

[104] G. Brozek, I. A. Zhuravin, D. Megirian, and J. Bures. “Localization of the central rhythm generator involved in spontaneous consummatory licking in rats: Functional ablation and electrical brain stimulation studies.” In: *Proceedings of the National Academy of Sciences* 93.8 (Apr. 1996), pp. 3325–3329.

[105] W. D. Hutchison et al. “Neurophysiological identification of the subthalamic nucleus in surgery for Parkinson’s disease”. In: *Annals of Neurology* 44.4 (Oct. 1998), pp. 622–628.

[106] J. J. Lemaire et al. “Direct Stereotactic MRI Location in the Globus Pallidus for Chronic Stimulation in Parkinson’s Disease”. In: *Acta Neurochirurgica* 141.7 (July 1999), pp. 759–766.

[107] Michael S. Yoon and Michael Munz. “Placement of Deep Brain Stimulators into the Subthalamic Nucleus”. In: *Stereotactic and Functional Neurosurgery* 72.2-4 (1999), pp. 145–149.

[108] P. A. Tass, A. N. Silchenko, C. Hauptmann, U. B. Barnikol, and E.-J. Speckmann. “Long-lasting desynchronization in rat hippocampal slice induced by coordinated reset stimulation”. In: *Physical Review E* 80.1 (July 2009), p. 011902.

[109] Magteld Zeitler and Peter A. Tass. “Augmented brain function by coordinated reset stimulation with slowly varying sequences”. In: *Frontiers in Systems Neuroscience* 9 (Mar. 2015), p. 49.

[110] Marom Bikson et al. “Suppression of epileptiform activity by high frequency sinusoidal fields in rat hippocampal slices”. In: *The Journal of Physiology* 531.1 (Feb. 2001), pp. 181–191.

[111] Matthew D. Johnson, Svjetlana Miocinovic, Cameron C. McIntyre, and Jerrold L. Vitek. “Mechanisms and targets of deep brain stimulation in movement disorders”. In: *Neurotherapeutics : the journal of the American Society for Experimental NeuroTherapeutics* 5.2 (Apr. 2008), pp. 294–308.

[112] Viviana Gradinaru, Murtaza Mogri, Kimberly R. Thompson, Jaimie M. Henderson, and Karl Deisseroth. “Optical Deconstruction of Parkinsonian Neural Circuitry”. In: *Science (New York, N.Y.)* 324.5925 (Apr. 2009), pp. 354–359.

[113] Jean-Michel Deniau, Bertrand Degos, Clémentine Bosch, and Nicolas Maurice. “Deep brain stimulation mechanisms: Beyond the concept of local functional inhibition. Deep brain stimulation mechanisms”. In: *European Journal of Neuroscience* 32.7 (Oct. 2010), pp. 1080–1091.

[114] Coralie de Hemptinne et al. “Therapeutic deep brain stimulation reduces cortical phase-amplitude coupling in Parkinson’s disease”. In: *Nature Neuroscience* 18.5 (Apr. 2015), pp. 779–786.

[115] Nealen G. Laxpati, Willard S. Kasoff, and Robert E. Gross. "Deep Brain Stimulation for the Treatment of Epilepsy: Circuits, Targets, and Trials". In: *Neurotherapeutics : the journal of the American Society for Experimental NeuroTherapeutics* 11.3 (June 2014), pp. 508–526.

[116] Gilles van Luijtelaar et al. "Methods of automated absence seizure detection, interference by stimulation, and possibilities for prediction in genetic absence models". In: *Journal of Neuroscience Methods* 260 (Feb. 2016), pp. 144–158.

[117] Vladimir A. Maksimenko et al. "Absence Seizure Control by a Brain Computer Interface". In: *Scientific Reports* 7.1 (May 2017), p. 2487.

[118] Christian Hauptmann and Peter A. Tass. "Therapeutic rewiring by means of desynchronizing brain stimulation". In: *Biosystems* 89.1-3 (May 2007), pp. 173–181.

[119] Dan Wilson and Jeff Moehlis. "Locally optimal extracellular stimulation for chaotic desynchronization of neural populations". In: *Journal of Computational Neuroscience* 37.2 (June 2014), pp. 243–257.

[120] Oleksandr V. Popovych, Borys Lysyansky, Michael Rosenblum, Arkady Pikovsky, and Peter A. Tass. "Pulsatile desynchronizing delayed feedback for closed-loop deep brain stimulation". In: *Plos One* 12.3 (Mar. 2017), e0173363.

[121] Oleksandr V. Popovych, Borys Lysyansky, and Peter A. Tass. "Closed-loop deep brain stimulation by pulsatile delayed feedback with increased gap between pulse phases". In: *Scientific Reports* 7.1 (Apr. 2017), p. 1033.

[122] Oleksandr V. Popovych and Peter A. Tass. "Multisite Delayed Feedback for Electrical Brain Stimulation". In: *Frontiers in Physiology* 9 (Feb. 2018), p. 46.

[123] Arthur T. Winfree. *The Geometry of Biological Time*. Springer New York, 2001.

[124] Arkady Pikovsky, Michael Rosenblum, and Jürgen Kurths. *Synchronization. A Universal Concept in Nonlinear Sciences*. Cambridge University Press, Oct. 2001.

[125] Peter J. Uhlhaas and Wolf Singer. "Abnormal neural oscillations and synchrony in schizophrenia". In: *Nature Reviews Neuroscience* 11.2 (Feb. 2010), pp. 100–113.

[126] P. Temperli et al. "How do parkinsonian signs return after discontinuation of subthalamic DBS?" In: *Neurology* 60.1 (Jan. 2003), pp. 78–81.

[127] Andrea A. Kühn et al. “High-Frequency Stimulation of the Subthalamic Nucleus Suppresses Oscillatory β Activity in Patients with Parkinson’s Disease in Parallel with Improvement in Motor Performance”. In: *Journal of Neuroscience* 28 (2008), pp. 6165–6173.

[128] Peter A. Tass and Milan Majtanik. “Long-term anti-kindling effects of desynchronizing brain stimulation: A theoretical study”. In: *Biological Cybernetics* 94.1 (Nov. 2005), pp. 58–66.

[129] Martin A. Horn et al. “A New Stimulation Mode for Deep Brain Stimulation in Parkinson’s Disease: Theta Burst Stimulation”. In: *Movement Disorders* 35.8 (May 2020), pp. 1471–1475.

[130] Xiao-Jiang Feng, Eric Shea-Brown, Brian Greenwald, Robert Kosut, and Herschel Rabitz. “Optimal deep brain stimulation of the subthalamic nucleus—a computational study”. In: *Journal of Computational Neuroscience* 23.3 (May 2007), pp. 265–282.

[131] Kevin M. Hannay, Victoria Booth, and Daniel B. Forger. “Collective phase response curves for heterogeneous coupled oscillators”. In: *Physical Review E* 92.2 (Aug. 2015), p. 022923.

[132] Grégory Dumont, G. Bard Ermentrout, and Boris Gutkin. “Macroscopic phase-resetting curves for spiking neural networks”. In: *Physical Review E* 96.4 (Oct. 2017), p. 042311.

[133] D. Terman, J. E. Rubin, A. C. Yew, and C. J. Wilson. “Activity Patterns in a Model for the Subthalamopallidal Network of the Basal Ganglia”. In: *The Journal of Neuroscience* 22.7 (Apr. 2002), pp. 2963–2976.

[134] H. Kita and S.T. Kitai. “Intracellular study of rat globus pallidus neurons: Membrane properties and responses to neostriatal, subthalamic and nigral stimulation”. In: *Brain Research* 564.2 (Nov. 1991), pp. 296–305.

[135] A. Dhooge, W. Govaerts, and Yu. A. Kuznetsov. “Matcont. A MATLAB package for numerical bifurcation analysis of ODEs”. In: *ACM Transactions on Mathematical Software* 29.2 (June 2003), pp. 141–164.

[136] Jan A. Sanders and Ferdinand Verhulst. *Averaging Methods in Nonlinear Dynamical Systems*. Springer New York, 1985.

[137] P. L. Kapitza. “Dynamic Stability of a Pendulum When Its Point of Suspension Vibrates”. In: *Soviet Phys. JETP* 21 (1951), pp. 588–597.

[138] Eugene I. Butikov. “On the dynamic stabilization of an inverted pendulum”. In: *American Journal of Physics* 69.7 (July 2001), pp. 755–768.

[139] Irmantas Ratas and Kestutis Pyragas. “Pulse propagation and failure in the discrete FitzHugh-Nagumo model subject to high-frequency stimulation”. In: *Physical Review E* 86.4 (Oct. 2012), p. 046211.

[140] Alain Destexhe and Terrence J. Sejnowski. “The Wilson–Cowan model, 36 years later”. In: *Biological Cybernetics* 101.1 (July 2009), pp. 1–2.

[141] Stephen Coombes and Áine Byrne. “Next Generation Neural Mass Models”. In: *Nonlinear Dynamics in Computational Neuroscience*. Ed. by F. Corinto and A. Torcini. Springer International Publishing, June 2018. Chap. Next Generation Neural Mass Models, pp. 1–16.

Santrauka

Įvadas

Sinchronizacijos procesai didelėse sąveikaujančių dinaminių sistemų populiacijose yra intensyvių fizikinių, technologinių ir biologinių sistemų tyrimų dėmesio centre [1–6]. Neuronų tinkluose sinchronizacija gali atlikti dvejopą vaidmenį. Normaliomis sąlygomis sinchronizacija yra atsakinga už pažinimą ir mokymąsi [7, 8], tačiau perteklinė sinchronizacija gali sukelti neurologinius sutrikimus, tokius kaip Parkinsono liga [9] ir kt. [10, 11]

Daugelyje pritaikymų yra svarbu optimizuoti netiesinių osciliatorių sinchronizaciją su išoriniu signalu. Tipiškas pavyzdys yra giluminė smegenų stimuliacija (GSS) [27, 33]. Neuromokslų srityje stimuliacijos optimizavimo tyrimai daugiausia orientuoti į *minimalios energijos* arba *minimalios galios* valdymo algoritmų kūrimą [34–43]. Energija arba galia yra natūralus efektyvumo matas siekiant minimizuoti įsikišimą į biologinę sistemą ir sumažinti implantuojamo impulsų generatoriaus energijos sąnaudas, tačiau netinkamai suprojektuota elektrinės stimuliacijos sistema gali pažeisti nervinį audinį ir/ar patį GSS elektrodą [44].

Neurochirurgijoje taikomuose stimuliacijos protokoluose paprastai naudojami periodiniai, subalansuoto krūvio dvifaziai signalai [45]. Krūvio balansas yra būtinas siekiant išvengti ilgalaikių nepageidaujamų poveikių [46–49]. Nervinio audinio pažeidimas taikant tokius stimuliacijos protokolus priklauso nuo elektrodo ir elektrinio impulso savybių [50–53]. Audinių pažeidimo slenkstį nulemia krūvio tankis bei stimuliacijos impulso fazei tenkantis krūvis [50, 51]. Todėl, siekiant minimizuoti nervinio audinio pažaidą, kaip stimuliacijos srovės

parametrų optimizavimo rodiklį galima pasirinkti valdymo srovės modulio vidurkį [49, 54].

Naujausi dinaminių sistemų teorijos pasiekimai, tokie kaip didelio masto osciliatorių tinklų mikroskopinių modelių lygčių vidutinio lauko redukcija į mažos dimensijos diferencialinių lygčių sistemas, tiksliai nusakančias makroskopinę sistemos raidą begalinio dydžio riboje, leidžia ne tik geriau suprasti sinchronizacijos atsiradimą tokiuose tinkluose, bet taip pat gali paaiškinti stimuliacijos poveikį sinchronizacijos procesams.

Tikslai

1. Pritaikyti fazinės redukcijos, vidurkinimo ir vidutinio lauko redukcijos sistemoms termodinaminėje riboje metodus netiesinių osciliatorių tinklų sinchronizacijos valdymo uždaviniams;

2. Išvesti optimalios subalansuoto krūvio valdymo srovės išraišką, kuri užtikrina impulsus generuojančio neurono sinchronizaciją su periodine išorine stimuliacija minimizuojant šios stimuliacijos srovės modulio vidurkį;

3. Išplėsti ir pritaikyti neurono valdymo minimaliu krūviu algoritmą sąveikaujančių dinaminių elementų tinklams bei makroskopinėms lygtims, išvestoms impulsus generuojančių neuronų tinklams termodinaminėje riboje;

4. Ištirti įvairių stimuliacijos algoritmų poveikį didelio masto tinklui, sudarytam iš dviejų sąveikaujančių eksitatorinių ir inhibitorinių *quadratic integrate-and-fire* (QIF) neuronų populiacijų.

Mokslinis naujumas

- Siekiant minimizuoti nervinio audinio pažaidą, kaip optimaliojo valdymo efektyvumo matas pasirinktas stimuliacijos srovės modulio vidurkis. Suformuluotas valdymo minimaliu krūviu uždavinys skiriasi nuo anksčiau nagrinėtų valdymo uždavinių. Paprastai impulsus generuojančio

neurono sinchronizacijos su valdymo srove uždavinio tikslas yra minimizuoti vidutinės energijos funkcionalą. Neuronui tenkanti energija yra proporcinga stimuliacijos srovės kvadratui, o ne jos moduliui. Dėl šios priežasties šiame darbe išvesta valdymo minimaliu krūviu srovė reikšmingai skiriasi nuo minimalios galios valdymo srovės.

- Be audinio pažaidos sumažinimo, valdymo minimaliu krūviu algoritmas turi dar vieną praktinį pranašumą. Esant mažam dažnių skirtumui, minimalios galios valdymo srovė yra proporcinga neurono fazinei atsako funkcijai (FAF), todėl jos sudarymui būtina žinoti visą FAF. Priešingai, minimalaus krūvio valdymo srovė priklauso tik nuo atstumo tarp FAF absoliučių ekstremumų ir jos amplitudės. Tai leidžia empiriškai nustatyti optimalios srovės parametrus, nenaudojant neurono modelio ir fazinės redukcijos teorijos. Be to, nagrinėjama optimizavimo uždavinio formuluotė atsižvelgia į asimetrinį valdymo srovės amplitudės ribojimą. Tai yra labai svarbu, nes *in vivo* taikomuose stimuliacijos protokoluose paprastai naudojami asimetriniai valdymo signalai.

- Optimalios valdymo srovės sudarymo algoritmas gali būti pritaikytas kolektyvinius periodinius virpesius generuojančiam sąveikaujančių neuronų tinklui. Šiam tikslui reikalinga žinoti tinklo FAF. Kaip ir vieno neurono atveju, esant mažam dažnių skirtumui, užtenka žinoti atstumą tarp tinklo FAF absoliučių ekstremumų ir jos amplitudę.

- Išsami dviejų eksitatorinių ir inhibitorinių QIF neuronų populiacijų sistemos bifurkacijų analizė atskleidė įvairių stimuliacijos algoritmų veikimo mechanizmus. Aukšto dažnio (AD) stimuliacijos poveikis paaiškinamas naudojant vidutinio lauko lygtis, suvidurkintas per stimuliacijos periodą. Ši metodika gali pasitarnauti kaip veiksminga priemonė kuriant didelio masto neuronų tinklų sinchronizacijos valdymo algoritmus.

Ginamieji teiginiai

1. Optimali valdymo srovė, užtikrinanti impulsus generuojančio neurono sinchronizaciją su periodine subalansuoto krūvio išorine stimuliacija yra

sudaryta iš teigiamo ir neigiamo impulsų, centruotų ties neurono FAF ekstremumais.

2. Esant mažam dažnių skirtumui, tiesinėje Arnoldo liežuvio dalyje, kuomet srovės ribojimas yra nereikšmingas, minimalaus krūvio valdymo srovė priklauso tik nuo atstumo tarp FAF absoliučių ekstremumų ir jos amplitudės.

3. Pakeitus vieno neurono FAF efektyviąja tinklo FAF, tas pats valdymo metodas gali būti pritaikytas sąveikaujančių neuronui tinklui; optimali neuronų tinklo valdymo srovė taip pat sudaryta iš periodiškai pasikartojančių stačiakampių impulsų, kurių amplitudės ir pločiai bendruoju atveju skiriasi.

4. Inhibitorinės dviejų sąveikaujančių eksitatorinių ir inhibitorinių QIF neuronų pilnojo tinklo populiacijos AD stimuliacija pakeičia sužadinimo parametro skirstinio centrą, taip padidindama aktyvių neuronų dalį toje populiacijoje. Tokiu būdu stabilizuojama nekoherentinė rimties būsena ir kolektyviniai tinklo virpesiai nutrūksta.

5. Slenkstinė AD stimuliacijos amplitudė, stabilizuojanti nestabilią nekoherentinę rimties būseną, AD srityje yra proporcinga stimuliacijos dažniui.

6. Tinklo virpesių slopinimas veikiant eksitatorinę populiaciją yra galimas, jei sistemos parametrai yra bistabiliame režime. Paveikus eksitatorinę populiaciją stačiakampiu slopinančiuoju impulsu, tinklo būsena perjungiama iš stabilaus ribinio ciklo į stabilų rimties tašką, atitinkantį nekoherentinę tinklo būseną.

Publikacijų sąrašas

Moksliniai straipsniai

1. Kestutis Pyragas, Augustinas P. Fedaravičius, Tatjana Pyragienė, ir Peter A. Tass. „Optimal waveform for entrainment of a spiking neuron with

minimum stimulating charge“. *Physical Review E* 98.4 (spalis 2018), p. 042216.

2. Kestutis Pyragas, Augustinas P. Fedaravičius, Tatjana Pyragienė, ir Peter A. Tass. „Entrainment of a network of interacting neurons with minimum stimulating charge“. *Physical Review E* 102.1 (liepa 2020), p. 012221.

3. Kestutis Pyragas, Augustinas P. Fedaravičius, ir Tatjana Pyragienė. „Suppression of synchronous spiking in two interacting populations of excitatory and inhibitory quadratic integrate-and-fire neurons“. *Physical Review E* 104.1 (liepa 2021), p. 014203.

Pranešimai konferencijose

1. Augustinas P. Fedaravičius ir Kestutis Pyragas. „Optimal waveform for the entrainment of a spiking neuron with the minimum mean absolute value of the stimulating current“. *Open Readings 2018*. Vilnius, kov. 2018, p. 77.

2. Augustinas P. Fedaravičius, Kestutis Pyragas, Tatjana Pyragienė, ir Peter A Tass. „Optimal entrainment of a network of interacting neurons with minimum stimulating charge“. *Dynamics Days Digital 2020*. Rugpj. 2020, p. 48.

3. Tatjana Pyragienė, Kęstutis Pyragas, ir Augustinas P. Fedaravičius. „Sinchronizacijos slopinimas dviejose sąveikaujančiose neuronų populiacijose“. *44-oji Lietuvos nacionalinė fizikos konferencija*. Vilnius, spalis 2021, p. 169.

Asmeninis indėlis

Autorius kartu su publikacijų bendraautoriais išvedė krūviu optimalios valdymo srovės išraišką, užtikrinančią neurono bei sąveikaujančių neuronų tinklo sinchronizaciją su periodine išorine stimuliacija, atliko dviejų populiacijų QIF neuronų didelio masto tinklo, veikiamo išorinės AD stimuliacijos, bifurkacijų

analizę ir vidurkinimą, bei patvirtino teorinius rezultatus atlikdamas skaitinį modeliavimą.

Padėka

Norėčiau nuoširdžiai padėkoti savo moksliniam vadovui prof. habil. dr. Kęstučiui Pyragui už suteiktas žinias, aiškumą ir tikslumą tiek fizikoje, redukuojant ir valdant sudėtingas sistemas, tiek kasdieniame bendravime, ir begalinę kantrybę, neabejoju, chaotiškiausiam per ilgą akademinę karjerą vadovautam doktorantui;

Bakalauro ir magistro darbų vadovui prof. habil. dr. Minvydui Ragulskiui už tai, kad supažindino mane su netiesine dinamika ir chaosu, ir tokiu būdu dar labiau pastūmėjo į neuromokslų sritį;

Savo tėvams Lilijai ir Algimantui už tai, kad savo auklėjimu ir palaikymu sudarė sąlygas gilintis į visas dominančias sritis;

Eglei Preckailaitei už tai, kad palaiko mano nervų sistemą kritinėje būsenoje (fizikine prasme).

1 Pagrindai

Šiame skyriuje remiantis literatūros šaltiniais trumpai apžvelgiamas disertacijos mokslinis kontekstas bei naudojami matematiniai metodai.

Pirmajame skyrelyje apibūdinama neuronų sandara, jų kaip dirgliųjų ląstelių savybės, plazminės membranos fiziologija, jos elektrinis aktyvumas bei veikimo potencialo generavimas, pateikiamas Hodgkin-Huxley (HH) neurono modelis.

Antras skyrelis skirtas supaprastinam neuronų modeliavimui, trumpai išdėstoma stabiliame ribiniame cikle svyruojančių neuronų fazinės redukcijos teorija, kuomet neuronai traktuojami kaip osciliatoriai. Tokiu atveju, neurono ar net viso neuronų tinklo lygčių sistema redukuojama į vieną skaliarinę fazės lygtį. Taip pat pateikiami fazinių osciliatorių sinchronizacijos režimų apibrėžimai.

Trečiajame skyrelyje aprašoma vidutinio lauko redukcijos teorija, leidžianti tiksliai apibūdinti makroskopinę neuronų tinklo būseną termodinaminėje riboje. Šią būseną charakterizuoja biofiziškai reiškingi kintamieji – tinklo vidutinis membranos potencialas bei impulsų generavimo dažnis.

Ketvirtajame skyrelyje pateikiama būtinosios optimaliojo valdymo sąlygos – Pontriagino maksimumo principo – formuluotė.

2 Optimali valdymo srovė neurono sinchronizacijai minimizuojant stimuliacijos krūvį

2.1 Uždavinio formuluotė

Nagrinėjamas bendrasis HH tipo neurono modelis su periodiniu žadinimu

$$C_m \dot{v} = F(v, \mathbf{w}) + I(\omega t), \tag{2.1a}$$

$$\dot{\mathbf{w}} = \mathbf{G}(v, \mathbf{w}). \tag{2.1b}$$

Čia C_m yra membranos elektrinė talpa, v yra membranos potencialas. Funkcija $F(v, \mathbf{w})$ apibūdina pro membranos kanalus tekančių jonų sroves. $I(\omega t)$ yra išorinis periodinis žadinimas, tenkinantis sąlygą $I(\omega t + 2\pi) = I(\omega t)$, kur ω yra stimuliacijos dažnis, o $T = 2\pi/\omega$ – periodas. (2.1b) lygtis aprašo atstatomojo kintamojo $\mathbf{w}$, kuris bendruoju atveju yra vektorius $\mathbf{w} = (w_1, \ldots, w_n)$, dinamiką. Funkcija $\mathbf{G}(v, \mathbf{w})$ nusako jonų kanalų dinamiką.

Daroma prielaida, jog, nesant stimuliacijos [$I(\omega t) = 0$], neuronas generuoja impulsus (veikimo potencialus) periodu T_0. Esant pakankamai silpnai stimuliacijos srovei $I(\omega t)$, galima taikyti fazinės redukcijos metodą [73, 81, 95] ir redukuoti (2.1) lygtis į vieną skaliarinę fazės lygtį

$$\dot{\vartheta} = \omega_0 + z(\vartheta) I(\omega t), \tag{2.2}$$

kur ϑ yra fazė, $\omega_0 = 2\pi/T_0$ yra laisvo neurono impulsų generavimo dažnis, $z(\vartheta)$ yra 2π-periodinė fazės atsako funkcija (FAF). FAF gaunama iš laisvo neurono modelio; ji nusako neurono atsaką į bet kokį silpną išorinį žadinimą.

Pagrindinis šio skyriaus tikslas – išvesti optimalią stimuliacijos srovės $I(\omega t)$ signalo formą, užtikrinančią neurono sinchronizaciją su šios srovės dažniu minimizuojant srovės modulio vidurkį. Minimizuojamas funkcionalas

$$\mathcal{J}[I] = \frac{1}{T} \int_0^T |I(\omega t)| \, \mathrm{d}t \, . \tag{2.3}$$

Reikalaujama, kad stimuliacijos srovė neviršytų iš anksto nustatytos minimalios $I_- < 0$ bei maksimalios $I_+ > 0$ vertės, t.y.,

$$I_- \leq I(\omega t) \leq I_+. \tag{2.4}$$

Taip pat įvedama kliniškai būtina krūvio balanso sąlyga $\int_0^T I(\omega t)\,\mathrm{d}t = 0$. Krūvis q tenkina diferencialinę lygtį

$$\dot{q} = I(\omega t), \tag{2.5}$$

todėl krūvio balanso sąlygą galima užrašyti

$$q(0) = 0, \quad q(T) = 0. \tag{2.6}$$

Sinchronizacija galima jei egzistuoja sistemos (2.2) sprendinys, tenkinantis kraštines sąlygas

$$\vartheta(0) = 0, \quad \vartheta(T) = 2\pi. \tag{2.7}$$

Apibendrinant, norint rasti optimalią stimuliacijos srovės išraišką, reikia minimizuoti (2.3) funkcionalą, kintamiesiems ϑ ir q tenkinant (2.2) ir (2.5) diferencialines lygtis su kraštinėmis sąlygomis (2.6) ir (2.7). Taip pat reikia atsižvelgti į stimuliacijos amplitudės ribojimą (2.4).

2.2 Optimizavimo uždavinio sprendimas

Aukščiau suformuluoto uždavinio sprendimui pasitelktas Pontriagino maksimumo principas [94, 96]. Parenkama Lagranžo funkcija $\mathcal{L}(I) = |I|$ ir apibrėžiama sistemos Hamiltono funkcija: $\mathcal{H}(q, \vartheta, I, p, \mu) = p(t)\dot{\vartheta} + \mu(t)\dot{q} - \mathcal{L}$, arba

$$\mathcal{H}(\vartheta, I, p, \mu) = [\omega_0 + z(\vartheta)I]p + \mu I - |I|. \tag{2.8}$$

Oilerio lygtys, apibrėžiančios (2.3) funkcionalo minimalią reikšmę sutampa su Hamiltono lygtimis:

$$\dot{\vartheta} = \frac{\partial \mathcal{H}}{\partial p}, \quad \dot{q} = \frac{\partial \mathcal{H}}{\partial \mu}, \quad \dot{p} = -\frac{\partial \mathcal{H}}{\partial \vartheta}, \quad \dot{\mu} = -\frac{\partial \mathcal{H}}{\partial q}. \tag{2.9}$$

Mechanikoje $p(t)$ and $\mu(t)$ yra judesio kiekio komponentės, o Oilerio formalizme – Lagranžo daugikliai. Hamiltono funkciją galima perrašyti

$$\mathcal{H}(\vartheta, I, p, \mu) = \begin{cases} \omega_0 p + [z(\vartheta)p + \mu - 1]I, & \text{jei} \quad I \geq 0, \\ \omega_0 p + [z(\vartheta)p + \mu + 1]I, & \text{jei} \quad I \leq 0. \end{cases} \tag{2.10}$$

Pritaikius Pontriagino maksimumo principą, kuris teigia, jog optimalioje trajektorijoje Hamiltono funkcija yra pastovi ir įgyja maksimalią reikšmę, Hamiltono funkcijai (2.10), išvestas algoritmas optimaliai stimuliacijos srovei sukonstruoti.

Bendruoju atveju, turi būti žinoma konkretaus neurono modelio FAF $z(\vartheta)$ bei srovės amplitudės rėžiai I_- ir I_+. Optimalios srovės išraiška (žymima $I^*(\vartheta)$) įgyja atkarpomis pastovios funkcijos pavidalą:

$$I^*(\vartheta) = I_\pm H[z(\vartheta) - z_2] + I_\mp H[z_1 - z(\vartheta)], \tag{2.11}$$

kur $H(\cdot)$ yra Hevisaido vienetinė funkcija. Optimali srovė priklauso nuo dažnių skirtumo $\Delta\omega = \omega - \omega_0$ ženklo. Čia ir toliau viršutinis (apatinis) indeksas atitinka $\Delta\omega > 0$ ($\Delta\omega < 0$). Parametrai z_1 ir z_2 tenkina nelygybę $z_1 < z_2$. Jų reikšmės nustatomos iš lygčių

$$I_\pm M_+(z_2) + I_\mp M_-(z_1) = \Delta\omega, \tag{2.12a}$$

$$I_\pm N_+(z_2) + I_\mp N_-(z_1) = 0, \tag{2.12b}$$

kurios bendruoju atveju skiriasi kai $\Delta\omega > 0$ ir $\Delta\omega < 0$. Šiose lygtyse figūruoja keturios pagalbinės funkcijos

$$M_+(\xi) = \langle z(\vartheta)H[z(\vartheta) - \xi]\rangle_\vartheta, \tag{2.13a}$$

$$M_-(\xi) = \langle z(\vartheta)H[\xi - z(\vartheta)]\rangle_\vartheta, \tag{2.13b}$$

$$N_+(\xi) = \langle H[z(\vartheta) - \xi]\rangle_\vartheta, \tag{2.13c}$$

$$N_-(\xi) = \langle H[\xi - z(\vartheta)]\rangle_\vartheta, \tag{2.13d}$$

kur kampiniai skliaustai su indeksu ϑ reiškia funkcijos vidurkį kintamojo ϑ atžvilgiu:

$$\langle f(\vartheta)\rangle_\vartheta \equiv \frac{1}{2\pi}\int_0^{2\pi} f(\vartheta)\,\mathrm{d}\vartheta\,. \tag{2.14}$$

Funkcionalo (2.3) vertė optimalioje trajektorijoje (2.11) yra

$$\mathcal{J}^* \equiv \mathcal{J}[I^*] = |I_\pm|N_+(z_2) + |I_\mp|N_-(z_1). \tag{2.15}$$

2.3 Analizinis pavyzdys: Stuart-Landau osciliatorius

Nagrinėjamas Stuart-Landau osciliatorius, kuriam optimalią srovę galima rasti analiziniu būdu:

$$\dot{x} = -y + x\Big(1 - x^2 - y^2\Big) + I(\omega t), \tag{2.16a}$$

$$\dot{y} = \quad x + y\Big(1 - x^2 - y^2\Big). \tag{2.16b}$$

Nesant išorinio žadinimo, egzistuoja ribinis ciklas $x_c = \cos(t),\ y_c = \sin(t)$, kurio dažnis $\omega_0 = 1$. Sistemos FAF yra

$$z(\vartheta) = \sin(\vartheta). \tag{2.17}$$

Esant silpnam išoriniam žadinimui, (2.16) sistema redukuojama į fazės lygtį:

$$\dot{\vartheta} = 1 + \sin(\vartheta)I(\omega t). \tag{2.18}$$

Šiai FAF geometrinė pagalbinių funkcijų (2.13) prasmė pateikta 2.1 pav. Įstačius (2.17) lygtį į (2.13) sistemą ir suintegravus, gaunama pagalbinių funkcijų (2.13) analizinė išraiška

$$M_{+,-}(\xi) = \pm\sqrt{1-\xi^2}/\pi, \tag{2.19a}$$

$$N_{+,-}(\xi) = 1/2 \mp \arcsin(\xi)/\pi, \tag{2.19b}$$

Šių funkcijų grafikai pavaizduoti 2.2 pav.

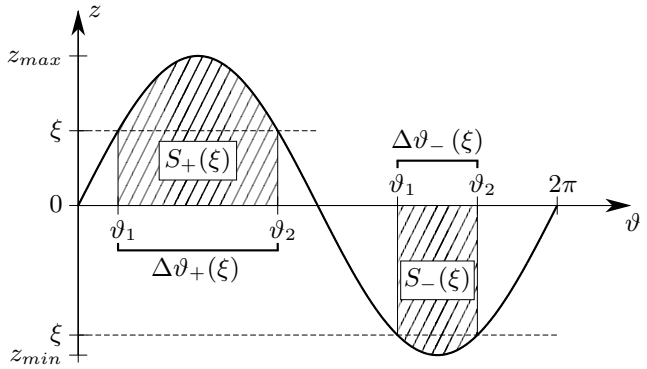

2.1 pav. Pagalbinių funkcijų (2.13) geometrinė prasmė. Ištisine linija pavaizduota FAF. Užštrichuotos sritys, pažymėtos $S_+(\xi)$ ir $S_-(\xi)$, žymi funkcijų $M_+(\xi) = S_+(\xi)/2\pi$ ir $M_-(\xi) = S_-(\xi)/2\pi$ vertes. Funkcijos $N_+(\xi) = \Delta\vartheta_+/2\pi$ ir $N_-(\xi) = \Delta\vartheta_-/2\pi$ apibrėžia fazinio kintamojo ϑ intervalus, kuriuose FAF yra atitinkamai aukščiau ir žemiau horizontalios tiesės $z = \xi$.

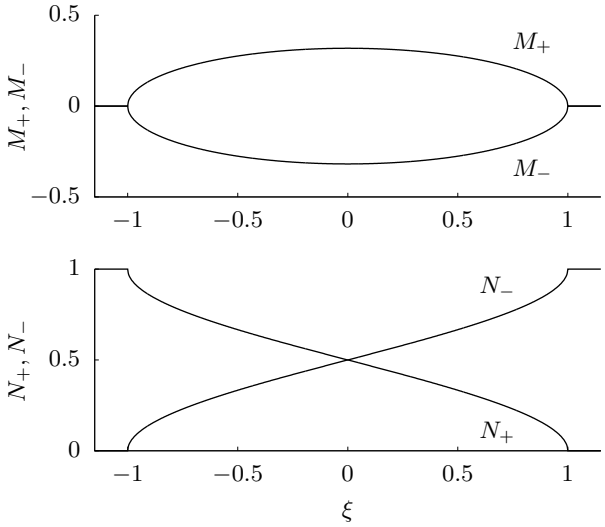

2.2 pav. Pagalbinės funkcijos $M_+(\xi)$ ir $M_-(\xi)$ (viršuje) bei $N_+(\xi)$ ir $N_-(\xi)$ (apačioje) Stuart-Landau osciliatoriui.

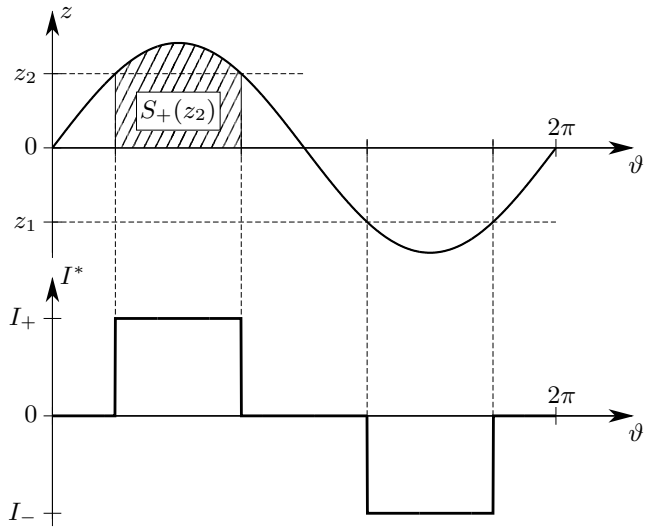

2.3 pav. Geometrinis optimalios valdymo srovės sudarymas Stuart-Landau osciliatoriui. Tiesė $z = z_2$ parinkta taip, kad užštrichuotos sritys tenkintų lygtį $S_+(z_2) \equiv 2\pi M_+(z_2) = \pi|\Delta\omega|/I_0$. Optimalios srovės (2.20) išraiška gaunama suprojektavus tiesių $z = z_2$ ir $z = z_1 = -z_2$ sankirtos su FAF taškus į ϑ ašį. Pavaizduota optimali srovė atitinka $\Delta\omega > 0$. $\Delta\omega < 0$ atveju, optimali srovė įgyja priešingą ženklą.

Kadangi FAF (2.17) yra nelyginė funkcija, natūralu parinkti simetrinį stimuliacijos amplitudės ribojimą, $I_+ = -I_- \equiv I_0$. Tokiu atveju, optimali srovė (2.11) keičia ženklą priklausomai nuo $\Delta\omega$ ženklo:

$$I^*(\vartheta) = I_0\{H[z(\vartheta) - z_2] - H[z_1 - z(\vartheta)]\}\,\mathrm{sgn}(\Delta\omega). \tag{2.20}$$

2.3 pav. pavaizduotas optimalios srovės sudarymo algoritmas. Parametrai $z_{1,2}$ apskaičiuojami iš lygčių:

$$z_{1,2} = \mp\sqrt{1 - (\pi\Delta\omega/2I_0)^2}. \tag{2.21}$$

Optimali funkcionalo (2.15) išraiška (2.4 pav.):

$$\mathcal{J}^* = \frac{2I_0}{\pi}\arcsin\left(\frac{\pi|\Delta\omega|}{2I_0}\right). \tag{2.22}$$

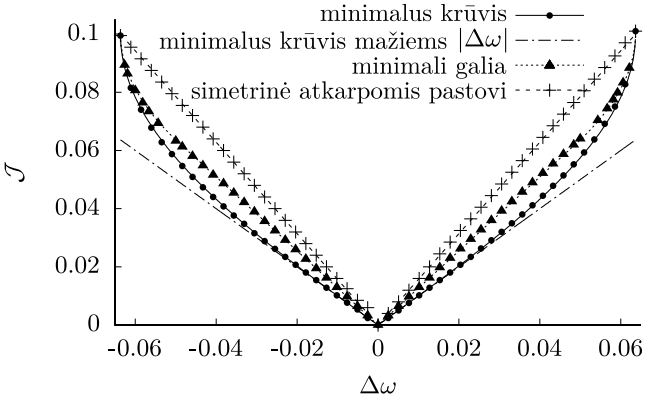

2.4 pav. Arnoldo liežuviai Stuart-Landau osciliatoriui. Stimuliacijos srovės $\mathcal{J}$ modulio vidurkio [(2.3) lygtis] priklausomybė nuo dažnių skirtumo $\Delta\omega$, pavaizduota trims srovės formoms. Ištisine linija nubrėžta kreivė su taškais atitinka minimalaus krūvio srovę (2.20). Brūkšnine-taškine linija pavaizduota aproksimacija (2.26). Taškinė linija su trikampiais vaizduoja minimalios galios srovę (2.25). Punktyrinė linija su „+“ simboliais atitinka simetrinę atkarpomis pastovią srovę (2.24). Linijos žymi teorines kreives, simboliai – skaitinių eksperimentų rezultatus.

Osciliatoriaus sinchronizacija su optimalia srove (2.20) galima baigtiniame dažnių intervale:

$$|\Delta\omega| \leq 2I_0/\pi. \tag{2.23}$$

2.3.1 Rezultatų palyginimas skirtingoms valdymo srovėms

Norint patikrinti išvestos signalo formos (2.20) optimalumą, apskaičiuoti Arnoldo liežuviai dar dviems valdymo srovės formoms (2.5 pav): simetrinei atkarpomis pastoviai srovei

$$I_{sb}(\vartheta) = I_0\{H[\sin(\vartheta)] - H[-\sin(\vartheta)]\}, \tag{2.24}$$

ir srovei, užtikrinančiai sinchronizaciją minimalia galia [41]

$$I_E^*(\vartheta) = \begin{cases} -I_0, & \text{jei } \tilde{I}_E(\vartheta) \leq -I_0, \\ \tilde{I}_E(\vartheta) = 2|\Delta\omega|\sin(\vartheta), & \text{jei } \left|\tilde{I}_E(\vartheta)\right| < I_0, \\ I_0, & \text{jei } \tilde{I}_E(\vartheta) \geq I_0. \end{cases} \tag{2.25}$$

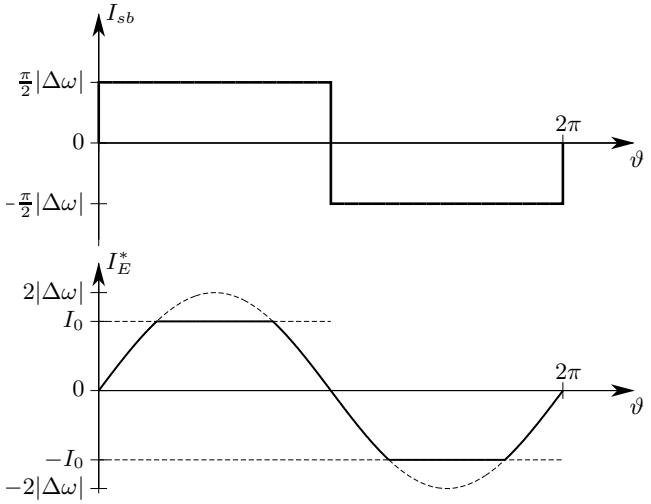

2.5 pav. Simetrinė atkarpomis pastovi (viršuje) bei minimalios galios (apačioje) srovės Stuart-Landau osciliatoriui. Arnoldo liežuviai šiems signalams pateikti 2.4 pav.

$\mathcal{J}^*$ priklausomybė nuo dažnių skirtumo $\Delta\omega$ šioms dviems srovės formoms palyginta su krūviu optimaliuoju valdymu (su ir be amplitudės ribojimo) 2.4 pav. Skaitinių eksperimentų rezultatai sutampa su teoriniais skaičiavimais ir patvirtina optimizavimo uždavinio sprendimo teisingumą.

2.3.2 Mažas dažnių skirtumas

Esant mažam dažnių skirtumui, $|\Delta\omega| \ll 2I_0/\pi$, kuomet valdymo srovės amplitudės ribojimas yra nereikšmingas, (2.22) lygtis tampa

$$\mathcal{J}^* \approx |\Delta\omega|, \tag{2.26}$$

t.y. Arnoldo liežuviai yra tiesės (brūkšninės-taškinės linijos 2.4 pav.). Iš (2.22) lygties išplaukia $z_{1,2} \approx \mp[1-(\pi\Delta\omega/2I_0)^2/2]$. Kai $|\Delta\omega| \to 0$, parametro z_2 vertė artėja prie FAF maksimumo, $z_2 \to \max[z(\vartheta)] = 1$, o parametro z_1 vertė – prie FAF minimumo, $z_1 \to \min[z(\vartheta)] = -1$. Iš to seka, kad optimali valdymo srovė yra sudaryta iš dviejų siaurų stačiakampių I_0 aukščio impulsų, vieno teigiamo, kito neigiamo, centruotų ties FAF maksimumu ir minimumu.

Impulsų plotis artėja prie nulio, kai $|\Delta\omega| \to 0$. Galima daryti išvadą, kad optimalus valdymas priklauso tik nuo FAF formos ties jos ekstremumais.

2.4 Optimalus valdymas mažoms $|\Delta\omega|$ vertėms bendruoju atveju

Nagrinėjamas apibendrintas optimizavimo uždavinys esant mažam dažnių skirtumui $|\Delta\omega|$ bet kokiai FAF $z(\vartheta)$ ir nesimetriniam valdymo srovės apribojimui $I_- \le I(\omega t) \le I_+$. $|\Delta\omega|$ vertės yra mažos lyginant su sinchronizacijos intervalu, kuris priklauso nuo amplitudės rėžių I_- ir I_+.

Daroma prielaida, kad FAF $z(\vartheta)$ yra tolydi 2π-periodinė funkcija, įgyjanti absoliutų maksimumą $z_{max} > 0$ taške $\vartheta = \vartheta_{max}$ ir absoliutų minimumą $z_{min} < 0$ taške $\vartheta = \vartheta_{min}$. Nesunku pastebėti, kad kai $|\Delta\omega| \to 0$, (2.12) lygčių sprendiniai tenkina išraiškas $z_1 \to z_{min}$ ir $z_2 \to z_{max}$. Apruoksimuojant FAF parabolėmis jos ekstremumų ϑ_{max} ir ϑ_{min} aplinkose, gaunamos apytikrės pagalbinių funkcijų $M_+(\xi)$ ir $N_+(\xi)$ vertės z_{max} aplinkoje bei funkcijų $M_-(\xi)$ ir $N_-(\xi)$ vertės z_{min} aplinkoje. Išsprendus (2.12) lygtis, gaunama optimalios valdymo srovės išraiška:

$$I^*(\vartheta) = I_+\Pi\left(\frac{\vartheta}{\Delta\vartheta_+}\right) + I_-\Pi\left(\frac{\vartheta \pm \Delta\vartheta_z}{\Delta\vartheta_-}\right), \tag{2.27}$$

kur pliusas (minusas) atitinka $\Delta\omega > 0$ ($\Delta\omega < 0$). $\Pi(x)$ yra stačiakampė funkcija, įgyjanti reikšmes $\Pi(x) = 1$, kai $|x| < 1/2$, ir $\Pi(x) = 0$, kai $|x| > 1/2$. Vadinasi, valdymo srovė (2.27) sudaryta iš teigiamo ir neigiamo impulsų, centruotų atitinkamai ties ϑ_{max} ir ϑ_{min}. Teigiamo (neigiamo) impulso aukštis yra I_+ (I_-), o plotis – $\Delta\vartheta_+$ ($\Delta\vartheta_-$). Impulsų pločiai $\Delta\vartheta_{+,-}$ apskaičiuojami iš lygties

$$\Delta\vartheta_{+,-} = \frac{2\pi\Delta\omega}{I_{+,-}(z_{max} - z_{min})}. \tag{2.28}$$

Optimaliai valdymo srovei sudaryti užtenka žinoti dvi FAF savybes: atstumą tarp jos ekstremumų $\Delta\vartheta_z = \vartheta_{max} - \vartheta_{min}$ bei amplitudę $z_{max} - z_{min}$. Optimali

funkcionalo $\mathcal{J}^*$ vertė yra

$$\mathcal{J}^* = \frac{2|\Delta\omega|}{z_{max} - z_{min}}. \tag{2.29}$$

2.5 Skaitiniai pavyzdžiai

(2.27) išraiškos pagrindu sudaroma eksperimentinė valdymo srovė, sudaryta iš teigiamo ir neigiamo impulsų

$$I(\vartheta) = a\left[\Pi\left(\frac{s\vartheta}{l}\right) - \frac{1}{s}\Pi\left(\frac{\vartheta + d}{l}\right)\right], \tag{2.30}$$

atskirtų atstumu d. Parametras s nusako impulsų asimetriją: teigiamo impulso plotis yra l/s, amplitudė a, o centras – taške $\vartheta = 0$, neigiamo impulso plotis l, amplitudė a/s, centras $\vartheta = -d$. Varijuojant parametrus l ir d, apskaičiuojama slenkstinė amplitudės vertė $a = a_{th}$, kurią pasiekus įvyksta sinchronizacija su valdymo srove. Funkcionalo (2.3) vertė ties sinchronizacijos slenksčiu yra

$$\mathcal{J}_{th} = a_{th} l/s\pi. \tag{2.31}$$

Skaitinio eksperimento rezultatai atsitiktinai sugeneruotai FAF

$$\begin{aligned} z(\vartheta) = {} & 0.745705\cos(\vartheta) - 0.666276\sin(\vartheta) \\ & - 0.134064\cos(2\vartheta) - 0.940493\sin(2\vartheta) \\ & - 0.222622\cos(3\vartheta) + 0.768401\sin(3\vartheta) \end{aligned} \tag{2.32}$$

naudotai [97] šaltinyje, pateikti 2.6 ir 2.7 pav. Teorinės optimalios vertės $d = -\Delta\vartheta_z$ ir $d = \Delta\vartheta_z$ atitinka $\mathcal{J}_{th}$ minimumą ir sutampa su teorine verte $\mathcal{J}^*$, gauta iš (2.29) lygties.

Arnoldo liežuviai, apskaičiuoti klasikiniam HH neurono modeliui (2.8 pav.), naudojant tris skirtingas valdymo sroves, pateikti 2.9 pav. Skaitiniu būdu apskaičiuotos vertės sutampa su teorinėmis, o tikslo funkcionalo vertės optimaliai srovei (2.27) yra mažiausios.

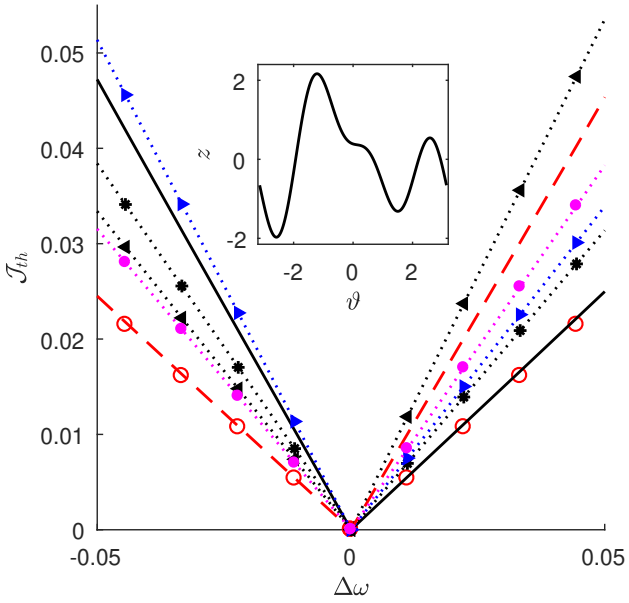

2.6 pav. Arnoldo liežuviai osciliatoriui, apibrėžtam (2.32) FAF. Valdymo srovės modulio vidurkio $\mathcal{J}_{th}$ [(2.31) lygtis] priklausomybė nuo dažnių skirtumo $\Delta\omega$ eksperimentinei srovei (2.30). Parametrų vertės $s = 2$ ir $I_+ = 1$ fiksuotos. Kreivės atitinka skirtingas atstumo tarp teigiamo ir neigiamo impulso d vertes: $d = -2$ (juodos taškinės linijos su žvaigždutėmis), $d = -\Delta\vartheta_z \approx -1.3660$ (juodos ištisinės linijos), $d = -0.7$ (mėlynos taškinės linijos su dešinėn nukreiptais trikampiais), d=0.7 (juodos taškinės linijos su kairėn nukreiptais trikampiais), $d = \Delta\vartheta_z$ (raudonos punktyrinės linijos) and $d = 2$ (magenta spalvos taškinės linijos su skrituliais). Parametrų vertės $d = -\Delta\vartheta_z$ ir $d = \Delta\vartheta_z$ atitinka teorinius optimalius atstumus kai $\Delta\omega > 0$ ir $\Delta\omega < 0$. Raudoni apskritimai žymi teorines optimalias funkcionalo $\mathcal{J}^*$ vertes, gautas iš (2.29) lygties. Įdėtiniame paveiksle pavaizduota (2.32) FAF.

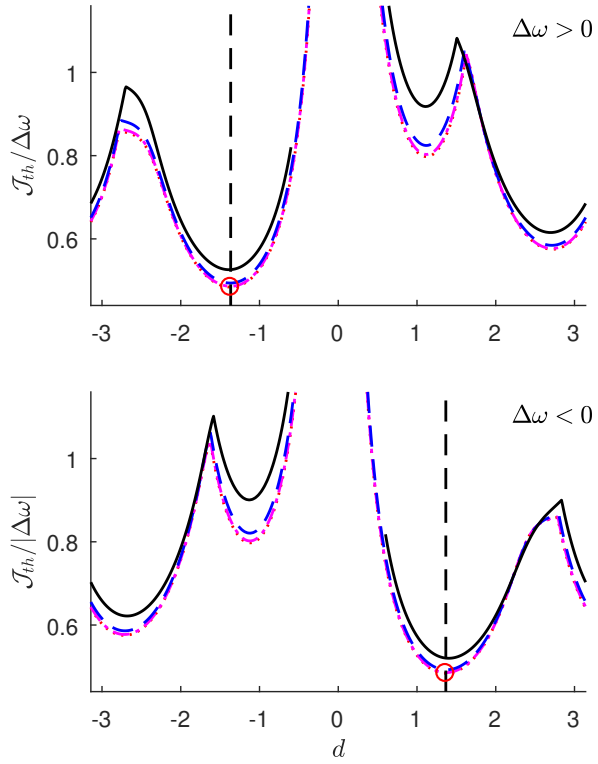

2.7 pav. $\mathcal{J}_{th}/|\Delta\omega|$ priklausomybė nuo d osciliatoriui, apibrėžtam (2.32) FAF. Čia d yra atstumas tarp eksperimentinės srovės (2.30) teigiamo ir neigiamo impulso. Viršutinis (apatinis) grafikas atitinka $\Delta\omega > 0$ ($\Delta\omega < 0$). Impulsų asimetrijos parametro vertė $s = 2$ fiksuota. Kreivės atitinka skirtingas impulso pločio l vertes: $l = 0.1$ (raudonos taškinės linijos), $l = 0.2$ (magenta spalvos brūkšninės-taškinės linijos), $l = 0.4$ (mėlynos punktyrinės linijos) ir $l = 0.8$ (juodos ištisinės linijos). Vertikalios punktyrinės tiesės žymi teorinius optimalius atstumus tarp impulsų: $d = -\Delta\vartheta_z \approx -1.3660$, kai $\Delta\omega > 0$, ir $d = \Delta\vartheta_z$, kai $\Delta\omega < 0$. Raudoni apskritimai žymi teorines optimalias funkcionalo $\mathcal{J}^*$ vertes, gautas iš (2.29) lygties.

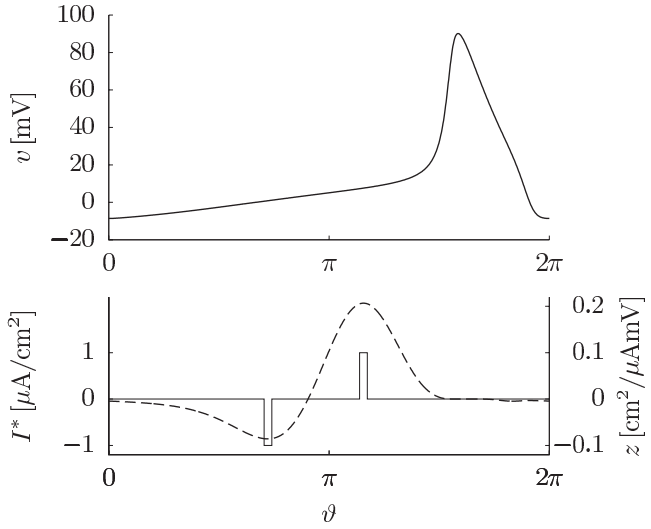

2.8 pav. (Viršuje) Hodgkin-Huxley neurono veikimo potencialas nesant stimuliacijos [$I(\omega t) = 0$]. (Apačioje) FAF (punktyrinė linija) ir optimali valdymo srovė [(2.27) lygtis] (ištisinė linija), parametrai $I_+ = -I_- = 1$ μA/cm^2 ir $\Delta\omega = 0.01$ rad/ms.

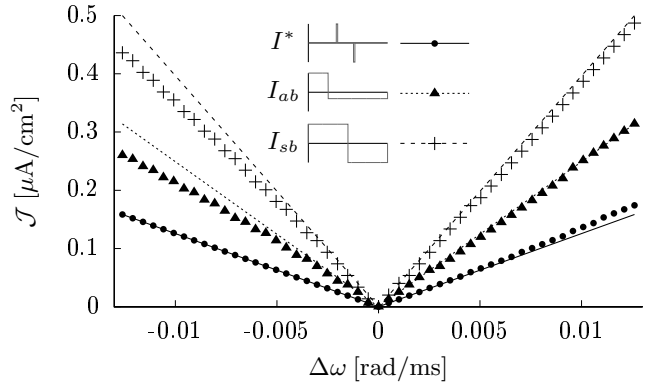

2.9 pav. Arnoldo liežuviai Hodgkin-Huxley neurono modeliui. Vaizduojama valdymo srovės modulio vidurkio $\mathcal{J}$ [(2.3) lygtis] priklausomybė nuo dažnių skirtumo $\Delta\omega$ trims valdymo srovėms. Tiesėmis pavaizduoti analiziškai gauti rezultatai, simboliai žymi skaitinių sprendinių vertes. Ištisinės linijos ir taškai atitinka optimalią valdymo srovę, apibrėžtą (2.27) ir (2.28) lygtimis. Taškinės linijos ir trikampiai atitinka asimetrinę atkarpomis pastovią srovę. Punktyrinės linijos su pliuso simboliais žymi simetrinę atkarpomis pastovią srovę.

3 Sąveikaujančių neuronų tinklo sinchronizacija minimizuojant stimuliacijos krūvį

Šiame skyriuje aukščiau aprašyta optimaliojo valdymo metodika pritaikoma sinchronizuotam sąveikaujančių neuronų tinklui. Tam tikslui naudojama heterogeninių dinaminių elementų tinklų fazinės redukcijos teorija [82]. Taip pat nagrinėjamas didelio masto pilnai susieto heterogeninių *quadratic integrate-and-fire* (QIF) neuronų tinklo valdymas. Begalinio neuronų skaičiaus riboje toks tinklas gali būti redukuotas į mažos dimensijos makroskopinį tinklo modelį [85, 86]. Makroskopinės lygtys leidžia nesunkiai apskaičiuoti tinklo FAF bei sudaryti optimalią valdymo srovę.

3.1 Uždavinio formuluotė

Nagrinėjamas iš N susietų HH tipo heterogeninių neuronų sudarytas tinklas, veikiamas periodinio išorinio žadinimo

$$\dot{v}_i = F_i(v_i, \mathbf{w}_i) + \sum_{j=1}^{N} H_{ij}(v_i, v_j) + I_i(\omega t), \tag{3.1a}$$

$$\dot{\mathbf{w}}_i = \mathbf{G}_i(v_i, \mathbf{w}_i), \quad (i = 1, \ldots, N). \tag{3.1b}$$

Čia skaliaras v_i ir vektorius $\mathbf{w}_i \in \mathbb{R}^n$ atitinkamai yra i-tojo neurono membranos potencialas ir atstatomasis kintamasis. Funkcija $F_i(v_i, \mathbf{w}_i)$ aprašo pro i-tojo neurono jonų kanalus tekančias sroves; funkcija $H_{ij}(v_i, v_j)$ apibrėžia i-tojo neurono poveikį j-ajam neuronui. $I_i(\omega t)$ yra i-tąjį neuroną veikianti 2π-periodinė stimuliacijos srovė, kurios dažnis yra ω, o periodas yra $T = 2\pi/\omega$. (3.1b) lygtis apibrėžia atstatamojo kintamojo $\mathbf{w}_i$ dinamiką, kur funkcija $\mathbf{G}_i(v_i, \mathbf{w}_i)$ aprašo jonų kanalų dinamiką. Vektoriaus $\mathbf{w}_i$ bei funkcijų F_i ir $\mathbf{G}_i$ dimensija n priklauso nuo konkretaus neurono modelio.

Daroma prielaida, kad, nesant stimuliacijos [$I_i(\omega t) = 0$], visas tinklas osciliuoja bendrame ribiniame cikle periodu T_0 bei dažniu $\omega_0 = 2\pi/T_0$. Tikslas – rasti optimalią valdymo formą $I_i(\omega t)$, užtikrinančią tinklo sinchronizaciją su valdymo srovės dažniu ω minimizuojant stimuliacijos periodu neuronams

tenkantį krūvį. Turi būti tenkinamos visos ankstesniame skyriuje aprašytos sąlygos: krūvio balanso sąlyga, valdymo srovės amplitudės rėžiai bei uždavinio kraštinės sąlygos.

Esant pakankamai silpnai valdymo srovei $I_i(\omega t)$, pritaikius fazinės redukcijos metodą [73, 83, 95], $(n+1)N$ dimensijos (3.1) lygčių sistema redukuojama į vieną skaliarinę lygtį

$$\dot{\vartheta} = \omega_0 + \sum_{i=1}^{N} z_i(\vartheta) I_i(\omega t), \tag{3.2}$$

kurioje $\vartheta(t)$ yra kolektyvinė tinklo fazė. Čia $z_i(\vartheta)$ yra 2π-periodinė i-tojo neurono FAF.

3.2 Optimali valdymo srovė sąveikaujančių neuronų tinklo sinchronizacijai

Nagrinėjamas atvejis, kai ta pačia valdymo srove $I(\omega t)$ stimuliuojamas neuronų tinklo poaibis $i \in \{i_k\} \equiv \{i_1, i_2, \ldots, i_M\}$, kur $M \leq N$, t.y.

$$I_i(\omega t) = \begin{cases} I(\omega t), & \text{kai } i \in \{i_1, i_2, \ldots, i_M\}, \\ 0, & \text{kitu atveju.} \end{cases} \tag{3.3}$$

Tuomet fazės lygtis (3.2) tampa

$$\dot{\vartheta} = \omega_0 + z(\vartheta) I(\omega t), \tag{3.4}$$

kur

$$z(\vartheta) = \sum_{k=1}^{M} z_{i_k}(\vartheta). \tag{3.5}$$

Neuronų tinklo fazės lygtis (3.4) sutampa su vieno neurono fazės lygtimi, skiriasi tik FAF $z(\vartheta)$, kuri šiuo atveju yra stimuliuojamų neuronų FAF suma. Todėl galima tiesiogiai taikyti ankstesniame skyriuje gautus rezultatus.

3.3 Skaitiniai pavyzdžiai

Norint patikrinti valdymo srovės (2.27) optimalumą, naudojama eksperimentinė valdymo srovė (2.30).

Slenkstinė sinchronizacijos amplitudė a_{th} apskaičiuojama dviem metodais: (i) skaitiniu būdu tiesiogiai integruojant netiesinę sistemą (3.1) ir (ii) naudojant apytikrę fazę (3.4). Pirmuoju metodu fiksuojamos parametrų s, l ir d vertės, tuomet varijuojant eksperimentinės srovės (2.30) amplitudę a, randama minimali a vertė a_{th}, užtikrinanti (3.1) lygčių sinchronizaciją su valdymo srove. Antruoju metodu įvedamas fazių skirtumas $\varphi = \vartheta - \omega t$ ir iš (3.4) lygties gaunama šio kintamojo atžvilgiu suvidurkinta lygtis:

$$\dot{\varphi} = -\Delta\omega + \frac{1}{2\pi}\int_{-\pi}^{\pi} z(\vartheta+\varphi)I(\vartheta)\,\mathrm{d}\vartheta\,. \tag{3.6}$$

Apibrėžiama pagalbinė funkcija

$$\Phi(\varphi|s,l,d) = \frac{1}{2\pi a}\int_{-\pi}^{\pi} z(\vartheta+\varphi)I(\vartheta)\,\mathrm{d}\vartheta\,, \tag{3.7}$$

leidžianti apskaičiuoti slenkstinę amplitudės vertę:

$$a_{th} = \Delta\omega \begin{cases} 1/\max\limits_{\varphi}[\Phi(\varphi|s,l,d)], & \text{kai} \quad \Delta\omega > 0, \\ 1/\min\limits_{\varphi}[\Phi(\varphi|s,l,d)], & \text{kai} \quad \Delta\omega < 0. \end{cases} \tag{3.8}$$

Išnagrinėta santykio $\mathcal{J}_{th}/|\Delta\omega|$ priklausomybė nuo atstumo tarp valdymo srovės impulsų d esant fiksuotoms parametrų s bei l vertėms. Patikrinta, ar $\mathcal{J}_{th}/|\Delta\omega|$ įgyja absoliutų minimumą taške $d = \Delta\vartheta_z$ ($d = -\Delta\vartheta_z$), kai $\Delta\omega > 0$ ($\Delta\omega < 0$), ir ar šių minimų reikšmės sutampa su teorinėmis vertėmis $\mathcal{J}^*/|\Delta\omega|$, gautomis iš (2.29) lygties. Optimalios vertės priklauso tik nuo FAF amplitudės $\mathcal{J}^*/|\Delta\omega| = 2/(z_{max} - z_{min})$ ir nepriklauso nuo kitų valdymo algoritmo parametrų, tokių kaip valdymo srovės amplitudės rėžiai I_- ir I_+.

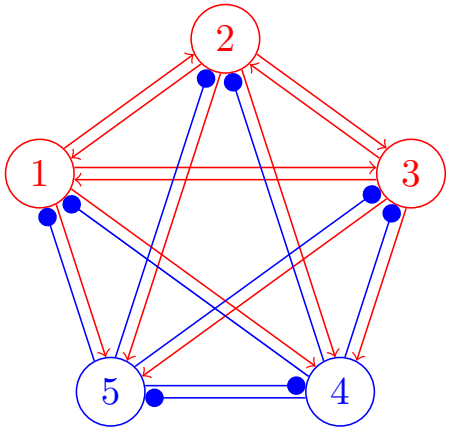

3.1 pav. Penkių sinapsėmis susietų FHN neuronų tinklas. Skaičiais 1, 2 ir 3 paženklinti raudoni apskritimai žymi eksitatorinius neuronus, mėlyni skaičiais 4 ir 5 pažymėti apskritimai – inhibitorinius. Raudonos rodyklės bei mėlynos tiesės su apskritimais žymi atitinkamai eksitatorines bei inhibitorines sinapses. Eksitatoriniai neuronai yra savaime osciliuojantys ($\gamma_i = 0.8$, $i = 1, 2, 3$), inhibitoriniai yra sužadinamieji ($\gamma_i = 0.2$, $i = 4, 5$).

3.3.1 Sinapsėmis susietų FHN neuronų tinklas

Patikriname optimaliojo valdymo teorijos teisingumą sinapsėmis susietų FitzHugh-Nagumo (FHN) neuronų tinklui:

$$F_i(v_i, w_i) = v_i - v_i^3/3 - w_i + \gamma_i, \tag{3.9a}$$

$$G_i(v_i, w_i) = \delta(\alpha + v_i - \beta w_i), \tag{3.9b}$$

$$H_{ij}(v_i, v_j) = K_{ij} S_j(v_j). \tag{3.9c}$$

$N = 5$ FHN neuronų tinklo schema pavaizduota 3.1 pav. Parametrų vertės $\alpha = 0.7$, $\beta = 0.8$ ir $\delta = 0.08$ vienodos visiems neuronams, tačiau skiriasi γ_i vertės. Pirmi trys neuronai, $i = 1, 2, 3$, yra savaime osciliuojantys, jų parametras $\gamma_i = 0.8$. Kiti du neuronai, $i = 4, 5$, spontaniškai neaktyvūs, tačiau gali būti sužadinti įeinančių signalų; jų parametro vertė $\gamma_i = 0.2$.

Daroma prielaida, jog sinapsės yra greitos, ir j-tojo presinapsinio neurono i-tajam postsinapsiniam neuronui indukuota srovė gali būti aprašyta (3.9c) lygtimi, kur K_{ij} yra j-tojo neurono poveikio i-tajam neuronui stipris. $S_j(v_j)$ yra

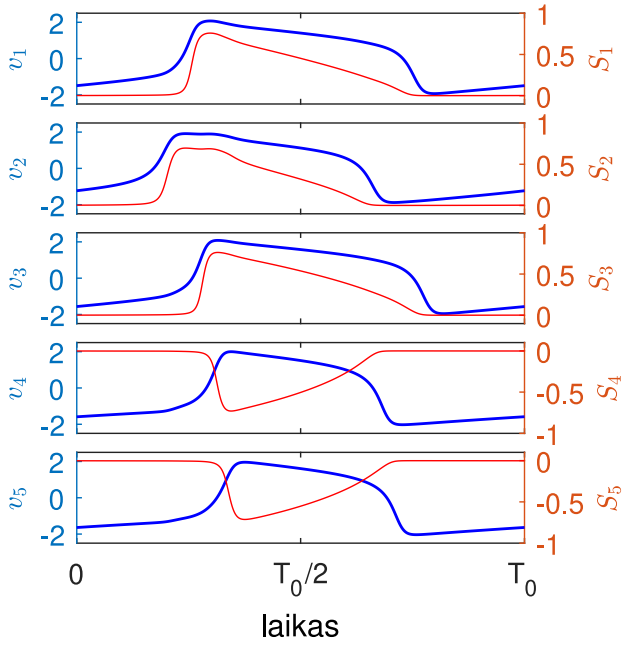

3.2 pav. Sinapsėmis susietų FHN neuronų membranos potencialų v_j (paryškintos mėlynos kreivės) ir sinapsinių kintamųjų S_j (plonos raudonos kreivės) dinamika nesant išorinės stimuliacijos.

sinapsinė srovė, generuojama j-tojo presinapsinio neurono:

$$S_j(v_j) = p_j \left[1 + \exp\left(-\frac{v_j - v_{th}}{\sigma}\right)\right]^{-1}, \tag{3.10}$$

čia $v_{th} = 1.5$ ir $\sigma = 0.5$ yra sinapsės parametrai, o p_j nustato sinapsinio impulso ženklą: $p_j = +1$ eksitatorinėms ir $p_j = -1$ inhibitorinėms sinapsėms. Sąveikos matricos elementai K_{ij} yra atsitiktiniai tolygiai intervale $[0, 0.5]$ pasiskirstę nepriklausomi dydžiai. Tinklo neuronų membranos ir sinapsinių potencialų, $v_j(t)$ ir $S_j(v_j(t))$, dinamika pavaizduota 3.2 pav. 3.3 pav. pateiktos neuronų FAF $z_j(\vartheta)$.

3.1 pav. pavaizduoto neuronų tinklo architektūra atitinka pogumburio branduolio (lot. *nucleus subthalamicus* (STN)) bei blyškiojo kamuolio (lot. *globus pallidus*) išorinio segmento (GPe) neuroninio tinklo struktūrą. STN sudaro eksitatoriniai osciliuojantys neuronai, GPe – sužadinamieji inhibtoriniai

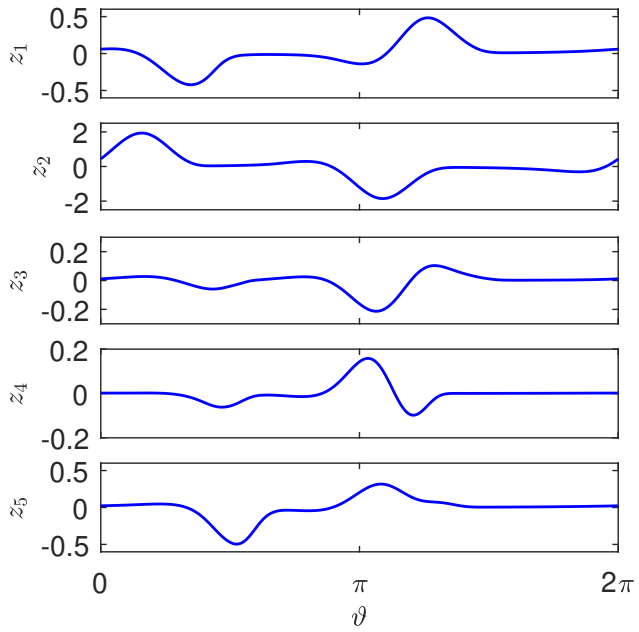

3.3 pav. Sinapsėmis susietų FHN neuronų tinklo fazės atsako funkcijos.

neuronai. Šių branduolių neuroninis tinklas veikia kaip ritmo vedlys ir yra plačiai taikomas Parkinsono ligos modeliavimui [133].

Nagrinėjami du stimuliavimo protokolai: (i) stimuliuojami tik eksitatoriniai neuronai, kurių indeksai $j = 1, 2, 3$. Šiuo atveju, FAF $z = z_1 + z_2 + z_3$; (ii) stimuliuojami tik inhibitoriniai neuronai, kurių indeksai $j = 4, 5$. Tuomet FAF yra $z = z_4 + z_5$. Šios FAF bei santykio $\mathcal{J}_{th}/|\Delta\omega|$ priklausomybė nuo atstumo d tarp valdymo srovės (2.30) impulsų (i) ir (ii) stimuliavimo protokolui pavaizduota atitinkamai 3.4 ir 3.5 pav.

Abiem atvejais, suvidurkintos fazės lygties (3.6) sprendiniai ir tiesioginio (3.1) netiesinės sistemos modeliavimo rezultatai patvirtina 3.2 skyrelyje pateiktos teorijos teisingumą. Tikslo funkcionalo minimalios vertės sutampa su teoriškai prognozuotomis vertėmis (2.29).

Pirmasis stimuliavimo protokolas yra efektyvesnis. Taip yra todėl, kad eksitatoriniai neuronai yra jautresni išoriniam žadinimui – jų FAF amplitudė keturis kartus didesnė.

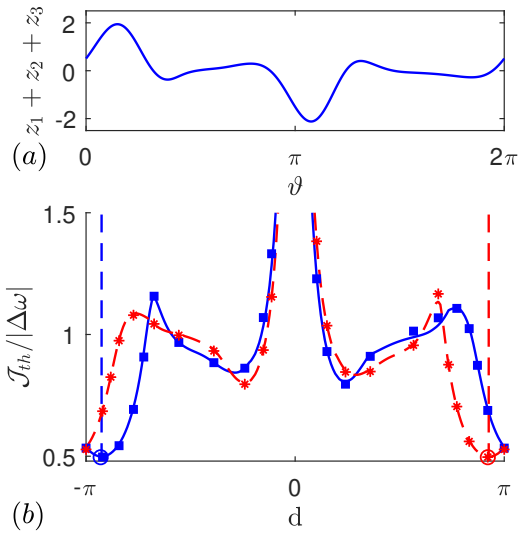

3.4 pav. Sinapsėmis susietų FHN neuronų tinklo valdymo minimaliu krūviu teorijos patikrinimas stimuliuojant tik eksitatorinius neuronus, kurių indeksai $j = 1, 2, 3$. (a) FAF $z = z_1 + z_2 + z_3$, fazinis atstumas tarp jos maksimumo ir minimumo $\Delta\vartheta_z = -2.9084$, amplitudė $z_{max} - z_{min} = 4.0634$. (b) Slenkstinės (2.3) funkcionalo vertės $\mathcal{J}_{th}$, normalizuotos pagal dažnių skirtumą $|\Delta\omega|$, priklausomybė nuo atstumo d tarp valdymo srovės (2.30), esant fiksuotiems parametrams $l = 0.2$ ir $s = 2$. Paryškinta mėlyna bei plona raudona kreivė atitinka rezultatus, gautus iš vidurkintos fazės lygties (3.6) esant $\Delta\omega > 0$ bei $\Delta\omega < 0$. Mėlyni kvadratai bei raudonos žvaigždutės atitinka rezultatus, gautus integruojant (3.1) netiesines lygtis. Vertikalios punktyrinės tiesės žymi teorinius optimalius atstumus $d = \pm\Delta\vartheta_z$. Apskritimai žymi teorines optimalias vertes (2.29).

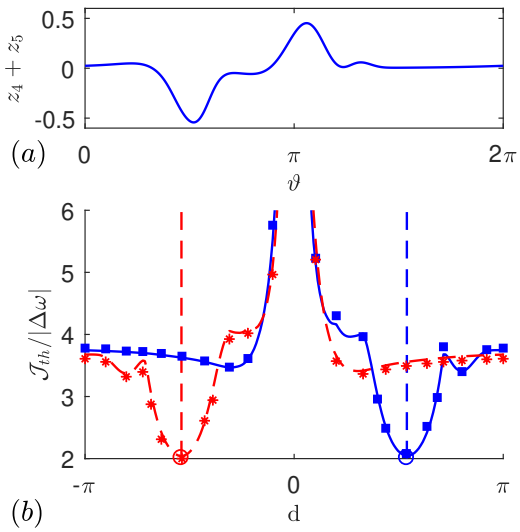

3.5 pav. Grafikai analogiški pateiktiems 3.4 pav., tačiau stimuliuojami inhibitoriniai neuronai, kurių indeksai $j = 4, 5$. FAF šiuo atveju yra $z = z_4 + z_5$, fazinis atstumas tarp jos ekstremumų yra $\Delta\vartheta_z = 1.6935$, amplitudė $z_{max} - z_{min} = 0.9949$. Kitų parametrų vertės tokios pat kaip 3.4 pav.

3.3.2 Elektriniu ryšiu susietų FHN neuronų tinklas

Nagrinėsime $N = 10$ elektriniu ryšiu susietų FHN neuronų tinklą [82]. Fiziologinis tokio tinklo atitikmuo – plyšinėmis jungtimis (angl. *gap junctions*) susietų nervinių ląstelių tinklas. Kaip ir anksčiau, funkcijos $F_i(v_i, w_i)$ ir $G_i(v_i, w_i)$ apibrėžiamos (3.9a) ir (3.9b) išraiškomis, o funkcija $H_{ij}(v_i, v_j)$ tampa

$$H_{ij}(v_i, v_j) = K_{ij}(v_j - v_i). \tag{3.11}$$

Parametrai $\alpha = 0.7$, $\beta = 0.8$ ir $\delta = 0.08$ yra tokie patys visiems neuronams; inhibitorinių neuronų su indeksais $i = 1, \ldots, 7$ parametras $\gamma_i = 0.2$, tuo tarpu eksitatorinių neuronų su indeksais $i = 8, 9, 10$ parametras $\gamma_i = 0.8$. 10×10 dydžio sąveikos matricos elementai K_{ij} sugeneruoti atsitiktiniu būdu.

3.6 pav. pateikti eksitatorinių neuronų su indeksais $i = 8, 9, 10$ stimuliavimo rezultatai. FAF forma ir $\mathcal{J}_{th}/|\Delta\omega|$ priklausomybė nuo d [3.6(b) pav.] yra sudėtingesnė, tačiau, kaip ir ankstesniuose pavyzdžiuose, absoliutus minimumas yra taške $d = \vartheta_z$, kai $\Delta\omega < 0$, ir taške $d = -\vartheta_z$, kai $\Delta\omega < 0$. Čia

$\vartheta_z \approx -0.5154$ yra atstumas tarp FAF ekstremumų. Absoliutusis $\mathcal{J}_{th}/|\Delta\omega|$ minimumas sutampa su (2.29). Galima daryti išvadą, kad išvesta optimaliojo valdymo teorija galioja ir sudėtingų tinklų modeliams.

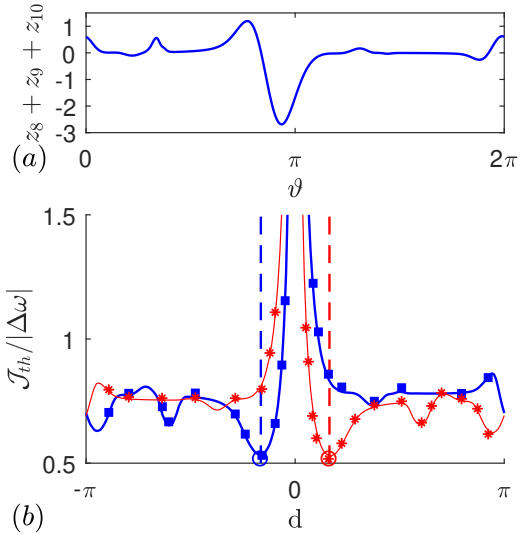

3.6 pav. Elektriniu ryšiu susietų FHN neuronų tinklo valdymo minimaliu krūviu teorijos patikrinimas stimuliuojant tik eksitatorinius neuronus, kurių indeksai $j = 8, 9, 10$. (a) Tinklo FAF $z = z_8 + z_9 + z_{10}$, fazinis atstumas tarp jos ekstremumų $\Delta\vartheta_z = -0.5154$, amplitudė $z_{max} - z_{min} = 3.8814$. (b) $\mathcal{J}_{th}/|\Delta\omega|$ priklausomybė nuo d esant fiksuotiems parametrams $l = 0.2$ ir $s = 2$. Žymėjimas toks pat kaip 3.4 pav.

3.3.3 Didelio masto sinapsėmis susietų kvadratinių integrate-and-fire neuronų tinklas

Nagrinėjamas heterogeninis pilnasis tinklas, sudarytas iš didelio kiekio sinapsėmis susietų QIF neuronų. Mikroskopinė tinklo būsena priklauso nuo neuronų membranos potencialų v_i, kurių dinamiką aprašo lygtys [80]:

$$\dot{v}_i = v_i^2 + \eta_i + S(t) + I(\omega t), \quad (i = 1, \ldots, N). \tag{3.12}$$

Čia konstantos η_i nustato individualių neuronų elgseną, $S(t)$ yra sinapsinė srovė, o $I(\omega t)$ yra išorinis periodinis žadinimas. Daroma prielaida, kad visi tinklo neuronai yra vienodai veikiami išorinės stimuliacijos. Kai membranos

potencialas v_i pasiekia didžiausią vertę v_{peak}, įtampa atstatoma į vertę v_{reset}. Nustatomos vertės $v_{peak} = -v_{reset} \to \infty$. Jei sinapsių dinamika yra greita, jos gali būti modeliuojamos funkcija [86]:

$$S(t) = J\frac{v_{th}}{N}\sum_{j=1}^{N} H(v_j(t) - v_{th}). \tag{3.13}$$

Čia J yra sąveikos stipris, $H(\cdot)$ yra Hevisaido vienetinė funkcija, v_{th} – slenkstinis potencialas. Parametro J ženklas eksitatorinėms (inhibitorinėms) sinapsėms yra teigiamas (neigiamas). Baigtinis sinapsinio impulso plotis yra esminis veiksnys savaiminių makroskopinių tinklo svyravimų atsiradimui [86].

Kai $\eta_i < 0$, neuronas yra sužadinimajame režime, kai $\eta_i > 0$, jis periodiškai generuoja impulsus. Jei parametro η_i reikšmės yra pasikirsčiusios pagal Lorenco skirstinį, termodinaminėje riboje, kai $N \to \infty$, galima išvesti paprastųjų diferencialinių lygčių sistemą dviems biofiziškai reikšmingiems makroskopiniams dydžiams – vidutiniam membranos potencialui $v(t)$ ir impulsų generavimo dažniui $r(t)$ [86]:

$$\dot{v} = \bar{\eta} + v^2 - \pi^2 r^2 + S(v, r) + I(\omega t), \tag{3.14a}$$

$$\dot{r} = \Delta/\pi + 2rv. \tag{3.14b}$$

Čia sinapsinės srovės $S = S(v, r)$ išraiška yra:

$$S(v, r) = J\frac{v_{th}}{\pi}\left[\frac{\pi}{2} - \arctan\left(\frac{v_{th} - v}{\pi r}\right)\right]. \tag{3.15}$$

Didelėms N vertėms, makroskopinis modelis (3.14) gerai atitinka mikroskopinio modelio (3.12) sprendinius, todėl mikroskopinio modelio FAF galima apskaičiuoti iš (3.14) sistemos.

Nagrinėjamas tinklas, sudarytas iš $N = 10^4$ QIF neuronų, kurių parametrų vertės $v_{th} = 50$, $J = 30$, $\Delta = 1$ ir $\bar{\eta} = 0$. Parinkus $\bar{\eta} = 0$, pusė neuronų yra osciliuojantys, kita pusė – sužadinamieji. Su tokiomis parametrų vertėmis (3.14) makroskopinis modelis svyruoja ribiniame cikle periodu $T_0 \approx 1.130132$.

Siekiant palyginti iš mikroskopinio modelio gautus rezultatus su redukuotos sistemos (3.14) sprendiniais, apskaičiuojamas Kuramoto tvarkos paramet-

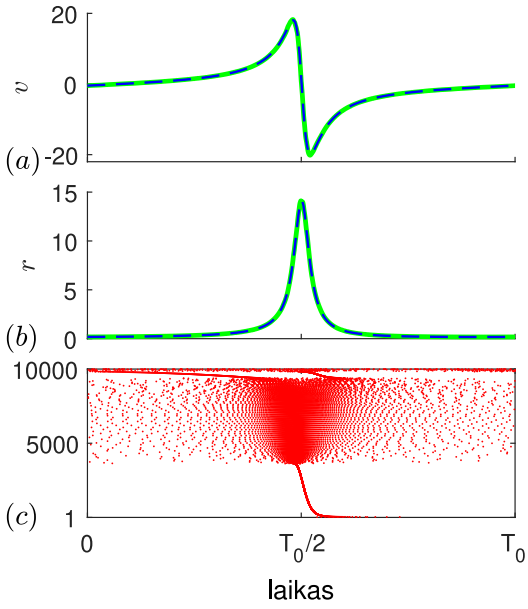

3.7 pav. Heterogeninio 10^4 sinapsėmis susietų QIF neuronų tinklo dinamika nesant stimuliacijos. Parametrų vertės $v_{th} = 50$, $J = 30$, $\Delta = 1$, $\bar{\eta} = 0$. (a) Vidutinio membranos potencialo $v(t)$ ir (b) impulsų generavimo dažnio $r(t)$ kitimas laike. Plonos punktyrinės mėlynos kreivės žymi redukuotos sistemos (3.14) sprendinius, paryškintos žalios ištisinės kreivės žymi mikroskopinio $N = 10^4$ neuronų tinklų skaitinio modeliavimo rezultatus. (c) Rastrinis brėžinys. Taškai žymi kiekvieno neurono impulsų laikus, vertikalioje ašyje atidėti individualūs neuronai.

ras [83]

$$Z = \frac{1}{N}\sum_{j=1}^{N}\exp\left(i\theta_j\right), \tag{3.16}$$

kurį su makroskopiniais parametrais v ir r sieja sąryšis [85]:

$$v = \mathrm{Im}\left(\frac{1-Z^*}{1+Z^*}\right), \quad r = \frac{1}{\pi}\,\mathrm{Re}\left(\frac{1-Z^*}{1+Z^*}\right), \tag{3.17}$$

čia Z^* žymimas kompleksinis jungtinis skaičius. Kintamųjų $v(t)$ ir $r(t)$ dinamika, apskaičiuota iš mikroskopinio modelio, gerai atitinka makroskopinio modelio (3.14) sprendinius (3.7 pav.).

Nepaisant sudėtingos mikroskopinės tinklo dinamikos, jo makroskopinį elgesį gerai apibūdina redukuota lygčių sistema (3.14). Tinklo FAF, gauta iš redukuotos lygčių sistemos, ir $\mathcal{J}_{th}/|\Delta\omega|$ priklausomybė nuo d pateikta 3.8 pav. $\mathcal{J}_{th}/|\Delta\omega|$ įgyja minimalią reikšmę taške $d = \vartheta_z$, kai $\Delta\omega > 0$, ir taške $d = -\vartheta_z$, kai $\Delta\omega < 0$; čia $\vartheta_z \approx 2.5832$ yra atstumas tarp FAF ekstremumų. Minimali $\mathcal{J}_{th}/|\Delta\omega|$ vertė atitinka teoriškai apskaičiuotą optimalią vertę (2.29).

Galima daryti išvadą, kad išvesta optimaliojo valdymo teorija galioja ne tik mažiems neuronų tinklams, bet ir didelio masto sąveikaujančių QIF neuronų tinklui, kurio kolektyvinė dinamika pasižymi periodiniais makroskopiniais virpesiais.

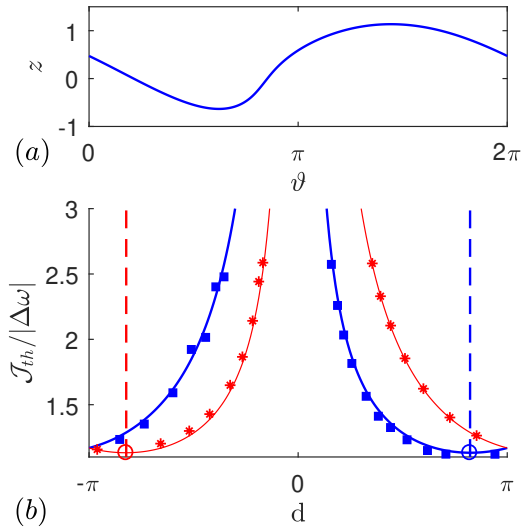

3.8 pav. 10^4 sinapsėmis susietų QIF neuronų tinklo valdymo minimaliu krūviu teorijos patikrinimas. (a) Tinklo FAF stimuliuojant visus tinklo neuronus. FAF apskaičuojama iš redukuotos lygčių sistemos. Fazinis atstumas tarp FAF ekstremumų $\Delta\vartheta_z = 2.5832$, amplitudė $z_{max} - z_{min} = 1.7696$. (b) $\mathcal{J}_{th}/|\Delta\omega|$ priklausomybė nuo d esant fiksuotiems parametrams $l = 0.2$ ir $s = 2$. Paryškintos mėlynos ir plonos raudonos kreivės gautos tuo pat būdu kaip ir 3.4 pav. Simboliai žymi 10^4 mikroskopinių lygčių, veikiamų (2.30) srovės, skaitinio modeliavimo rezultatus.

4 Sinchronizacijos slopinimas dviejose sąveikaujančiose eksitatorinių ir inhibitorinių neuronų populiacijose

Šiame skyriuje parodoma, kad vidutinio lauko lygtys yra naudingos norint suprasti ne tik kolektyvinių virpesių atsiradimą didelio masto neuronų tinkluose, bet ir stimuliacijos poveikį sinchronizacijos procesams. Kaip pavyzdys nagrinėjamas dviejų sąveikaujančių eksitatorinių (E) bei inhibitorinių (I) *quadratic integrate-and-fire* (QIF) neuronų populiacijų tinklas. Parodoma, kad I populiacijos aukšto dažnio (AD) stimuliacija yra labai veiksminga slopinant kolektyvinį sinchronizuotą nervinių impulsų generavimą abiejose populiacijose. Slopinimo mechanizmas paaiškinamas nestabilios nekoherentinės tinklo būsenos stabilizavimu. Taip pat paaiškinamas virpesių slopinimo efektas, kurį sukelia slopinamasis impulsas, veikiantis E populiaciją.

4.1 Neuronų tinklo modelis

4.1.1 Mikroskopinis modelis

Nagrinėjamas heterogeninis dviejų sąveikaujančių eksitatorinių ir inhibitorinių populiacijų QIF neuronų tinklas. Mikroskopinė tinklo būsena priklauso nuo $2N$ neuronų membranos potencialų $\{V_j^{(E,I)}\}_{j=1,\ldots,N}$, tenkinančių $2N$ paprastųjų diferencialinių lygčių sistemą [80]:

$$\begin{aligned} \tau \dot{V}_j^{(E,I)} &= (V_j^{(E,I)})^2 + \eta_j^{(E,I)} + \mathcal{I}_j^{(E,I)}, \\ &\text{jei } V_j^{(E,I)} \geq V_p, \text{ tai } V_j^{(E,I)} \leftarrow V_r. \end{aligned} \tag{4.1}$$

Čia τ yra membranos laiko konstanta. Paprastumo dėlei, abiejų populiacijų neuronų skaičius N ir laiko konstanta τ sutampa. Heterogeninis sužadinimo parametras $\eta_j^{(E,I)}$ nusako izoliuoto neurono elgesį, o narys $\mathcal{I}_j^{(E,I)}$ apibrėžia sinapsinę sąveiką tarp neuronų ir išorinį žadinimą. Izoliuoti ($\mathcal{I}_j^{(E,I)} = 0$) neuronai, kurių parametro vertė neigiama, $\eta_j^{(E,I)} < 0$, yra ramybės būsenoje, o neuronai, kurių parametro vertė teigiama, $\eta_j^{(E,I)} > 0$, generuoja periodinius

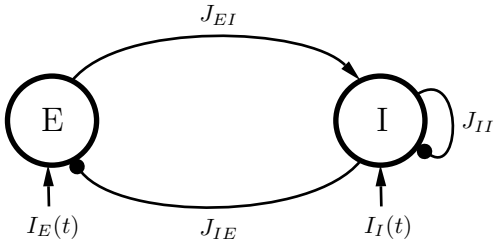

4.1 pav. Tinklo, susidedančio iš dviejų neuronų populiacijų, schema. Apskritimai, pažymėti „E“ ir „I“ žymi eksitatorinių bei inhibitorinių neuronų populiacijas. Rodyklė žymi E populiacijos žadinamąjį poveikį populiacijai I. J_{EI} yra sąveikos stipris. Kreivės su skrituliais žymi slopinantį I poveikį E, taip pat slopinantį grįžtamąjį ryšį I populiacijos viduje. J_{IE} ir J_{II} yra šių sąveikų stipris. Vertikalios rodyklės, pažymėtos $I_E(t)$ ir $I_I(t)$, žymi išorinį žadinimą, veikiantį E ir I populiacijas.

veikimo potencialus, kuriuos galima aproksimuoti Dirako delta funkcija. Impulsas generuojamas membranos potencialui $V_j^{(E,I)}$ viršijus vertę V_p. Iškart po to membranos potencialo vertė atstatoma į V_r. Nustačius $V_p = -V_r \to \infty$, QIF neuroną galima transformuoti į teta neuroną (angl. *theta neuron*). Ši prielaida taip pat esminė analizuojant (4.1) sistemą begalinio tinklo dydžio riboje $N \to \infty$ [85]. Abiejų populiacijų neuronų parametrai $\eta_j^{(E,I)}$ gaunami iš Lorenco skirstinio:

$$g_{E,I}(\eta) = \frac{1}{\pi} \frac{\Delta_{E,I}}{(\eta - \bar{\eta}_{E,I})^2 + \Delta_{E,I}^2}, \tag{4.2}$$

kur $\Delta_{E,I}$ ir $\bar{\eta}_{E,I}$ atitinkamai yra E ir I populiacijos skirstinio plotis ir centras. Paskutinis (4.1) lygties narys $\mathcal{I}_j^{(E,I)}$ nusako sinapsinę sąveiką bei išorinę stimuliaciją:

$$\mathcal{I}_j^{(E)} = -J_{IE} S_I(t) + I_E(t), \tag{4.3a}$$

$$\mathcal{I}_j^{(I)} = J_{EI} S_E(t) - J_{II} S_I(t) + I_I(t). \tag{4.3b}$$

Čia $S_E(t)$ ir $S_I(t)$ apibrėžia E ir I populiacijų vidutinę sinapsinę aktyvaciją:

$$S_{E,I}(t) = \frac{\tau}{N} \sum_{j=1}^{N} \sum_{k \setminus (t_j^k)_{E,I} < t} \delta(t - (t_j^k)_{E,I}), \tag{4.4}$$

kur $(t_j^k)_{E,I}$ yra j-tojo neurono k-tojo impulso laikas, o $\delta(t)$ yra Dirako delta funkcija. Parametrai J_{EI}, J_{IE} ir J_{II} apibrėžia sinapsinės sąveikos stiprį (žr. 4.1 pav.). Srovės $I_E(t)$ ir $I_I(t)$ aprašo homogeninę išorinę atitinkamai E ir I populiacijos stimuliaciją. Nagrinėjami stimuliacijos protokolai, kai stimuliuojama atskirai I ($I_E(t) = 0$, $I_I(t) \neq 0$) arba E ($I_E(t) \neq 0$, $I_I(t) = 0$) populiacija.

Tinklo architektūra, pavaizduota 4.1 pav., imituoja pogumburio branduolio (STN – E populiacija) ir blyškiojo kamuolio išorinio segmento (GPe – I populiacija) neuronų tinklą, dažnai naudojamą modeliuojant Parkinsono ligą (žr. pvz. [133]).

4.1.2 Makroskopinis modelis: vidutinio lauko lygtys riboje, kai $N \to \infty$

Nagrinėjamo tinklo makroskopinę dinamiką charakterizuoja keturi biofiziškai reikšmingi dydžiai – E ir I populiacijos vidutinis membranos potencialas ir bedimensis impulsų generavimų dažnis:

$$v_{E,I} = \frac{1}{N} \sum_{j=1}^{N} V_j^{(E,I)}, \quad r_{E,I} = \tau \frac{M^{(E,I)}(\Delta t)}{N \Delta t}, \tag{4.5}$$

Čia $M^{(E,I)}(\Delta t)$ yra nervinių impulsų skaičius mažame laiko intervale Δt. Riboje, kai $N \to \infty$, dydžių $r_{E,I}(t)$ ir $v_{E,I}(t)$ dinamiką aprašo keturių paprastųjų diferencialinių lygčių sistema [85]:

$$\tau \dot{r}_E = \Delta_E / \pi + 2 r_E v_E, \tag{4.6a}$$

$$\tau \dot{v}_E = \bar{\eta}_E + v_E^2 - \pi^2 r_E^2 - J_{IE} r_I + I_E(t), \tag{4.6b}$$

$$\tau \dot{r}_I = \Delta_I / \pi + 2 r_I v_I, \tag{4.6c}$$

$$\tau \dot{v}_I = \bar{\eta}_I + v_I^2 - \pi^2 r_I^2 + J_{EI} r_E - J_{II} r_I + I_I(t). \tag{4.6d}$$

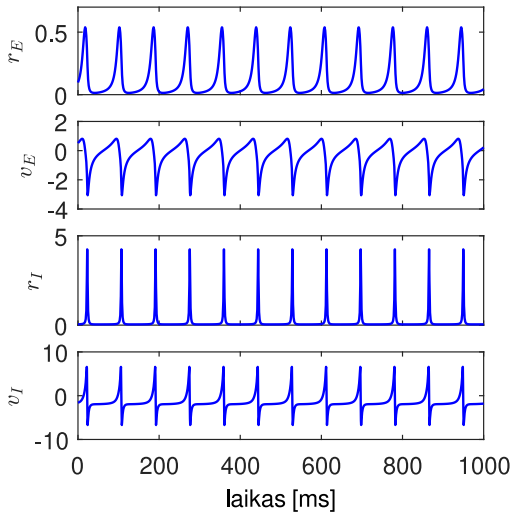

4.2 pav. Makroskopinių kintamųjų $r_E(t)$, $v_E(t)$, $r_I(t)$ ir $v_I(t)$ dinamika išsprendus vidutinio lauko lygtis (4.6) nesant stimuliacijos, $I_E(t) = I_I(t) = 0$. Parametrų vertės: $\Delta_E = 0.05$, $\bar{\eta}_E = 0.5$, $\Delta_I = 0.5$, $\bar{\eta}_I = -4$, $J_{EI} = 20$, $J_{IE} = 5$, $J_{II} = 0.5$ ir $\tau = 14$ ms.

Šios vidutinio lauko lygtys ženkliai supaprastina tinklo dinamikos bei stimuliacijos poveikio jai analizę.

4.2 Tinklo dinamika nesant stimuliacijos

Nesant stimuliacijos, $I_E(t) = I_I(t) = 0$, makroskopiniai tinklo virpesiai, gauti išsprendus (4.6) sistemą, pavaizduoti 4.2 pav. Sąlyginai paprastos vidutinio lauko lygtys leidžia atlikti išsamią įvairių tinklo dinaminių režimų bifurkacijų analizę ir atskleisti stimuliavimo algoritmų veikimo principus. Išanalizavus tinklo dinamikos priklausomybę nuo sąveikos stiprių J_{EI}, J_{IE} ir J_{II} bei sudarius bifurkacijų diagramą parametrų plokštumoje $(\bar{\eta}_I, \bar{\eta}_E)$, buvo nustatyta, kad sistema gali turėti stabilų rimties tašką, stabilų ribinį ciklą, arba būti bistabiliame režime su šiais dviem kartu egzistuojančiais atraktoriais. Bistabilumo sritys matomos vieno parametro bifurkacijų diagramose, pateiktose 4.3 pav. 4.4(a) ir 4.4(b) pav. pateikiamos dviejų parametrų bifurkacijų diagramos (J_{IE}, J_{EI}) ir (J_{II}, J_{EI}) plokštumose. Visi trys režimai užima pa-

kankamai didelius plotus parametrų erdvėje, todėl jie yra atsparūs parametrų pokyčiams plačiose ribose.

4.3 Sinchroninių virpesių slopinimas

4.3.1 Inhibitorinės populiacijos aukšto dažnio stimuliacija

Nagrinėjama tinklo dinamika, kai $I_E(t) = 0$ ir

$$I_I(t) = a\cos(\omega t), \tag{4.7}$$

kur a yra AD stimuliacijos amplitudė, o ω – kampinis dažnis. Stimuliacijos srovė (4.7) tenkina kliniškai būtiną krūvio balanso sąlygą $\int_0^T I_I(t)dt = 0$, kur $T = 2\pi/\omega$ yra stimuliacijos periodas. Daroma prielaida, kad laisvas tinklas turi vieną stabilų atraktorių – ribinį ciklą ir kad stimuliacijos dažnis $\nu = 1/T$ yra žymiai didesnis nei ribinio ciklo dažnis ν_0.

AD stimuliacijos poveikio tinklo dinamikai modeliavimo rezultatai pateikti 4.5 pav.: I populiacijos AD stimuliacija veiksmingai nuslopina sinchroninius tinklo virpesius.

Siekiant suprasti, kodėl inhibitorinių neuronų AD stimuliacija yra tokia veiksminga, atliekamas vidutinio lauko lygčių vidurkinimas per AD stimuliacijos periodą [136]:

$$\tau\dot{\bar{r}}_E = \Delta_E/\pi + 2\bar{r}_E\bar{v}_E, \tag{4.8a}$$

$$\tau\dot{\bar{v}}_E = \bar{\eta}_E + \bar{v}_E^2 - \pi^2\bar{r}_E^2 - J_{IE}\bar{r}_I, \tag{4.8b}$$

$$\tau\dot{\bar{r}}_I = \Delta_I/\pi + 2\bar{r}_I\bar{v}_I, \tag{4.8c}$$

$$\tau\dot{\bar{v}}_I = \bar{\eta}_I^A + \bar{v}_I^2 - \pi^2\bar{r}_I^2 + J_{EI}\bar{r}_E - J_{II}\bar{r}_I. \tag{4.8d}$$

Šios lygtys skiriasi nuo pradinių lygčių (4.6) tik tuo, kad parametras $\bar{\eta}_I$ pakeičiamas $\bar{\eta}_I^A$, kuris priklauso nuo stimuliacijos parametro A:

$$\bar{\eta}_I^A = \bar{\eta}_I + A^2/2. \tag{4.9}$$

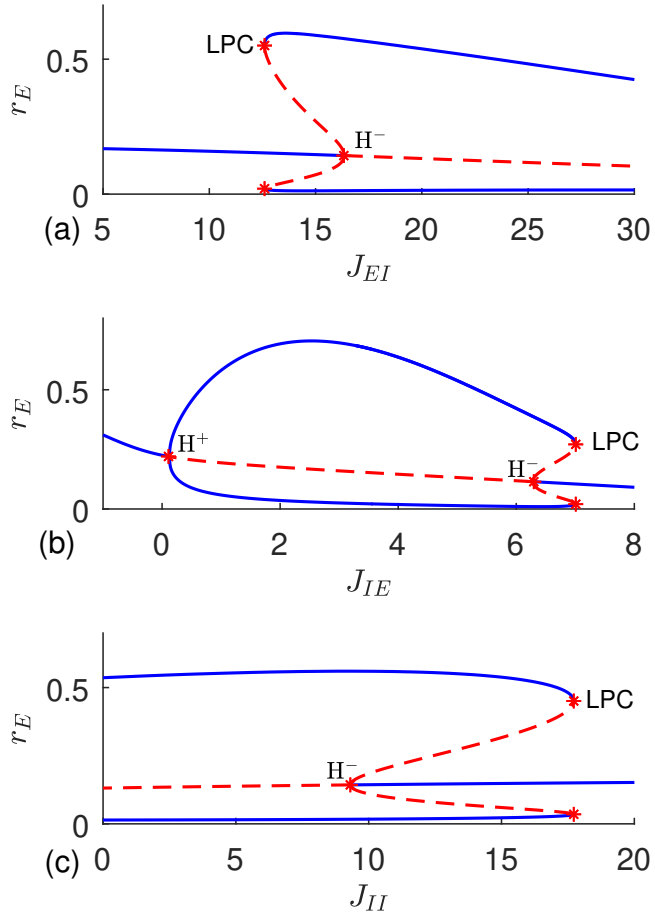

4.3 pav. Vieno parametro bifurkacijų diagramos, rodančios impulsų generavimo dažnio r_E priklausomybę nuo sąveikos stiprio (a) J_{EI}, (b) J_{IE} ir (c) J_{II}. Kitų parametrų vertės tokios pat kaip 4.2 pav. Mėlynos kreivės žymi stabilų rimties tašką bei stabilaus ribinio ciklo maksimumą ir minimumą. Raudonos punktyrinės linijos žymi nestabilų rimties tašką bei nestabilaus ribinio ciklo maksimumą ir minimumą. Raudonos žvaigždutės, pažymėtos LPC, H^+ ir H^-, atitinkamai žymi ciklų ribinio taško (angl. *limit point of cycles*) bifurkaciją, superkritinę Hopfo bifurkaciją ir subkritinę Hopfo bifurkaciją.

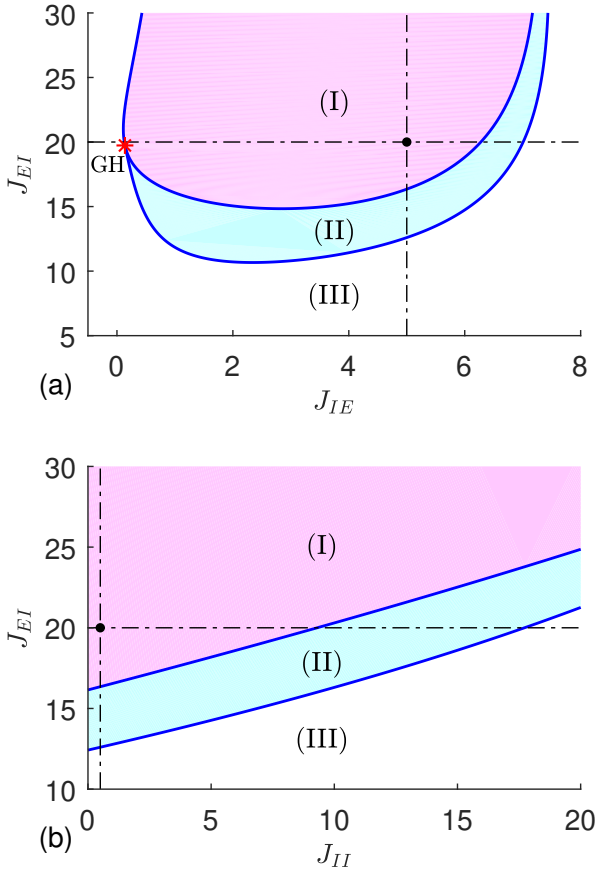

4.4 pav. Dviejų parametrų bifurkacijų diagramos parametrų plokštumose (a) (J_{IE}, J_{EI}) ir (b) (J_{II}, J_{EI}). Kitų parametrų vertės tokios pat kaip 4.2 pav. Plotai, pažymėti romėniškais skaitmenimis: (I) - egzistuoja tik stabilus ribinis ciklas, (II) - bistabilumo sritis su stabiliu ribiniu ciklu bei stabiliu rimties tašku, ir (III) - egzistuoja tik stabilus rimties taškas. Raudona žvaigždutė, pažymėta GH, nurodo bendrosios Hopfo bifurkacijos tašką. Horizontalios punktyrinės tiesės $J_{EI} = 20$ (a) ir (b) pav. atitinka vieno parametro bifurkacijų diagramų 4.3(b) ir 4.3(c) pav. plokštumas. Vertikalios punktyrinės tiesės $J_{IE} = 5$ (a) pav. ir $J_{II} = 0.5$ (b) pav. atitinka vieno parametro bifurkacijų diagramą 4.3(a). Horizontalių ir vertikalių tiesių sankirtos taškai atitinka parametrų vertes, naudotas 4.2 pav.

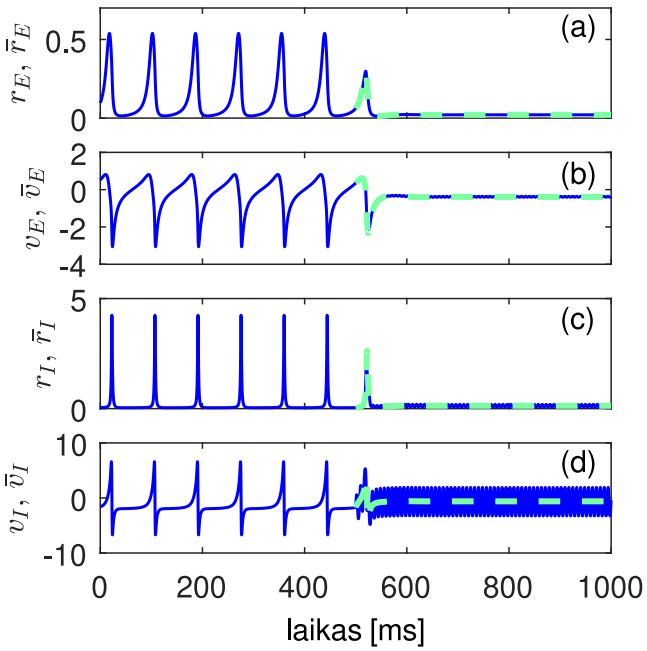

4.5 pav. Tinklo virpesių slopinimas taikant I populiacijos AD stimuliaciją. Mėlynos kreivės žymi kintamųjų $r_E(t)$, $v_E(t)$, $r_I(t)$ ir $v_I(t)$ dinamiką, nustatytą išsprendus (4.6) lygtis, esant toms pačioms parametrų vertėms kaip 4.2 pav. Iki stimuliacijos įjungimo ($t < 500$ ms) tinklo dinamika sutampa su 4.2 pav. Laiko momentu $t = 500$ ms pradedama I populiacijos stimuliacija $\nu = 130$ Hz dažnio ir $a = 30$ amplitudės srove. Žalios paryškintos punktyrinės linijos rodo kintamųjų $\bar{r}_E(t)$, $\bar{v}_E(t)$, $\bar{r}_I(t)$ ir $\bar{v}_I(t)$ dinamiką, nustatytą išsprendus suvidurkintas lygtis (4.8).

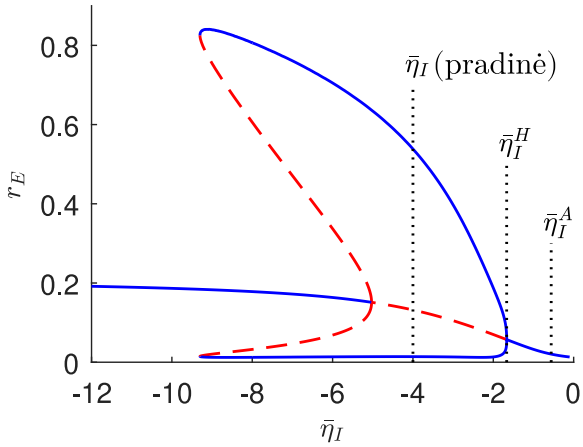

4.6 pav. Vieno parametro bifurkacijų diagrama, rodanti impulsų generavimo dažnio r_E priklausomynę nuo parametro $\bar{\eta}_I$. Kiti parametrai tokie pat kaip 4.2 pav. Žymėjimai tokie pat kaip 4.3 pav. Trys vertikalios taškinės linijos žymi bifurkacijos parametro pradinę vertę $\bar{\eta}_I = -4$, superkritinės Hopfo bifurkacijos vertę $\bar{\eta}_I^H \approx -1.667$, ir vertę $\bar{\eta}_I^A \approx -0.559$, gautą iš (4.9) lygties, nustačius stimuliacijos dažnį $\nu = 130$ Hz ir amplitudę $a = 30$.

4.5 pav. parodyta, kad suvidurkintos lygtys (4.8) gerai aproksimuoja pradinių lygčių (4.6) sprendinius.

Iš (4.9) lygties galima daryti išvadą, kad AD stimuliacija paslenka inhibitorinių neuronų Lorenco skirstinio $g_I(\eta)$ centrą į dešinę atstumu $A^2/2$. Dėl to I populiacija tampa labiau aktyvi. Pakankamai padidinus parametrą $\bar{\eta}_I$ stabilizuojamas nestabilus rimties taškas ir tokiu būdu nuslopinami tinklo virpesiai (4.6 pav.).

Bendruoju atveju, rimties būsenos stabilumo sąlygą $\bar{\eta}_I^A > \bar{\eta}_I^H$ arba $A^2 > 2(\bar{\eta}_I^H - \bar{\eta}_I)$ galima užrašyti

$$a > a_{\text{th}} \equiv 2\pi\nu\tau\sqrt{2(\bar{\eta}_I^H - \bar{\eta}_I)}, \tag{4.10}$$

kur a_{th} yra slenkstinė AD stimuliacijos amplitudė, kurią viršijus stabilizuojama suvidurkintų lygčių (4.8) rimties būsena ir nuslopinami pradinės lygčių sistemos (4.6) virpesiai. 4.7 pav. pateikti (4.6) sistemos modeliavimo rezultatai keičiant abu stimuliacijos parametrus: amplitudę a ir dažnį ν. Tinklo atsako

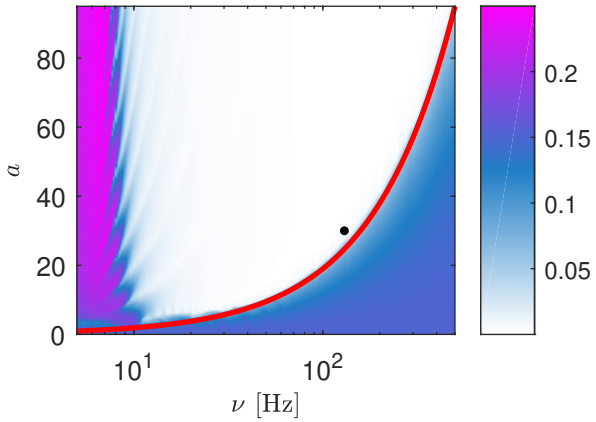

4.7 pav. Tinklo atsako priklausomybė nuo stimuliacijos dažnio ν ir amplitudės a. Spalvos žymi standartinio nuokrypio σ vertes, nustatytas iš (4.11) lygties 5000 ms intervalą vidurkio skaičiavimui. Balta spalva pažymėta nuslopintų virpesių sritis. Nesant stimuliacijos ($a = 0$), standartinis nuokrypis $\sigma \approx 0.15$. Raudone kreive pavaizduota analizinė slenkstinė amplitudė (4.10). Juodas taškas žymi parametrų vertes (ν, a), naudojamas 4.5 pav.

į stimuliaciją matu pasirinktas E populiacijos impulsų generavimo dažnio standartinis nuokrypis

$$\sigma = \sqrt{\langle [r_E(t) - \langle r_E(t) \rangle]^2 \rangle}, \tag{4.11}$$

kur kampiniai skliaustai žymi vidurkį laike. Mažos šio parametro vertės atitinka tinklo rimties būseną, didelės vertės – aukštos amplitudės virpesius. Įdomu, kad balta sritis 4.7 pav. panaši į eksperimentiškai nustatytą parametrų plokštumos sritį, kurioje nuslopinamas Parkinsono liga sergančių pacientų tremoras stimuliuojant ventralinį tarpinį gumburo branduolį (lot. *nucleus ventralis intermedius thalami*) [25].

4.3.2 Virpesių slopinimas stimuliuojant eksitatorinę populiaciją

Nagrinėjamas AD stimuliacijos poveikį E populiacijai, t. y. $I_I(t) = 0$ ir

$$I_E(t) = a \cos(\omega t). \tag{4.12}$$

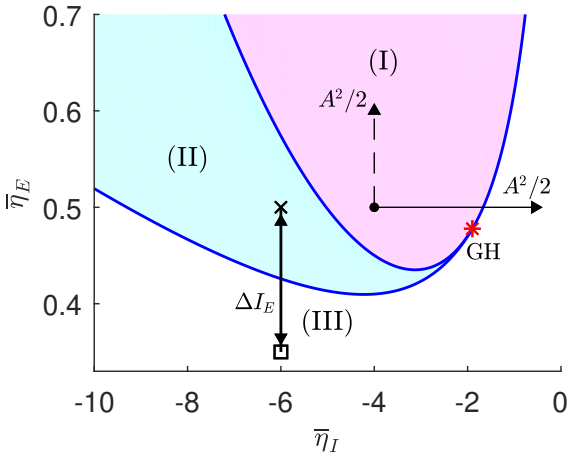

4.8 pav. Dviejų parametrų bifurkacijų diagrama plokštumoje $(\bar{\eta}_I, \bar{\eta}_E)$ nesant stimuliacijos. Žymėjimai tokie pat kaip 4.4 pav. Juodas taškas (I) srityje žymi parametrų vertes, naudotas 4.5 pav. AD stimuliacijos poveikis I populiacijai pažymėtas horizontalia rodykle. Vertikali punktyrinė rodyklė žymi AD stimuliacijos poveikį E populiacijai. Kryželis (II) srityje žymi parametrų vertes, naudotas 4.9 pav. Dviguba vertikali rodyklė žymi slopinančio impulso poveikį E populiacijai. Impulso poveikis sistemos dinamikai pateiktas 4.9 pav.

Taikant vidurkinimo metodą (4.6) lygtims, gaunama panaši į (4.8) lygčių sistema, tik šiuo atveju parametras $\bar{\eta}_I$ išlieka nepakitęs, o parametras $\bar{\eta}_E$ tampa

$$\bar{\eta}_E \to \bar{\eta}_E^A = \bar{\eta}_E + A^2/2. \tag{4.13}$$

Didinant $\bar{\eta}_E$ eksitatoriniai neuronai tampa aktyvesni ir tinklo virpesiai dar labiau sustriprėja. 4.8 pav. pateikiamas grafinis paaiškinimas, kodėl skiriasi E ir I populiacijos stimuliacijos poveikis.

Nors E populiacijos AD stimuliacija yra neveiksminga, sistemai esant bistabiliame režime tinklo virpesių slopinimas įmanomas taikant kitą valdymo protokolą. E populiaciją paveikus stačiakampiu slopinančiuoju impulsu, tinklo būsena perjungiama iš stabilaus ribinio ciklo į stabilų rimties tašką. Toks impulsas perkelia sistemos parametrus į sritį, kurioje rimties taškas yra vienintelis atraktorius. Išjungus stimuliaciją, sistema grįžta į bistabilų režimą, tačiau lieka rimties taške (žr. 4.8 pav.). Šio valdymo algoritmo efektyvumas parodytas 4.9 pav.

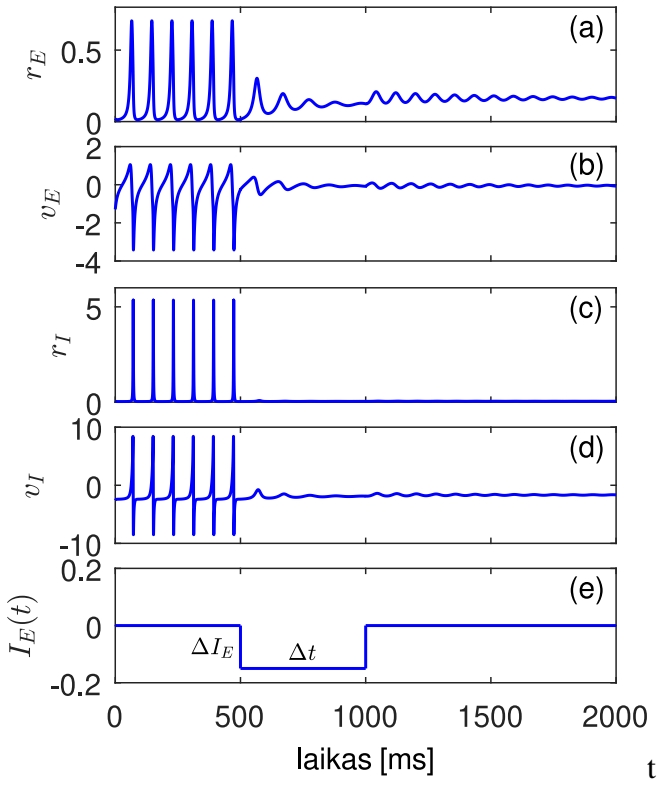

4.9 pav. Tinklo virpesių panaikinimas slopinančiu impulsu veikiant E populiaciją. Kintamųjų (a) $r_E(t)$, (b) $v_E(t)$, (c) $r_I(t)$ ir (d) $v_I(t)$ dinamika, gauta (4.6) lygtis veikiant slopinančiu impulsu $I_E(t)$, parodytu (e) pav. Impulso amplitudė $\Delta I_E = -0.15$, trukmė $\Delta t = 500$ ms. Parametrų vertės, išskyrus $\bar{\eta}_I = -6$, tokios pat kaip 4.2 pav.

4.4 Mikroskopinės dinamikos modeliavimas

Redukuotos vidutinio lauko lygtys (4.6) išvestos begalinio tinklo dydžio riboje, tačiau realūs tinklai sudaryti iš baigtinio neuronų skaičiaus. Siekiant patikrinti, ar aukščiau aprašyti valdymo algoritmai yra veiksmingi baigtinio dydžio tinklams, atlikome tiesioginį (4.1) lygčių modeliavimą.

Norint palyginti modeliavimo rezultatus su redukuotos sistemos (4.6) sprendiniais, apskaičiuojamas Kuramoto tvarkos parametras (3.16) ir panaudojamas sąryšis (3.17) tarp $Z_{E,I}$ ir impulsų generavimo dažnio $r_{E,I}$.

Iš mikroskopinio modelio apskaičiuotas AD stimuliacijos poveikis I populiacijai pateiktas 4.10 pav., slopinančio impulso poveikis E populiacijai – 4.11 pav.

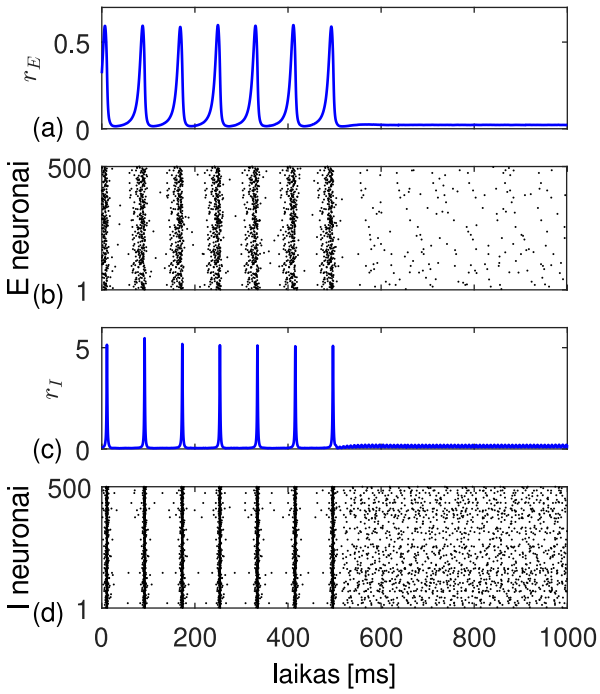

4.10 pav. Iš mikroskopinio modelio apskaičiuotas AD stimuliacijos poveikis I populiacijai. I ir E populiacijos neuronų skaičius sutampa, $N = 2000$. Visų parametrų vertės tokios pat kaip 4.5 pav. (a) ir (c) atitinkamai E ir I populiacijos impulsų generavimo dažnis. (b) ir (d) 500 atsitiktinai parinktų E ir I populiacijos neuronų rastriniai grafikai. Taškai žymi neuronų impulsų laikus.

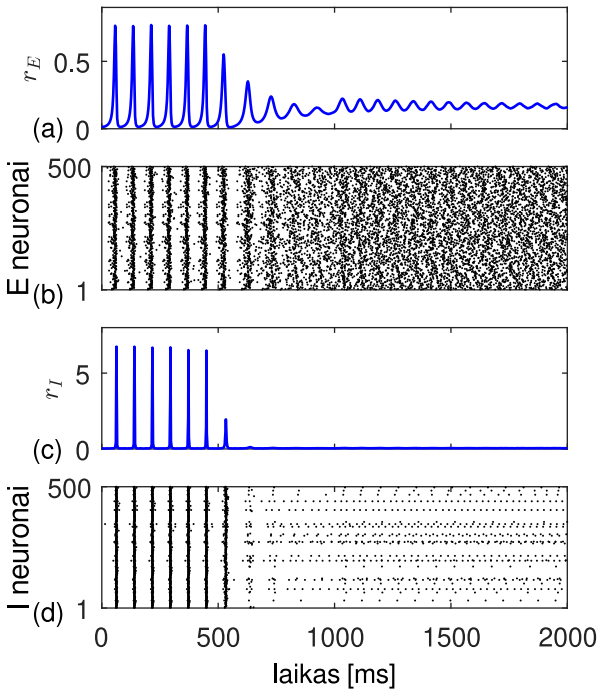

4.11 pav. Iš mikroskopinio modelio apskaičiuotas slopinančio impulso poveikis E populiacijai. E ir I populiacijos neuronų skaičius $N = 2000$. Visų parametrų vertės tokios pat kaip 4.9 pav. (a) ir (c) atitinkamai E ir I populiacijos impulsų generavimo dažnis. (b) ir (d) 500 atsitiktinai parinktų E ir I populiacijos neuronų rastriniai grafikai.

Rezultatai ir išvados

1. Optimali subalansuoto krūvio valdymo srovė, užtikrinanti impulsus generuojančio neurono sinchronizaciją su periodine išorine stimuliacija minimizuojant stimuliacijos srovės modulio vidurkį, yra sudaryta iš dviejų, bendruoju atveju skirtingo pločio ir amplitudės, teigiamo ir neigiamo impulsų, centruotų ties neurono FAF ekstremumais. Šios optimizavimo teorijos pagrįstumas patvirtintas analiziškai Stuart-Landau osciliatoriui, atsitiktinei FAF ir klasikiniam HH neurono modeliui.

2. Be audinio pažaidos sumažinimo, valdymo minimaliu krūviu algoritmas turi dar vieną praktinį pranašumą: esant mažam dažnių skirtumui, tiesinėje Arnoldo liežuvio dalyje, kuomet srovės ribojimas yra nereikšmingas, valdymo srovė priklauso tik nuo atstumo tarp FAF absoliučių ekstremumų ir jos amplitudės. Tai leidžia empiriškai nustatyti stimuliacijos parametrus, nežinant neurono modelio išraiškos ir netaikant fazinės redukcijos teorijos.

3. Neuronų tinklo lygtys taip pat gali būti redukuotos į tą pačią fazės lygtį, kaip ir vienas neuronas; šiuo atveju neurono FAF pakeičiama efektyviąja tinklo FAF. Optimalioji neuronų tinklo valdymo srovė taip pat sudaryta iš periodiškai pasikartojančių teigiamų ir neigiamų, bendruoju atveju skirtingo pločio ir amplitudės, stačiakampių impulsų, priklausančių nuo tinklo FAF amplitudės ir atstumo tarp jos globaliųjų ekstremumų.

4. Teorinius rezultatus patvirtina trys skaitiniai pavyzdžiai: optimalus valdymas pritaikytas dviems mažo masto sinapsėmis bei elektrine sąveika susietiems FHN neuronų tinklams ir didelio masto sinapsiškai susietų QIF neuronų tinklui. Pirmuoju atveju gauta, kad osciliuojančių eksitatorinių neuronų stimuliacija yra efektyvesnė nei kiti stimuliacijos protokolai – sinchronizacija pasiekiama su keturis kartus mažesniu stimuliacijos srovės modulio vidurkiu.

5. Pilnasis sinapsėmis sujungtų dviejų eksitatorinių ir inhibitorinių QIF neuronų populiacijų tinklas turi tris galimus dinaminius režimus: vieną

stabilų rimties tašką, vieną stabilų ribinį ciklą ir bistabilų režimą su šiais dviem kartu egzistuojančiais atraktoriais. Visi trys režimai užima pakankamai didelius plotus parametrų erdvėje, todėl jie yra atsparūs parametrų pokyčiams plačiose ribose.

6. Vidutinio lauko lygtys, suvidurkintos per AD stimuliacijos periodą, yra tapačios nesutrikdytoms vidutinio lauko lygtims, tačiau su pakeistu sužadinimo parametru. Taikant AD stimuliaciją inhibitorinei neuronų populiacijai padidėja impulsus generuojančių neuronų dalis, o tai lemia tinklo nekoherentinės nestabilios rimties būsenos stabilizavimą ir kolektyvinių virpesių nutraukimą. Slenkstinė stimuliacijos amplitudė, reikalinga šiam tikslui pasiekti, AD srityje yra proporcinga stimuliacijos dažniui.

7. Eksitatorinės neuronų populiacijos AD stimuliacija yra neefektyvi siekiant nuslopinti tinklo virpesius, nes padidina impulsus generuojančių neuronų dalį šioje populiacijoje. Nepaisant to, jei sistemos parametrai yra bistabiliame režime, galimas kitas stimuliacijos protokolas. Veikiant eksitatorinius neuronus stačiakampiu slopinančiuoju impulsu, sistemos parametrai pervedami į fazinės erdvės sritį, kurioje egzistuota vienintelis rimties taškas. Tokiu būdu, sistema pereina į stabilią nekoherentinę rimties būseną, kurioje ir lieka išjungus stimuliaciją ir parametrams grįžus į bistabilią sritį.

8. Remiantis atliktais tyrimais, galima teigti, kad vidutinio lauko lygtys, gautos iš sąveikaujančių QIF neuronų mikroskopinės dinamikos, gali būti efektyvus įrankis kuriant įvairius didelio masto neuronų tinklų sinchronizacijos valdymo algoritmus.

Santrumpos

AD aukšto dažnio (stimuliacija)

E eksitatorinė (populiacija)

FAF fazės atsako funkcija

FHN FitzHugh-Nagumo

GPe globus pallidus externus

GSS giluminė smegenų stimuliacija

HH Hodgkin-Huxley

I inhibitorinė (populiacija)

QIF quadratic integrate-and-fire

STN subthalamic nucleus (nucleus subthalamicus)

Vilnius University Press
9 Saulėtekio Ave., LT-10222, Vilnius, Lithuania
E-mail: info@leidykla.vu.lt, www.leidykla.vu.lt
bookshop.vu.lt, journals.vu.lt
Print run copies 20